

Dynamic Response of Droplets to Single Wave Electrowetting Perturbation

by
Juan Sebastian Marin Quintero

A thesis submitted in partial fulfillment of the requirements for the degree of
Master of Science

Department of Mechanical Engineering
University of Alberta

©Juan Sebastian Marin Quintero, 2019

Abstract

Active control over the spreading of a liquid can be the avenue of endless opportunities. This spreading is dictated by the surface energy of a solid surface in which the wetting of a given liquid is quantified by the Young's contact angle. This quantification is the outcome of the interactions and the magnitudes of the interfacial energies at the solid-liquid, the solid-medium, and the drop-medium interfaces. Electrowetting-on-dielectric (EWOD) is a technique that can permit the control over spreading and its rate without permanently altering the surface energies of these three interfaces. This is the key aspect and the most important advantage of electrowetting. The new equilibrium configuration of the drop, as a response to EWOD by means of an externally applied electric field, can be predicted by the Young-Lippmann's equation. Although electrowetting has been widely studied, there is limited knowledge on the initial response of the drop, mainly after exerting different kinds of electric fields. During the implementation of the electric field a spreading behaviour is triggered, and this initial reaction of the drop to electrowetting was investigated thoroughly in this study. The transient evolution in the drop's shape was analyzed meticulously while the drop acquired the new equilibrium position. If the applied electrical actuation is oscillatory (AC), the number of cycles of this actuation dictated the equilibrium configuration and, in some cases,

it deviates from the Young-Lippmann's equation prediction. Moreover, the system properties, i.e., the thermophysical properties of the droplet and the surrounding medium, along with the voltage and the frequency of the applied wave, completely altered the initial drop dynamics that eventually resulted in the corresponding equilibrium of the droplet. It is also observed that the first actuation cycle of AC EWOD had the greatest influence on the drop to achieve the maximum possible spreading. Hence, as an extension of this research, the transient dynamics of a drop submitted to a single electrokinetic excitation is scrutinized. The response time of the drop, defined as the time from the instant that the excitation is introduced until the maximum spreading reached during the single actuation cycle, is directly and inversely proportional to the viscosity of the liquids and the frequency of the actuation force, respectively. Based on the extensive parametric study, a unique definition of time scale is proposed to predict the time to reach the maximum spreading of AC electrowetting. This new time scale was based on the imposed actuation time by the frequency of the wave and on the viscous time scale modified by the electrowetting properties. The aftereffects of the actuation on the drop's motion, particularly at the drop-medium interface, are also investigated to find out the role of this induced perturbation on the equilibration process. The oscillatory motion at the drop-medium interface resembled an inertial capillarity response. An equivalent mass-spring-dampener model is also proposed to analyze these oscillations. Finally, with increased knowledge about the response of a single drop to electrowetting, a new technique for electrocoalescence is proposed. The in-house developed technique circumvented the repulsion at the point of merging between two drops, i.e., at the three-phase contact lines. The coalescence of sessile drops is characterized by the

evolution of a film bridge between the drops that represents a mass transfer phenomenon. If a redefined time scale for maximum spreading is considered for the coalescence analysis, initial bridge growth suggested a universal growth irrespective of the system properties.

Preface

This thesis is original work by Juan Sebastian Marin Quintero. Improvement of the numerical solution of Chapter 2 was performed with Hafijur Rahman. A part of the experiments of Chapter 3 were conducted in collaboration with Joana Tian, and experiments of Chapter 4 with Markus Cäsar. For all the chapters, I was responsible for data collection, presentation and preparing the manuscripts. The idea for this project was conceived by my supervisor Dr. Prashant R. Waghmare. The interpretation of data was performed by myself, with valuable discussions with all above mentioned researchers, which contributed with their best ability. Dr. Waghmare supervised this research with conceptualization, continuous assistant in improving the work, and revising the manuscripts.

A version of Chapter 2 of this thesis will be submitted to the Journal of Fluid Mechanics with authorship order as: Juan S. Marin Quintero, Hafijur Rahman, and Prashant R. Waghmare, “Drop Spreading on a Solid Substrate due to Electrowetting”. In addition, the results of Chapter 2 were presented as an oral presentation at the Bubble & Drop 2019 international conference in Sofia, Bulgaria, as : “A mathematical model for sessile drop spreading under liquid medium due to electrowetting”. A version of Chapter 3 of this thesis has been submitted in Langmuir

as: Juan S. Marin Quintero, Prashant R. Waghmare, “Sessile drop response to a single wave electrokinetic excitation”, which is under review. Also, a summarized version of this work was presented as a poster presentation at the Droplets 2019 international conference in Durham, United Kingdom, as: “Sessile drop response to a single wave electrokinetic excitation”. And lastly, a modified version of Chapter 4 of this thesis will be prepared for submission to an appropriate journal as: Juan S. Marin Quintero, Hafijur Rahman, Markus Cäsar, and Prashant R. Waghmare, “Induced coalescence of sessile droplets by a single wave of electrowetting”.

Acknowledgements

I want to express my sincere gratitude to my supervisor Dr. Prashant Waghmare for his guidance and continuous support during my entire studies at the University of Alberta, for giving me the opportunity to work with him during my exchange program as an undergraduate student in 2016, and for accepting me as an MSc student at the Mechanical Engineering department. I immensely appreciate his patience and constant example throughout my whole project. I am also grateful for all the conversations with him that inspired me to think outside the box, to have attention on small details, and to become a better thinker.

I would also thank all the members of the interfacial Science and Surface Engineering Lab. Especially I thank Dr. Aleksey Baldygin for providing me training in all the different equipment in the lab and his expertise when I was designing and arranging my experimental setup. I also want to thank Ryan Baily, who provided me with technical and engineering support during my projects. I am also extremely grateful with Joanna Tian, Markus Cäsar, Sujit Deshmukh, and Hafijur Rahman for all their contributions on performing the experiments, having meaningful conversations, and improving my research.

In addition I want to give my profound thanks to my partner Fernanda Torres for her love, support, and being the person I trust the most. Also, I want to thank my uncle Tere Quintero and my grandma Flor for always taking care of me and being my second mothers. Finally, words cannot express how grateful I am to my parents John Jairo Marin and Flor Maria Quintero for always believing in me and encouraging me to become a better person.

Contents

1	Introduction	1
1.1	Overview of key applications	8
1.2	Aim of the present work	13
1.3	Thesis Outline	15
2	Drop Spreading on a Solid Substrate due to Electrowetting	19
2.1	Introduction	19
2.2	Formulation of the mathematical model and solution	22
2.2.1	Kinetic energy, E_k	25
2.2.2	Surface potential energy, E_s	25
2.2.3	Viscous dissipation within the drop (W_d) and at the drop- medium interface (W_m)	27
2.2.4	Governing equation for the drop's height variation	28
2.3	Experimental study of drop's perturbation	30
2.4	Results and discussions	32
2.4.1	Effect of electrowetting number	35
2.4.2	Effect of Roshko number	38
2.4.3	Effect of viscosity ratio	45
2.5	Conclusion	47

3	Sessile drop response to a single wave electrokinetic excitation	49
3.1	Introduction	49
3.2	Material and Methods	53
3.3	Results and Discussions	56
3.3.1	Applied voltage effect	60
3.3.2	Applied frequency effect	64
3.3.3	Viscosity effect	69
3.3.4	Response time of the drop	72
3.4	Conclusions	74
4	Induced coalescence of sessile droplets by a single wave of electrowetting	76
4.1	Introduction	76
4.2	Experimental setup	85
4.3	Prediction of the bridge growth	87
4.4	Results and Discussions	91
4.4.1	Effect of electrowetting number	94
4.4.2	Effect of separation distance	98
4.4.3	Effect of Ohnesorge number	101
4.5	Conclusions	104
5	Conclusion and Future Work	106
5.1	Overview and summary	106
5.2	Future works	110
5.2.1	Liquid medium electrocoalescence	110

5.2.2	Design and characterization of a liquid lens	112
Bibliography		115
Appendix		141
A-1	Derivation of Young-Lippmann equation	141
A-2	Optical setup considerations	145
A-2.1	Image acquisition	145
A-2.2	Illumination	149
A-2.3	Data acquisition and processing	150

List of Tables

2.1	Liquid properties of water drop and oil medium	31
3.1	Liquid properties of electrosprea- ding drops and oil medium	55
A-1	Areas and volume equations, with the corresponding partial deriva- tives with respect to R and θ	144

List of Figures

1.1	Dielectric breakdown of Electrowetting on dielectric	5
1.2	Contact angle saturation of Electrowetting on dielectric	7
1.3	Digital microfluidic circuit based on electrowetting	10
1.4	Liquid lens device based on Electrowetting on dielectric	12
2.1	Schematic of a sessile drop following the spherical cap assumption .	23
2.2	Theoretical results for a water drop in an oil medium submitted to a single sine wave of electrowetting	33
2.3	Transient variation of droplet height for different electrowetting numbers	36
2.4	Transient variation of droplet height for different Roshko numbers .	40
2.5	Effect of Roshko number on drop's spreading dynamics	41
2.6	Minimum height achieved by a drop by a sequence of sine waves for different Roshko numbers	43
2.7	Effect of viscosity ratio on drop's spreading dynamics	46
3.1	Schemes of the response of a sessile droplet to an external defor- mative force	52
3.2	Drop's response to a wave perturbation by means of electric field . .	58
3.3	Effect of applied voltage on the drop spreading dynamics	63

3.4	Effect of applied frequency on the drop spreading dynamics	67
3.5	Effect of viscosity on the drop spreading dynamics	71
3.6	Response time of the drops for different electrowetting conditions	74
4.1	Schematic of proposed experimental setup for electrocoalescence	79
4.2	Drops response to electrowetting	82
4.3	Designed experimental setup for electrocoalescence	87
4.4	Proposed drops response to a single wave perturbation by electrowetting	92
4.5	Effect of electrowetting number on the bridge growth	96
4.6	Initial bridge height of water drops in air medium	99
4.7	Effect of separation distance on the bridge growth	101
4.8	Effect of separation Ohnesorge number on the bridge growth	103
5.1	Liquid medium electrocoalesce for a single wave perturbation of electrowetting	112
5.2	Focal length of a liquid lens as a function of the applied voltage	114
A-3	Schematic of the optical setup used for the experiments	146
A-4	Line profile for detecting drop's interface	152

Chapter 1

Introduction

Modifying the wetting properties of a solid substrates has been a topic of interest for the last three decades. To alter the wetting properties of a solid substrate, pretreatment of the solid surface of known surface energy is the most popular option [1–3]. Additional techniques, apart from the engineering of the substrates, include the introduction of additives or surfactant into the liquid [4, 5] or in some special cases the introduction of intermediate layers between the liquid and solid substrates [6]. However, above mentioned methods, either solid or liquid properties are permanently altered and it is an arduous task to regain the original properties of the solids or the liquids. A technique named electrowetting (EW), which was introduced in 1875 by G. Lippman [7], alters the wetting behaviour of liquids and has a high reversibility with minimal or null changes to the substrate. Initially, this phenomenon was observed by G. Quincke in 1870, where the mercury-water interfacial tension continuously decreased over time [8]. Yet, Quincke failed to give a satisfactory explanation, and he proposed this might be attributed to the deposition of impurities brought by the air or by the liquid, which were impossible to avoid [8]. Later on, Gabriel Lippmann discovered that this effect could be eliminated by applying a voltage between mercury and aqueous electrolytes, which was seen

in the capacity to control the position of the mercury meniscus in a capillary [7]. Hence, Lippmann formulated a theory for electrocapillarity effects for modifying the interfacial properties of liquids. Thereby inducing an electric field, the wetting characteristics could be changed resulting in the alteration of wettability of the substrate in a controlled manner. The mathematical relationship (Eq.1.1) between the applied electric potential (U) and the apparent surface tension (σ) is expressed in Lippmann's equation [7, 9]:

$$\sigma = \sigma_{sl} - \frac{1}{2}cU^2 \quad (1.1)$$

Where σ_{sl} is the surface tension of the solid-liquid interface when no voltage is applied, and c is the capacitance per unit area of the solid-liquid interface. During the next decades, EW received considerable attention, where aqueous electrolytes were used as a liquid on metal substrates [10–14]. The key breakthrough was witnessed when the electrolysis at the metal-liquid interface was circumvented [15]. In the case of aqueous electrolytes, which are in direct contact with electrodes, the electrolytic decomposition in H^+ and OH^- , within the voltage range of hundreds of millivolts, is inevitable [16]. This phenomenon limits the applied voltage and thus the maximum reversible spreading, one can achieve. The combination of a metal electrode and an aqueous electrolyte also suffers from the lack of reversibility primarily due to high contact angle hysteresis caused due to rough metal surface [12, 14, 17]. Two fold challenge, electrolysis and surface roughness, was address partially in the 1990's when Berge et al. [15] proposed an ingenious way of introducing a thin insulating layer between the conductive liquid and the metallic

electrode. This innovative concept, named electrowetting-on-dielectric (EWOD), eliminates the electrolysis and expands the selection of electrode materials and liquids. In case of EWOD, the insulator layer acts as an ideal dielectric and blocks the electron transfer from the electrode to the electrolyte, and at the same time, it maintains the high electric field at the electrode-electrolyte interface by redistributing the charges at the interface. Also, it is noteworthy to mention that EWOD is independent of the polarization at the interface, i.e., any magnitude of polarity can be used for EWOD experiments [18, 19].

The contact angle of a sessile drop on a solid substrate ($\cos\theta_Y$) is primarily governed by the Young's equation [20]. Traditionally, Young's equation can be very easily interpreted as a force balance at TPCL and one can get the expression for $\cos\theta_Y$. Similar approach fails to derive the expression for contact angle in the case of electrowetting, hence the minimization of energy was considered and an expression for the deviation from θ_Y was obtained. Details of this derivation are presented in Appendix A-1. After accounting the role of the dielectric and corresponding change in the surface energies, the contact angle (CA) as a function of the applied voltage is described by the Young-Lippmann equation as [21]:

$$\cos\theta_{app} = \cos\theta_Y + \frac{\varepsilon_o\varepsilon_d}{2d\sigma_{lv}}U^2 \quad (1.2)$$

where θ_Y is the initial equilibrium contact angle or Young's contact angle, ε_o is the permittivity of free space, ε_d is the dielectric constant of an insulating layer with a thickness d , σ_{lv} is the interfacial tension of the liquid and the surrounding medium,

and U is the applied voltage. Equation 1.2 is based on a very important assumption, i.e., an equilibrium state of drop, in which the dynamics involved in EWOD due to varied voltages and frequencies are ignored. This can be based on the actuation of electric field and its characteristics, i.e., alternating or direct current actuation. The direct current (DC) voltage presents the advantage of simplicity, where the voltage remains unchanged in time and the three phase contact line does not oscillate [22–25]. On the contrary, if the alternating current (AC) voltage is used, the drop’s response depends on the relationship between the applied frequency f and the relaxation time of charges $\tau = \varepsilon_0 \varepsilon_r / k$, where ε_r and k are the permittivity and conductivity of the liquid, respectively [26]. Jones et al. [26] proposed to categorize the drop’s response into three regimes: if $\tau \ll 1/f$ the droplet behaves as a perfect conductor and only coulombic forces act at the three phase contact line; if $\tau \gg 1/f$ the droplets behaves as a perfect dielectric and only the dielectrophoretic forces act on the drop; and if $\tau \approx 1/f$ the drop behaves as a leaky dielectric and both forces act on the drop. For the case when the droplet behaves as a perfect conductor, which is a basic assumption of the Young-Lippmann’s equation, the response depends on the time average voltage ($U = U_{RMS}$) and Eq.1.2 can be used for AC voltages [15, 27, 28].

Although DC voltage is easier to analyze and does not need to consider an additional factor, i.e. applied frequency, AC voltage is recurrent in EWOD studies [29, 30]. AC EWOD is preferred in microfluidic applications due to its ability to induce internal flows mixing inside the droplets while the droplet oscillates [13, 30–32]. In addition, AC has presented three more advantages that clearly make it the

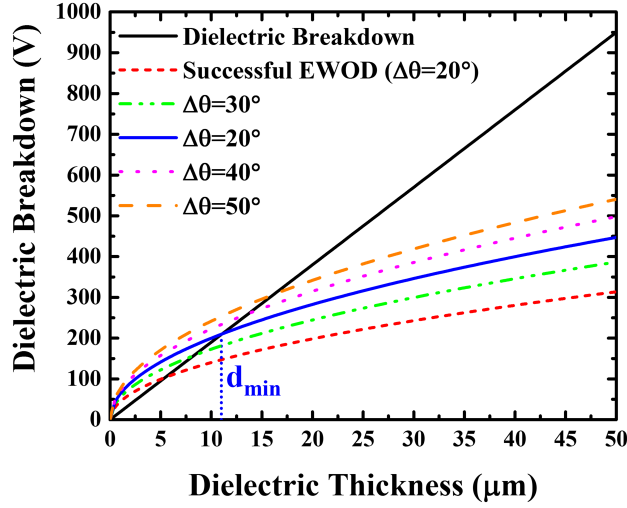


Figure 1.1: Dielectric breakdown of Electrowetting on dielectric. Successful EWOD and dielectric breakdown voltages versus the insulator thickness. The black line represents the insulator breakdown for PDMS ($E_{BD} = 19V/\mu m$ and $\epsilon_d = 2.8$) while the other lines represent the voltages required to obtain a desired reduction in the contact angle ($\Delta\theta$) from 115° of a water drop in air medium ($\sigma_w = 72.7mN/m$). The dashed blue line indicates the minimum insulator thickness ($d_{min} \approx 11\mu m$) to obtain a change in the contact angle of 20° .

best alternative for EWOD. First, the continuous motion of the charges at the three phase contact line induces oscillations in the base area of the drop that prevents the contact angle pinning, which leads to a reduction in the contact angle hysteresis [28, 33]. Second, as the polarity of the applied voltage is switching, the permanent ion adsorption at the liquid-solid interface is reduced [18, 19, 34, 35]. Third, and the most important aspect, is the delay of the contact angle saturation by effectively enhancing the maximum wetting envelope [36–39]. For both AC and DC voltages, the dielectric breakdown is one of the major limitations in EWOD. The dielectric breakdown occurs when the current flows in an electrical insulator because the voltage applied surpasses the breakdown voltage. Once the dielectric breakdown occurs, the insulator becomes electrically conductive and no longer behaves as a dielectric, which occurs at $U_{BD} = E_{BD}d$, where E_{BD} is the breakdown strength

of the dielectric material. The breakdown voltage for a given voltage is linearly dependent on the thickness of the material as shown in continuous line in Fig. 1.1. Nevertheless, in order to obtain a desired reduction in the contact angle of the drop due to electrowetting, the voltage required can be found as [40]:

$$U^2 = \frac{2\sigma_{lv}(\cos\theta_{app}(U) - \cos\theta_Y)}{\epsilon_o\epsilon_d}d \quad (1.3)$$

This equation is a rearrangement of Young-Lippmann's equation in which the applied voltage can be determined for a given system that can be further compared to the breakdown voltage, as demonstrated in Fig. 1.1. For a varied thickness and given $\Delta\theta$, i.e., maximum change in contact angle compared with the Young's contact angle, the corresponding voltage can be determined. The competition between the dielectric breakdown and the required voltage for EWOD is illustrated in Fig.1.1. The convergence of the two lines determines the minimum thickness required to successfully operate EWOD for a desired contact angle reduction. For the case of a PDMS layer, the breakdown strength is at $E_{BD} = 19V/\mu m$, and it has a dielectric constant of $\epsilon_d = 2.8$. In addition, for the case of a water drop in air medium, the surface tension is $\sigma_{lv} = 72.7mN/m$ with an initial contact close to 115° . In order to produce a change in the contact angle of approximately 20° , the minimum thickness required is theoretically $d_{min} \approx 11\mu m$.

Additionally, it has been observed that, after the voltage is significantly increased (but still under the dielectric breakdown) the denominated critical voltage is reached and the CA becomes independent from the applied voltage as seen in

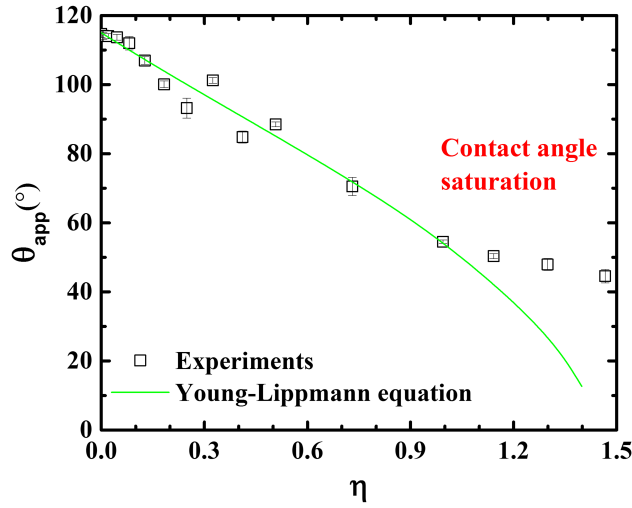


Figure 1.2: Contact angle saturation of Electrowetting on dielectric for a water drop in air medium. The contact angle becomes independent of the electrowetting number approximately after $\eta = 1$. A continuous AC voltage with $f = 100Hz$ was applied to a drop with $\sigma = 71.7mN/m$ on a dielectric with a thickness $d = 21\mu m$.

Fig.1.2. In other words, after a critical voltage is surpassed, the contact angle becomes independent of the applied voltage, which is referred to as the contact angle saturation [41]. Unanimous theory to explain the contact angle saturation has not been developed yet, but several academic groups have attributed this anomaly and suggested different hypothesis such as: air ionization close to the drop's edge, which suppresses the driving force of electrowetting [42]; the trapped charges in the dielectric layer that partially screen the applied electric field [18]; the surface energy of the solid-liquid interface approaches to zero and becomes unstable [10]; the assumptions of perfectly insulating dielectric or perfectly conducting liquid are violated, thus the net force acting on the contact line is reduced [43]; or even attributable to material deficiencies [44]. However, some attempts have been performed to correct Young-Lippmann's equation and accurately predict the observed contact angles beyond the critical voltage [45–47]. Interestingly, very few

researchers have devoted their attention to the transient dynamics or effect of different transient parameters involved in the electrowetting such as the frequency of the applied voltage or cycle of the applied voltage, etc.

In spite of these challenges, EWOD is widely used for numerous applications, but inadvertently without detailing the transient dynamics, and always below the CA saturation. EWOD has attracted the attention due to: its fast response (achieving contact angle changes at a range of 10-100ms with variations of several tens of degrees) [48, 49]; long-term reliability and stability [50]; reversible nature [18, 51]; and higher efficiency with low electricity and power consumption [16, 48]. Another aspect of EWOD-based devices is the exhibition of different phenomena without moving any mechanical components for its operation and the reduction of power usage [52]. Therefore, EWOD has raised a lot of attention recently for a range of applications including Lab-on-a-chip devices [19, 53–57], liquid lenses [22, 23, 29, 58, 59], displays [60, 61], reserve batteries [62, 63], communication technology [64], sustainable buildings [65], and microrobotics [66].

1.1 Overview of key applications

The reversibility and precise manipulation are key factors for allowing electrowetting to be the natural choice for a wide range of applications. The manipulation of small amounts of liquids (down to volumes of pico-liters) through micro-channels, for diagnostic or analysis purposes, is usually denoted as Lab-on-a-chip (LOC) [67, 68]. At the microscale, with such a small sample volume for analysis, surface forces becomes dominant, therefore, non-mechanical approaches are invented. The

manipulation of droplets with controlled maneuvering can be executed by dielectrophoresis [69], surface acoustic wave transport [70], and thermocapillary transport [71]. Electrowetting was introduced to microfluidic-based devices by Matsumoto et al. [13], where they replaced the use of piezoelectrically actuated micropumps by electrowetting for the manipulation of drops. It has been widely implemented for LOC devices [31, 55, 56] because it not only eliminates the requirement of mechanical connection/fittings, pumps and valves, but also gives a precise control over the transport. Further, electrowetting-based devices have been developed with interdigitated electrodes where individual electrodes act as guide for droplets, in which the drops can interact with other drops. This entire sequence is controlled externally and a desired path is the outcome of the activation sequence as seen in Fig.1.3. The liquid droplets are located between two parallel plates; the bottom electrode contains independently controlled electrodes, while the top electrode is a continuous and shared ground plate. The operational principle of liquid motion caused by electrowetting is to asymmetrically change the interfacial tension by applying a potential difference, and to induce a pressure difference inside the drop. The induced pressure gradient leads to an asymmetric deformation as well as the drop's motion [55]. As the drop is occupying more than one electrode, the side electrodes are activated to elongate the drop and the liquid moves from the high-pressure to the low-pressure region. Therefore, droplets can be manipulated without moving any mechanical part, more than one drop can be handled simultaneously, insignificant volumes of liquid are wasted, and automated programs can be implemented for the drop's control [72]. Electrowetting-based LOC operates following four fundamental fluidic's operations; generation, transporting, splitting, and merging of

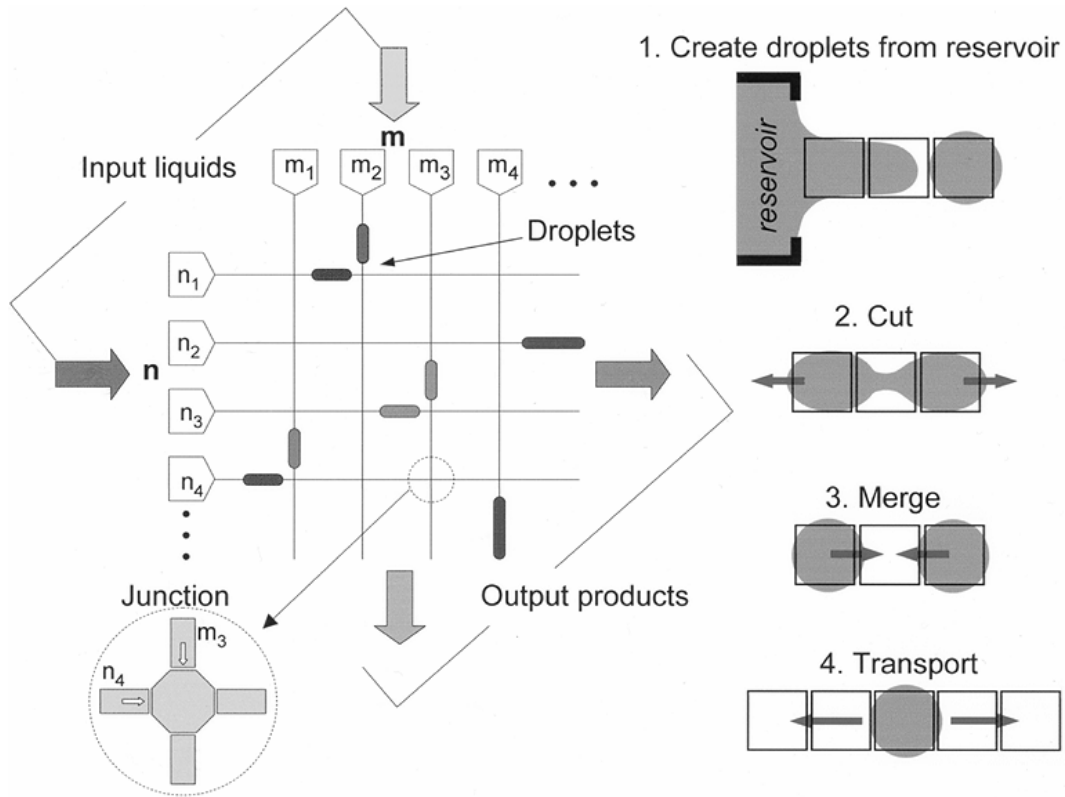


Figure 1.3: Digital microfluidic circuit based on electrowetting. A matrix of $m \times n$ different input liquids can be introduced. Also, the four fundamental droplet operations are represented; (1) Create droplets from reservoir; (2) Cut; (3) Merge; and (4) Transport (Adapted from Ref. [55] with permission of Journal of Microelectromechanical systems).

liquid droplets [55], as shown in Fig.1.3. In the microfluidic conduit on a series of electrode platforms, small droplets are taken from reservoirs, are transported along defined paths, and can be combined and mixed with other liquids to produce chemical reactions [54, 57]. Electrowetting has already been used to manipulate human physiological fluids, like blood, serum, plasma, urine, saliva, sweat and tears, demonstrating its promising future in biomedical applications [56].

The second broadest application field is related to adaptive optics. Many mechanical systems grant adjustable focus and magnification of the image, but the

device's size is compromised. In order to reduce the size of the optical instrument, the mechanical motion should be eliminated. Abundant solutions have been developed to design an operative tuneable micro-lens, but they have limited control on the change of the focal length [73–76]. A curved liquid-liquid interface can be used as a smooth lens, as the surface tension maintains a uniform curvature and restrains any irregularity at the interface. Following this order of ideas, if electrowetting is used to change the shape of the liquid-liquid interface, both the curvature and the focal length of the lens can be varied as a function of the applied voltage as shown in Fig.1.4. The cell typically consists of two immiscible liquids, an insulating liquid (usually oil), and a conducting water solution [22, 29]. The nature of a drop in a liquid medium guarantees the small contact angle hysteresis and the abolition of evaporation effects; thus, a continuously adjustable lens can be built. Also, as electrowetting exhibits a fast reaction, it allows the reduction in the operational time of the liquid lens. The optimized condition for reducing the response time of the lens is at the critically damped response, which is the fastest form to achieve the final shape without oscillations [23]. Hence, the viscosity of the oil and water solution should be considered carefully, as well as the comparison between the reaction time of the drop and the actuation time imposed by electrowetting.

The aim of this thesis is not to focus on the development or establishment of electrowetting in different domains with its applicability towards various applications. The prime objective is to identify the gap in the fundamental understanding of governing factors mainly the Young-Lippmann equation and further comment on the usefulness of such studies in real life application, primarily on the contact lens.

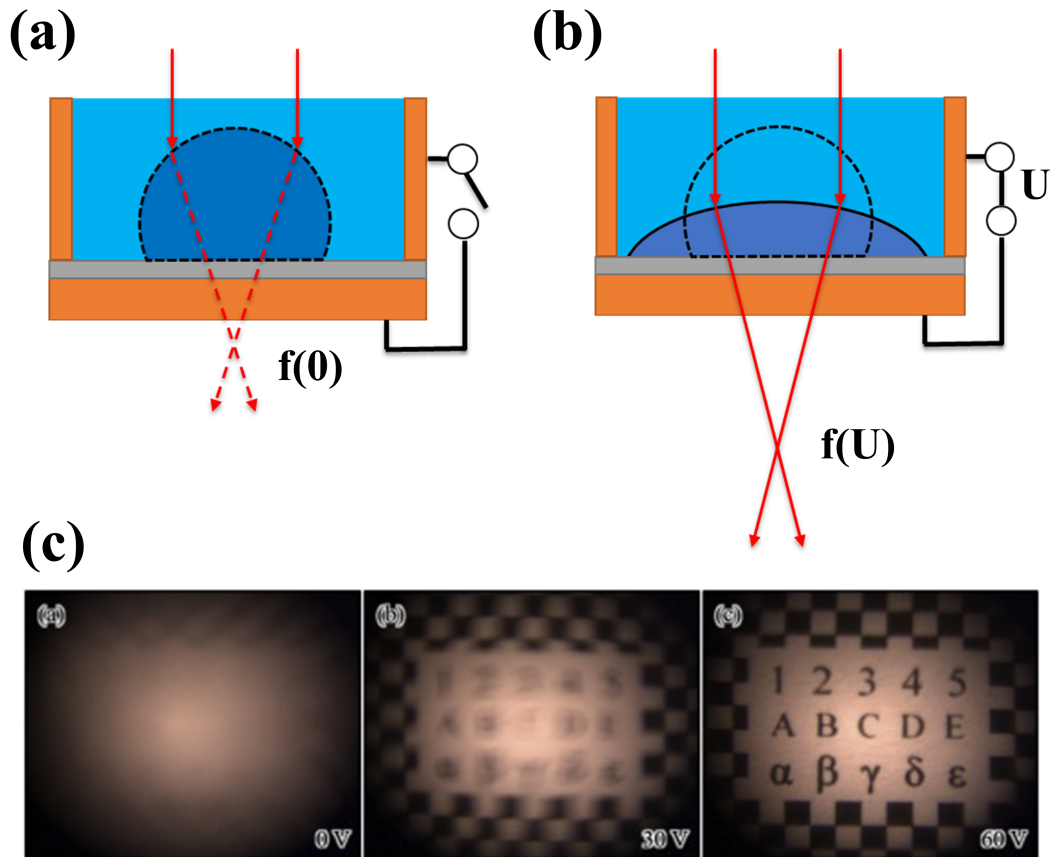


Figure 1.4: Liquid lens device based on Electrowetting on dielectric. (a) Schematic of a drop under equilibrium with no applied voltage acting as a lens, which converges the light rays into a fixed focal length. (b) Change in the focal length of the liquid lens by applying an electric field into the drop, which induces the drop's spreading and increases the drop's curvature. (c) Image focusing test of a liquid lens unit based operated by electrowetting. It is used a water-based conductive liquid and oil-based insulating liquid. The difference in the focal length can be seen for three different voltages (a) 0V, (b) 30V, and (c) 60V (Adapted from Ref. [77] with permission of Sensors and Actuators A: Physical).

1.2 Aim of the present work

Although Young-Lippmann's equation is widely recognized and mostly used to describe electrowetting, it has two very important limitations that very few researchers have studied. The first bounding limit of this equation is the contact angle saturation at high voltages, where the observed contact angle deviates from the theoretically predicted values and, as mentioned earlier, unified rationale for this behaviour has not been established. Therefore, it is accepted that the Young-Lippmann's formulation is only highly reliable for voltages below the threshold or before the critical voltage is reached [41]. The second defect of the Young-Lippmann's equation, which is borrowed from Young's equation, is the inability to describe the transient response of time, and therefore it is entirely unknown how the initial actuation of AC voltage alters the drop dynamics and equilibrium. Interestingly, based on previous works related to electrowetting, we noticed that minimal efforts had been devoted to understanding the initial reaction of the droplet in view of electrowetting. A thorough search of the relevant literature yielded that only DC voltage has brought special attention to the initial spreading of the drop due to electrowetting [25]. Consequently, the complete description of the drop's response caused by AC electrowetting is still missing, leading to a lack of information in the droplet dynamics immediately after the voltage is applied. The complete understanding of the time required for the drop to reach the new equilibrium position can be beneficial for the different applications where reducing the operational time or response time is essential [23].

The utilization of electrowetting inevitably generates the drop spreading, which is usually described as a function of the contact angle, the base radius, or the droplet's height [78–80]. Yet, the contact angle hysteresis and contact angle pinning spoil the drop's contact angle and base radius response [47, 81]. Thus, to circumvent this difficulty, which cannot be avoided, we focused on the height of the spreading droplets in our analysis. One of the aims of this research was to focus on the study of the droplet's dynamics based on the effect of essential actuation parameters such as voltage, frequency, drop's viscosity and medium's viscosity. It was observed that for experiments under air medium the drop experienced high oscillations on its height, which are a function of the applied wave, and the drop's thermophysical properties. In fact, the associated drop's shape response coincides with the inertial capillarity phenomenon [82], which inspired us to correlate the different studied parameters with the mass, spring, and dampener coefficients of the system.

In contrast, the response of a drop in a liquid medium completely differs from the case of air medium, where the droplet simply follows the applied wave and the oscillations completely vanish after the application of the potential difference. The reduction in some energy losses in the case of a liquid medium, as the contact angle hysteresis is almost negligible, allowed us to proposed and verified a theoretical model. This proposed model is able to predict the drop's transient response with respect to the AC actuation. The model was based on an overall energy balance approach that considered the most relevant energies as the kinetic and surface potential energies, as well as the work done by the drop the and medium dissipation

[83]. This model was tested to verify how the response of the drop will change according to the applied potential difference, the number of electrical waves, and the medium's viscosity.

And finally, with a better understanding of the early response of sessile droplets because of electrowetting, an experimental investigation of electrocoalescence was accomplished in the present thesis. Some studies have reported the presence of charges at the interface of the sessile drops, which create repulsion forces at the interface of the drops and prevent the drop coalescence [34, 84]. Thus, the drop's detachment from the electrodes is allowed, so the repulsion force at the interface of the drops weakens, and the drop coalescence can occur. The drop coalescence is characterized by the bridge that connects both drops, which grows fast with respect to time [85], where the initial contact angle of the drops dictates the bridge growth [86, 87] along with the viscosity of the drops [88–90]. In this context, electrowetting is used to study a wide variety of initial conditions for drop coalescence, as well as the effect of the applied voltage, separation distance and the role of the viscous forces in the process. In the upcoming section, the arrangement of the thesis with these three major studies is presented.

1.3 Thesis Outline

The primary purpose of this thesis is to describe and analyze the transient dynamics of the response of sessile droplets to the application of a single or a series of AC waves. Therefore, in this section, we attempt to delineate the thesis structure and the subjects covered in the succeeding chapters.

In Chapter 2, “initial drop spreading on a solid substrate due to electrowetting”, we developed a theoretical model for the description of a drop’s response to electrowetting in a liquid medium. A single or a sequence of AC waves, with different amplitudes and frequencies, were applied to a liquid droplet in an oil medium with different viscosities. In our proposed model, we considered the interaction of the kinematic energy, the surface energy, and the work due to the dissipation of the drop in an overall energy balance. The governing nondimensional parameters were the viscosity ratio (between the liquid drop and the oil mediums), the Electrowetting, the Roshko, and the Ohnesorge numbers. Experimental results captured by high speed imaging were compared with the theoretical results from the overall energy balance. A clear shift from in-phase to out-phase drop’s response and its dependency on the applied wave characteristics (amplitude, frequency) and the medium viscosity was established. We believe, our study in electrowetting can offer a better understanding of the transient dynamics of droplet spreading in a liquid medium along with the role of AC waves. The detailed understanding of this allowed us to comment on the attainment of steady state drop configuration after the decaying oscillatory behaviour. However, we noticed that the first half of the actuation cycle had the biggest impact on the drop response and a different time scale must be investigated to predict accurately the time required to reach the maximum spreading.

In Chapter 3, “sessile drop response to a single wave of electrokinetic excitation”, we provide an extensive experimental study regarding the drop’s response caused by electrowetting. In this work, an experimental mechanism was designed

to create a controlled perturbation or disturbances in a sessile droplet by applying an external electric field which induces the corresponding changes in the drop's shape. Single sine waves of AC voltage with different frequencies and voltages were applied, and the drop dynamics were investigated to scrutinize the drop's response while attaining its maximum deformation configuration. High-speed imaging of a sessile drop disclosed that the drop's response varies significantly according to the single wave characteristic (amplitude and frequency) and the properties of the drop (density, surface tension, and viscosity). The drop's shape response, after the actuation of the external field, resembles the inertial capillarity phenomenon; therefore the role of the drop and the medium viscosity is studied in detail. Experimental observations permitted us to propose a model, for the variations of the sessile drop's height, based on a mass-spring-damper system. The damping ratio of the system was observed to be a function of the Ohnesorge number, i.e., viscous, surface tension, and inertial forces in the system. In addition, we proposed a modified time scale that considers the applied frequency, as well as the applied voltage of the wave and the thermophysical properties of the liquids, to predict the time required for the drop to reach the maximum spreading.

After understanding the time required to reach the maximum spreading, we continued this work by introducing electrowetting at the interface of two liquids by observing the sessile droplet coalescence. In Chapter 4, "induced coalescence of sessile droplets by a single wave of electrowetting", the results obtained from previous chapters are used to predict the drop's motion and induce the coalescence of two sessile drops by electrowetting. Repulsion forces between the drops were

observed, which constraint the coalescence. Therefore, we proposed a new technique to study the drop coalescence under different initial conditions by applying a single electrowetting wave and generating drops detachment from the top electrode. The detachment of the drop guaranteed that the drops coalesce under all the different conditions of the applied electrical field, as long as the separation distance was under reasonable limits. The electrocoalescence study was focused on the growth of the bridge formed by the union of the drops, and how the different conditions influenced the initial bridge height and its growth.

Finally, the last chapter (Chapter 5) draws the conclusions from the analyses of the experimental results and the mathematical model along with a brief discussion about the future applications of this study. The results obtained in the previous chapters lead to a better understanding of the drop's response that can be applied to the droplet coalescence or the design of a micro-lens as an extension of this work. However, these two applications of electrowetting have been kept as future work and only the initial steps have been completed.

Chapter 2

Drop Spreading on a Solid Substrate due to Electrowetting¹

2.1 Introduction

Electrowetting is the induced effect of spreading of a liquid droplet on a conductor surface by applying an electrical potential [41]. In 1875, this phenomenon was discovered by Gabriel Lippmann [7], who observed that by applying a voltage difference between an aqueous solution and mercury, the liquid-liquid interface on a capillary could be controlled. In the case of electrowetting, an electrical double layer is spontaneously formed at the solid-liquid interface, which is made up of ions and counter ions at the solid-liquid interface, and is inherently charged or uncharged. The magnitude of the applied potential difference is tuned to control the charge distribution that reflects in a slip at the contact line. Thus, the desired contact angle can be obtained by applying the required voltage. For a solid-liquid interface, the maximum charge distribution is limited by the electrolysis. This is termed as the threshold voltage beyond which the disassociation of liquid molecules occurs with a marginal slip at the three phase contact line. Berge [15], in 1993, discovered that by

¹A version of this chapter will be submitted to the Journal of Fluid Mechanics as: Juan S. Marin Quintero, Hafijur Rahman, and Prashant R. Waghmare, “Drop Spreading on a Solid Substrate due to Electrowetting”

inserting a thin insulating layer (dielectric) between the liquid and underneath solid, the electrolysis could be eliminated and a higher contact angle reduction could be achieved. The introduction of the dielectric layer is known as electrowetting on dielectric (EWOD), and the layer works as an ideal dielectric, which enhances significantly the breakdown limit and simultaneously maintains the high electric field at the interface redistributing the charge at the surface [15].

Electrowetting is commonly characterized by quantifying the change in equilibrium contact angle (θ_0). The new equilibrium contact angle (θ_e), due to the applied voltage, can be deduced by energy minimization, as presented in Eq. 2.1 and a relationship between $\cos\theta_0$, commonly known as Young-Lippman's equation, and the electrowetting parameters [15, 21]. The details of this process can be found in Appendix A-1.

$$\cos\theta_e = \cos\theta_0 + \frac{\epsilon_0\epsilon_d U^2}{2d\sigma} = \cos\theta_0 + \eta \quad (2.1)$$

Here, ϵ_0 is the vacuum permittivity constant, ϵ_d is the dielectric constant of the insulator, d is the thickness of the dielectric layer, σ is the surface tension of the liquid-vapor interface, U is the applied voltage, and η is the electrowetting number which primarily governs the electrowetting phenomenon. Apart from material properties and interfacial tension, the applied voltage is only controlling parameters to tune the wettability. This applied voltage can be either direct (DC) or alternating (AC) current. Initially, the natural choice was DC for electrowetting [91, 92] but Magali et al. [93] performed electrowetting with AC, considering the voltage

as the root mean square voltage ($U_o = U/\sqrt{2}$) in Eq. 2.1. It was evident that the AC performed significantly better than DC because of: the reduction in the contact angle hysteresis due to the continuous motion of the three phase contact line [28, 33]; the reduction of ion adsorption at the liquid-solid interface [19]; and the delay of the contact angle saturation [37–39]. In addition, AC EWOD stood out because the possibility of effective internal flow mixing produced by droplet oscillations [30, 32, 94, 95], which is commonly required for microfluidics applications [13, 31, 55, 56]. Equation 2.1 is valid for both scenarios, provided the applied voltage is the root-mean-square voltage. This Young-Lippmann equation, predicts the change of the contact angle with respect to the applied voltage after attaining the equilibrium, but it fails to comment on the dynamic evolution or transience involved in the applied voltage, in particularly for AC scenario. A few studies [26, 30, 94, 96–98] have researched the role of applied frequency and its implication on the equilibrium contact angle, but the transience involved in this process is always missing. Also, the role of the actuation cycles is studied for a specific application [95], but prime attention was towards the internal flow of the drop and the implications towards the mixing. Hence, it is not fully understood how the drop attains the steady state and how the system parameters, primarily the medium viscosity, play a role on it. Here, we analyzed the role of electrowetting parameters, applied frequency, and the medium viscosity on the equilibrium contact angle. A detailed theoretical model is proposed to quantify the role of each energy component involved in this process and finally, the predicted drop shape evolution was compared with the experimental results. It is desirable to generate relatively simple models that can describe and predict the transient evolution of the drop spreading

[46, 47, 83, 99]. The complete understanding of the drop's response can increase the efficiency of EWOD-based devices by reducing operation times and having the entire description of the drop's evolution for a given actuation. Thus, the objective of the present study was to investigate and develop a theoretical approach that considers the effect of electrowetting and the fluids' properties, which can predict the drop's response and the transient dynamics of the drop spreading. An Overall Energy Balance (OEB) approach is proposed to study the sessile drop height in a varied viscous medium. This model can describe the transient evolution of the drop motion, and can predict the shift from in-phase to out-phase drop response from the applied waves.

2.2 Formulation of the mathematical model and solution

A liquid drop, when in contact with a smooth and homogeneous solid surface, wets the substrate and attains an equilibrium position, which is a function of interfacial energies. If the sessile drop is sufficiently small, the gravity has negligible effect compared to the capillarity. Therefore, it is safe to assume that the sessile drop shape resembles a spherical cap as shown in Fig. 2.1. By simple geometric exercise, the volume of the spherical cap can be deduced as presented in Eq. 2.2, which is a function of the radius of the sphere, r , or the height of the sessile drop, h , and the contact angle, θ , as:

$$V = \frac{\pi h^3}{3} \frac{2 + \cos\theta}{1 - \cos\theta} \quad (2.2)$$

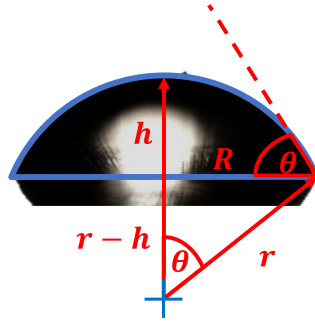


Figure 2.1: Schematic of a drop placed on a solid substrate that follows the spherical cap assumption. r represents the radius of the sphere, h is the height of the cap, R is the radius of the base of the cap, and θ is the contact angle of the drop.

For a constant drop volume, after ignoring the evaporation, the relationship between the transient variation in the contact angle and the height can be established as follows:

$$\frac{d\theta}{dt} = \left(\frac{(2 + \cos\theta)(1 - \cos\theta)}{h \sin\theta} \right) \frac{dh}{dt} \quad (2.3)$$

Similarly, one can get the relationship between the drop radius and height as presented in Eq. 2.4. It is often seen that either the base radius of the drop or the contact angle are used to describe the behaviour of the drop under the influence of different actuation mechanisms [100–102]. However, if the drop is submitted to continuous oscillatory disturbances, the contact angle hysteresis and pinning at three phase contact line influence the spreading dynamics and a corresponding erratic behaviour in the base radius or contact angle can be witnessed. This phenomenon becomes prominent in the case of air medium [47, 81]. Thus, to avoid any ambiguity and decipher the observed phenomena from these unavoidable circumstance, the height of the drop is considered as a variable for the analysis [103]. Therefore, along this

study, for theoretical as well as experimental exercise, the analysis is presented in terms of drop height:

$$\frac{dR}{dt} = \frac{d}{dt} \left(h \frac{\sin\theta}{1 - \cos\theta} \right) = -\frac{1}{\sin\theta} \frac{dh}{dt} \quad (2.4)$$

To theoretically determine the implication of induced drop deformation, due to applied electric actuation by means of electrowetting, the overall energy balanced (OEB) approached is considered. As performed for the prediction of advancing contact angle, the variation of drop's height can also be predicted with different energies involved in this process, namely kinetic, surface, and viscous dissipation due to drop and surrounding medium. Considering the sessile drop as the control volume, the applied electric energy (E_{in}) is utilized to move the contact line, i.e., the creation or destruction of the interfaces at a certain velocity (U). For this system, the energy balance can be written as:

$$\frac{dE_{in}}{dt} = \frac{d}{dt} (E_k + E_s) + \frac{d}{dt} (W_d + W_m) \quad (2.5)$$

Here, E_{in} is the energy added to the system, E_k and E_s are the kinetic and the surface energies of the drop. An additional work must be done to overcome the inherent resistance caused by the viscosity of the drop (W_d) and medium viscosity (W_m). For an isothermal system, an internal energy change can be ignored [83]. In the following section, the expression for all necessary energies that govern the energy balance are studied individually.

2.2.1 Kinetic energy, E_k

For an incompressible flow, the kinetic energy can be simplified as $E_k = \frac{mU^2}{2}$, where m is the mass of the drop and U is the bulk velocity of the internal flow in the droplet. It is to be noted that the effect of compressibility is limited ($\sim 0.5GPa^{-1}$) for water [104] and it can be ignored if the experiments are performed at atmospheric pressure [105]. Also, it is assumed that the mass of the drop is constant through the experiments, hence there is no mass transfer with the surrounding fluid. One can debate on the exact representation of U , which can be approximated to the velocity of the centre of mass of the drop (z) [99, 106]. Hence, the change in the kinetic energy with the location of centre of mass at height z from the drop base can be written as:

$$\frac{dE_k}{dt} = \frac{d}{dt} \left(\frac{mU^2}{2} \right) = mU \frac{dU}{dt} = m \frac{dz}{dt} \frac{d^2z}{dt^2} \quad (2.6)$$

After establishing the relationship between the drop's height and the centre of mass, the total rate of change of the kinetic energy of the drop can be found as:

$$\frac{dE_k}{dt} = m \frac{1}{2 + \cos\theta} \left(\frac{dh}{dt} \right) \left(\frac{1}{2 + \cos\theta} \frac{d^2h}{dt^2} + \frac{1 - \cos\theta}{h(2 + \cos\theta)} \left(\frac{dh}{dt} \right)^2 \right) \quad (2.7)$$

2.2.2 Surface potential energy, E_s

The total surface energy of the system is an amalgamation of surface energies of liquid-solid, liquid-fluid, and solid-fluid interfaces. Here, the liquid corresponds to the drop's phase, the solid is the underneath dielectric layer and the surrounding

medium is a representation of the fluid. For this system, the surface energy can be expressed as:

$$E_s = \sigma_{SD}A_{SD} + \sigma_{DM}A_{DM} - \sigma_{SM}A_{SM}. \quad (2.8)$$

In Eq. 2.8 σ and A are the respective surface energy and area whereas the subscripts denote the interface combinations, i.e., the substrate-drop (SD), the drop-medium (DM), and the substrate-medium (SM). At the three-phase contact line, it can be noticed that the substrate-drop and substrate-medium areas are equal ($A_{SD} = A_{SM}$). Thus, the rate of change of the surface energy is:

$$\frac{dE_s}{dt} = (\sigma_{SD} - \sigma_{SM})\frac{dA_{SD}}{dt} + \sigma_{DM}\frac{dA_{DM}}{dt} \quad (2.9)$$

By implementing the Young's equation with an equilibrium contact angle of the drop θ_e , the rate of change of the surface energy can be estimated as:

$$\frac{dE_s}{dt} = \frac{2\pi h\sigma}{1 - \cos\theta} \left(\cos\theta_e - \cos\theta \right) \frac{dh}{dt} \quad (2.10)$$

The only surface tension (σ) that appears in the equation is the drop-medium interfacial surface tension (σ_{DM}). The Young's equation fails to comment on the change in contact angle due to the application of the electric field, which was later modified by Lippmann as presented in Eq.2.1. Hence, the equilibrium contact angle θ_e was replaced by the instantaneous equilibrium contact angle θ_{ie} , which is

the manifestation of the applied actuation. To account the role of the applied frequency in the contact angle, the revised Eq.2.1 can be considered, where $U(t) = U_o \sin(2\pi ft)$ and f is the applied frequency [27, 28].

$$\cos\theta_{ie} = \cos\theta_0 + \frac{\epsilon_0 \epsilon_d U_o^2}{2d\sigma} \sin^2(2\pi ft) \quad (2.11)$$

2.2.3 Viscous dissipation within the drop (W_d) and at the drop-medium interface (W_m)

It is well accepted that the viscous dissipation during the drop's spreading can be deduced by considering the lubrication approximation [107]. As De Gennes proposed [108], the equivalent viscous force per unit length of the three-phase line can be estimated as:

$$F_v(t) = \frac{3\mu_d}{\theta} \ln(\epsilon^{-1}) \frac{dR}{dt} \quad (2.12)$$

where μ_d is the drop viscosity and ϵ is the ratio of the microscopic to macroscopic cut-off length. The logarithm ratio of the microscopic to macroscopic cut-off length, $\ln(\epsilon^{-1})$, was considered to be ten [109], as proposed in the literature. Bearing in mind the viscous force and the velocity ($\frac{dR}{dt}$) along the three phase contact line, the energy penalty due to drop viscosity can be found as:

$$\frac{dW_v}{dt} = \frac{6\pi\mu_d h}{\theta} \ln(\epsilon^{-1}) \frac{1}{\sin\theta(1 - \cos\theta)} \left(\frac{dh}{dt}\right)^2 \quad (2.13)$$

In the case of drop's deformation with a constant volume, due to the applied actuation, the fluctuation of the drop-medium interface (A_{DM}) can be observed. In most previous works, the increased drop volume scenario in an air medium [83] preclude the fluctuation and the resistance from the medium. The nature of volume increment is always continuous in nature, hence, the oscillatory motion was not noticed, whereas the viscous dissipation from the medium was ignored due to significantly higher drop viscosity compared to the air. Here, we attempt to account the role of medium viscosity since we have a medium with a viscosity comparable or higher than the drop's viscosity. The net rate of work due to the dissipation at the drop-medium interface can be calculated as $\frac{dw_m}{dt} = -\tau v dA$, where τ is the shear stress acting normal to the surface area dA_{DF} , considering the drop spreading at a velocity $v = 2\frac{dR}{dt}$. The shear stress at the drop's boundary is assumed to be $\tau = \mu_m \frac{\partial u_r}{\partial r} \Big|_{r=R}$, where μ_m is the medium viscosity, and u_r is the velocity at which the medium is getting displaced [110]. If a mass conservation analysis is performed at the boundary of the drop, the displacement velocity of the medium can be found to be $u_r = -\frac{2}{R} \frac{dR}{dt}$, and the net rate of work due to the dissipation at the drop-medium interface can be calculated as:

$$\frac{dW_m}{dt} = \frac{8\pi\mu_m h}{\sin^3\theta} \left(\frac{dh}{dt}\right)^2 \quad (2.14)$$

2.2.4 Governing equation for the drop's height variation

Combining equations from 2.7 to 2.14, the variations in the drop's height due to oscillatory actuation of the drop in a another liquid medium is:

$$\begin{aligned}
& \frac{m}{(2 + \cos\theta)^2} \frac{d^2h}{dt^2} + \frac{m(1 - \cos\theta)}{h(2 + \cos\theta)^2} \left(\frac{dh}{dt} \right)^2 \\
& + \left(\frac{6\pi\mu_d h}{\theta} \ln(\epsilon^{-1}) \frac{1}{\sin\theta(1 - \cos\theta)} + \frac{8\pi\mu_m h}{\sin^3\theta} \right) \left(\frac{dh}{dt} \right) \\
& + \frac{2\pi h\sigma}{1 - \cos\theta} [\cos\theta_{ie} - \cos\theta] = 0 \tag{2.15}
\end{aligned}$$

Furthermore, the mass of the drop is contemplated as $m = \Delta\rho V$, where V is the volume of the spherical cap, and $\Delta\rho = \rho_{water} - \rho_{oil}$ is the density difference between water and oil. To extract the key parameters from the governing equation, the governing equation was nondimensionalized as presented in Eq. 2.15. It is to be noted that the instantaneous contact angle and drop's height are two dependent parameters in this non-linear second order ordinary differential equation. With this approach, we have obtained a set of nondimensional numbers for which the characteristic length and time scale were chosen as drop's initial height (h_0) and the capillary time scale (τ_c), respectively where $\tau_c = (\Delta\rho h_0^3/\sigma)^{1/2}$.

$$\begin{aligned}
& \frac{h^{*2}}{3(1 - \cos\theta)(2 + \cos\theta)} \frac{d^2h^*}{dt^{*2}} + \frac{h^*}{3(2 + \cos\theta)} \left(\frac{dh^*}{dt^*} \right)^2 \\
& + \left(\frac{6\ln(\epsilon^{-1})}{\theta\sin\theta(1 - \cos\theta)} + \frac{8}{\sin^3\theta}\mu_r \right) Oh \left(\frac{dh^*}{dt^*} \right) \\
& + \frac{2(\cos\theta_{ie} - \cos\theta)}{1 - \cos\theta} = 0. \tag{2.16}
\end{aligned}$$

Here the μ_r is the ratio of the medium to the drop's viscosity and $Oh = \mu_d/(\Delta\rho\sigma h_0)^{1/2}$ is the well-known Ohnesorge number. In this nondimensionalization process, the equilibrium contact angle from Eq.2.11 gets appropriately changed to $\cos\theta_{ie} = \cos\theta_Y + \eta \sin^2(2\pi Ro Oh t^*)$, where $Ro = fh_0^2\Delta\rho/\mu_d$ is the Roshko number. In the present analysis, the solution of this second order differential equation was obtained

with a fourth order Runge-Kutta method with $h^* = 1$ and $dh^*/dt^* \approx 0$ as initial conditions. The proposed theoretical model is validated with the experimental results for a range of μ_r (10-1000), η (0.29 to 0.89), and Ro (0.44 to 44.49). The variation in the Oh for the considered parameters is marginal from $\approx 8.9 \times 10^{-3}$ to 9.7×10^{-3} , hence we have not considered this in our parametric analysis. In the upcoming section, experimental details are reviewed before the discussion of the comparison between the theoretical model and the experimental evidence.

2.3 Experimental study of drop's perturbation

The experiments were conducted by depositing $3\mu L$ drops of aqueous solutions (DI water and $0.1M$ sodium chloride) by means of a goniometer (DSA30, KRÜSS Scientific Instruments Inc.). A disposable syringe (NORM-JECT 1mL, Henke-Sass Wolf GmbH) was used to generate the drops inside a distortion-free cuvette (SC02, KRÜSS Scientific Instruments Inc.), which was prefilled with silicon oil (Paragon Scientific Ltd) with different viscosities, as shown in Table 2.1. The drops were deposited on a copper substrate, which was coated with a thin layer of Polydimethylsiloxane (PDMS), acting as electrode and dielectric. The dielectric layer was placed on the electrode by spin coating (WS-650Mz-23NPPB, Laurell Technologies) and the thickness of the dielectric layer was controlled by optimizing the rotational speed and the duration of the spinning process. The resulting dielectric layer thickness was approximately $21\mu m$ with a dielectric constant of $\varepsilon_d = 2.8$. The actuation by means of electrical signal was triggered by a waveform generator (294 100MS/s, FLUKE), which was further augmented by an amplifier (BOP 500, KEPCO) to obtain the desired output. The contact angle saturation [18] was

Table 2.1: Properties of water and liquid mediums. Viscosity μ , density ρ , and interfacial tension σ of different liquids at room temperature

Liquid	$\mu(mPas)$	$\rho(kg/m^3)$	$\sigma(mN/m)$
Water	0.91	997.1	71.7
D10	10.32	846.2	40.6
N35	59.19	853.6	40.6
S60	100.60	857.0	40.4
D500	541.40	869.9	40.5

the dictating factor to limit the maximum actuation signal in terms of maximum voltage. Finally, a copper wire, with a diameter of $60\mu m$, was used as positive electrode, and it was situated at centre of the droplet but with a separation distance equal to the initial radius of the drop from the bottom electrode.

The drop's perturbation and the associated changes in the shape of the drop were observed with a high-speed camera (Phantom V711, Vision Research Inc.) with a frame rate of 3,000 frames per second. An extended macro lens was attached to the high-speed camera to attain a spatial resolution of $\sim 5\mu m/pixel$ with a magnification factor close to four. A high intensity back light source (High Power LED Illumination, KRÜSS Scientific Instruments Inc.) was used as a back light illumination source. The camera exposure time, white intensity, focus, and colour balance were optimized to obtain the sharp drop-medium interface. The captured videos were calibrated and post-processed with an image analysis software (Image-Pro Premier 9.2, Media Cybernetics, Inc.) for the quantification of instantaneous drop's height. The drop-medium interface was identified by using an edge detector function in the image analysis software, so the height of the droplet could be measured.

2.4 Results and discussions

The dynamic response of the drop due to the electrical perturbation is compared with the solution of the overall energy balance equation, i.e., Eq. 2.16. Apart from the response to various operating conditions or to varied range of nondimensional numbers, the number of actuation waves is also studied for the sake of completeness of the analysis. The drops in all the different mediums attained an equilibrium, or initial height of $h_0 = 1.70 \pm 0.03mm$ with an associated contact angle $\theta_0 = 157.6 \pm 5.7^\circ$. However, the initial height and initial contact angle for the numerical study was selected as $h_0 = 1.70mm$ and $\theta_0 = 153.5^\circ$, respectively. In the following section, the theoretical predictions are represented by solid lines and only symbols are experimental observations.

The governing equation can be solved for the drop's height or the drop-medium interface velocity as shown in Fig. 2.2(a). This equation is a combination of different energy sources that can easily be quantified separately as depicted in 2.2(b). An analysis of the relative magnitude of the different energies considered provides a better understating on the drop's oscillations associated with the applied force. Figure 2.2(a) presents the height and the change in the height of the drop vs the time for the case of nondimensional parameters of $Ro = 0.22$, $Oh = 0.0093$, $\eta = 0.89$, and $\mu_r = 110$. The height's velocity has a zero magnitude at three times, i.e. at the initial position, and approximately when the voltage returns to a zero value in two occasions. Also, the velocity asymptotically attains a zero velocity as the drop

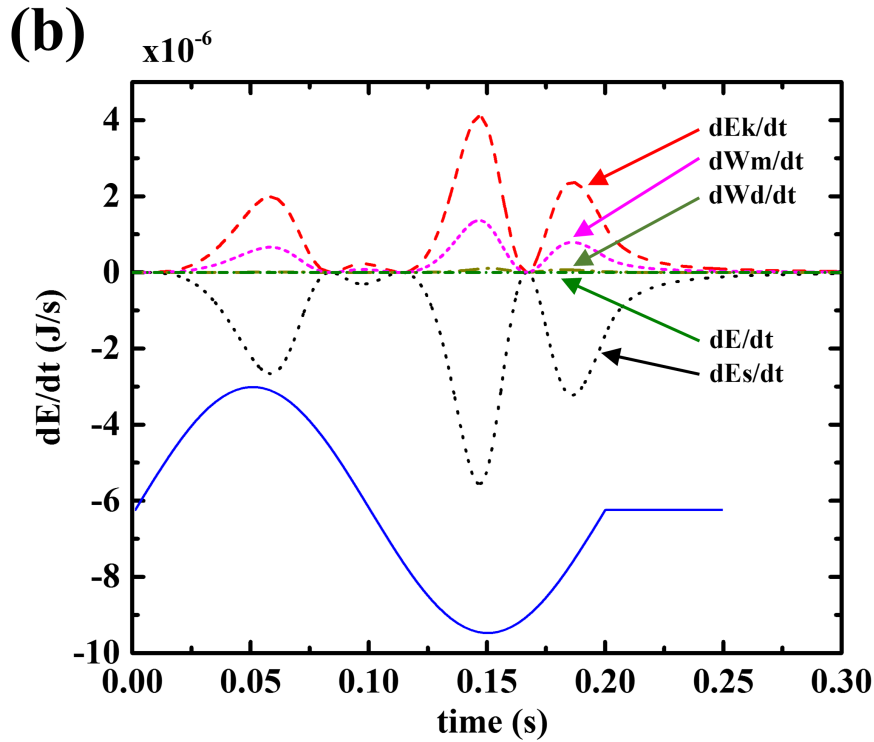
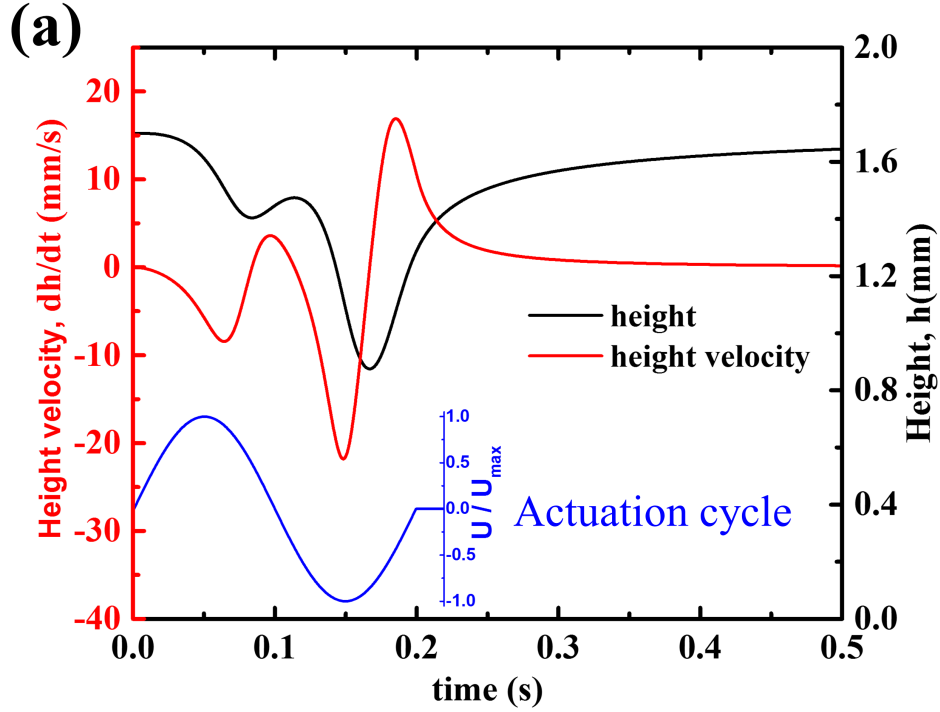


Figure 2.2: Theoretical results for a water drop ($\mu_d = 0.91mPas$) in an oil medium ($\mu_m = 100.60mPas$) submitted to a single sine wave of $U_{AC} = 350V$ at a frequency $f = 5Hz$, which corresponds to the nondimensional numbers of $Ro = 0.22$, $Oh = 0.0093$, $\eta = 0.89$ and $\mu_r = 110$. (a) Height and the rate of change of height with respect to time and (b) Comparison of all the different energies considered in the theoretical model.

returns to the initial position. At this point, all the energies from Eq.2.15 return to a zero value as shown in Fig.2.2(b). Also, it can be seen how the surface energy is transmitting the energy to the drop as in the form of velocity (kinetic energy), and to the surrounding as viscous dissipation (work due to drop and medium dissipation). The reason of the negative nature in the change of the surface energy can be understood from how the drop is attempting to reach the instantaneous equilibrium contact angle, and the difference between the cosines of the equilibrium and the actual contact angles, which is always negative or zero. The kinetic energy for almost the entire process was three times bigger than the work due to dissipation, and so the kinetic energy represented approximately 75% of the dielectric energy. It is worthwhile to mention that the negligible work due to the drop's viscous dissipation remained approximately 0.2% of the dielectric energy, which is consistent with the viscosity ratio for this particular case.

The maximum energy delivered to the system is nearly at $t = 0.15s$, which corresponds to the 75% of the period of the wave. At this point, the kinetic and the work due to medium dissipation reach their maximum value, while the surface potential energy reaches its minimum. This behaviour aligns with the application of the external force perturbation, where there are two moments when the voltage acquires the maximum amplitude, i.e. at 25% ($t = 0.05s$) and at 75% ($t = 0.15s$) of the applied period. At these two points, the instantaneous equilibrium contact angle from Eq.2.11 is equal to the apparent contact angle from Young-Lippman's (Eq.2.1), and so the difference between the equilibrium contact angle and the actual contact angle is the highest. However, when the electrical wave is at the 0.25% of its period,

the drop is still in an intermediate spreading point where the height velocity is not maximum, the minimum height has not been reached yet, and the substrate/droplet area (A_{SD}) has not reached its maximum value. Therefore, the energy peaks when the voltage is maximum are not identical, and the first peak is never greater than the second peak. The asymmetric spreading of the drop between the first half and second half of the electrical wave is detailed in the up coming sections. Following this order of ideas, a better understanding of the different nondimensional parameters is required to completely understand the drop's response and the oscillations linked with the application of a single or a sequence of electrical sinusoidal waves.

2.4.1 Effect of electrowetting number

The electrowetting number represents the ratio of the electrostatic energy to the surface energy, and it is the main governing parameter for a sessile droplet perturbed by an electric field. Literature already reported that by increasing the electrowetting number the apparent contact angle is further reduced [41], which leads to a lower instantaneous equilibrium contact angle that dictates the solution of Eq.2.16. In the case of electrowetting-induced spreading, a similar behaviour is presented in Fig.2.3. Figure 2.3 illustrates the change in the nondimensional height with respect to the nondimensional time multiplied by the Ohnesorge number (Oh) and Roshko number (Ro). The multiplication of the nondimensional time by the Ohnesorge and the Roshko numbers facilitates the analysis and comparison of the drop's dynamic response, which translates the time into the number of electrical cycles applied. For fixed values of Oh , Ro , and μ_r , the traditional outcome is observed,

i.e., a higher height diminution with the electrowetting number η . The voltage's range, and therefore the electrowetting number's range, was selected based on the dielectric breakdown of the insulator layer (the PDMS layer) that is a function of the dielectric thickness depicted as $E_{breakdown} = 19V\mu m^{-1}$. Thus, the maximum possible potential is approximately $400V$ before the occurrence of the electrolytic process. Yet, the maximum applied voltage was selected as $350V$ ($\eta = 0.89$) to avoid electrolysis and the saturation of the contact angle [18, 42]. The lower limit, $200V$ ($\eta = 0.29$), was chosen to observe a change in the drop's shape due to electrowetting. The height reduction for waves below this threshold voltage was observed to be less than 5%, as seen in Fig.2.3, resulting inconvenient for capturing the drop's response with the high-speed camera, and impractical to compare with the mathematical model.

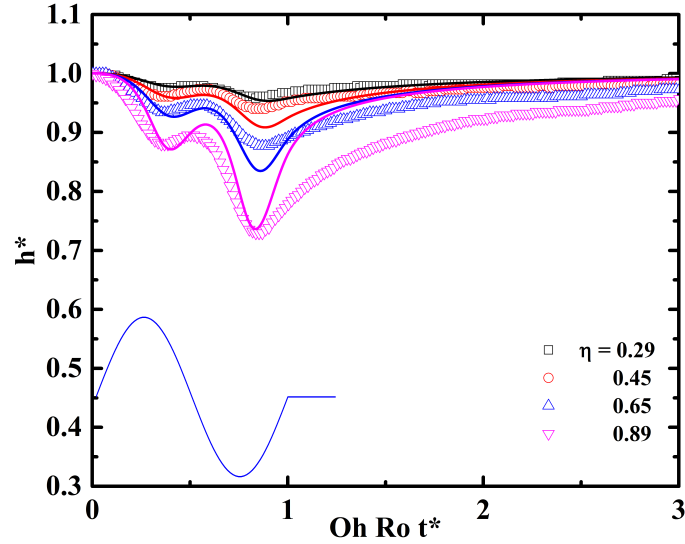


Figure 2.3: Transient variation of the droplet height for different electrowetting numbers. The additional terms are fixed to $Oh = 0.009$, $Ro = 4.45$, and $\mu_r = 110.55$. The experimental results are represented by symbols and the results obtained from the proposed model are represented by the solid lines.

For waves that generate a significant change in the drop's height, it can be seen how the drop does not symmetrically stretch following the applied sine wave, being more evident as the electrowetting number increases. Due to the additional resistance from the surrounding medium, the drop deviates from attaining the forced equilibrium contact angle, which leads to the dissipation of energy and to the delay in the spreading. This can be further seen as how the drop in the first quarter of the cycle spreads to an intermediate position, which does not correspond to the height calculated from the Young-Lippmann's equation (Eq.2.1). After the first quarter of the cycle has ended, when the voltage is starting to decrease, the drop momentarily continues to spread due to inertia, until it reaches a local minimum. As the voltage significantly reduces in magnitude, and the inertia vanishes in the second quarter of the cycle, the drop recoils to regain its original shape, but at a slower rate compared to the spreading in the first half. This phenomenon is directly attributed to the governing forces acting on the drop, i.e. during the first quarter of the cycle, the electrowetting is forcing the motion; while in the second quarter of the cycle, the electrowetting weakens, and the drop follows only the forces imposed by the interfacial tension. Before the drop can arrive at its original height, the second half of the electrical cycle starts, and the voltage restarts increasing in magnitude, leading to an additional spreading stage of the drop. However, in this second half of the actuation cycle, the drop further spreads due to the partial spreading occurred in the first half of the cycle. Then, a similar episode occurs as the voltage reaches again its maximum value at $Oh Rot^* = 0.75$, where it can be seen how the drop retraction is delayed due to inertia. Once the electrical cycle has been completed, the drop monotonically retracts to its original shape regardless of the applied voltage.

Nevertheless, it is worthwhile to observe how the drop reattains the initial position in a similar manner after the electrical wave vanishes.

2.4.2 Effect of Roshko number

The non-symmetric response of the electrowetting is directly related to the relaxation time of the drop and how fast the external force is applied [26]. As a consequence, there is an interplay between the properties of the liquids and the actuation by means of electrowetting. Hence, there are two key aspects one has to compare, the applied actuation frequency and the response in the drop oscillations, which is mostly due to the viscosity of the droplets. The first natural choice, in the case of considering nondimensional number, can be Strouhal number St , but we opted for Roshko number (Ro) instead. Anatol Roshko [111] introduced this nondimensional group as a dimensionless frequency to study vortex shedding in turbulent flows. Although Ro is commonly used to describe repetitiveness of vortex-street structures, in this work we proposed to use it to represent the repetitiveness in the drop's oscillations. This also allowed us to circumvent the use of contact line velocity for the analysis. For this research, the Ro describes the oscillating flow mechanisms and directly relates the applied frequency (f) and the drop's viscosity as the governing factors. Figure 2.4 represents the response of the drop's height to the varied range of the Ro number, where Ro is varied from 0.44 to 44.49. In any damped harmonic oscillator system, the existence of the resonance frequency can significantly alter the oscillations. The first resonance frequency (i.e. $n = 2$) for a drop of $3\mu L$ in oil medium is approximately $f_2 \approx 35 - 40Hz$ [112]. Therefore, we avoided fre-

quencies close to this, to avoid any implication from the resonance. Based on the experimental observations it was noticed that beyond $100Hz$ the drop's response was minimal, therefore, the highest frequency selected was $100Hz$ ($Ro = 44.49$). With this frequency noticeable response in drop's shape was observed. Below certain frequency, the drop has a tendency to slip away from its centre, also reported as 'wagging' [98]. Therefore, to avoid any asymmetric linear translation in the drop along the spreading direction, the lowest frequency of $1Hz$ ($Ro = 0.44$) was chosen. For this lowest frequency, i.e., for $Ro = 0.44$, it is clearly seen that the drop closely follows a symmetric spreading and both valleys, representing the minimum height in the drop, have a similar magnitude. The symmetric or uniform spreading of the drops is defined to be fulfilled if the difference between the magnitude of droplet's height at the maximum spreading position in both halves has a difference below 5%. The discrepancy between the experimental and theoretical predictions is off two folds, first, the predicted magnitude in the drop's height and second, the location of the minima. Interestingly, the time achieved to attain the first minima matches quite well with the experimental observations. The underprediction of height depression is significant for lower Ro , but for higher Ro (4.45 and above) it matches perfectly well. The proposed model is developed for AC voltage, whereas the lower frequency behaves similar to DC voltage scenario, hence, the discrepancies can be justified.

For a relatively low frequency ($Ro = 0.44$), the drop's response is in phase with the actuation, as we observed in the case of η . As Ro is increased, the actuation time scale is much faster than the response of the drop, hence, the deviation

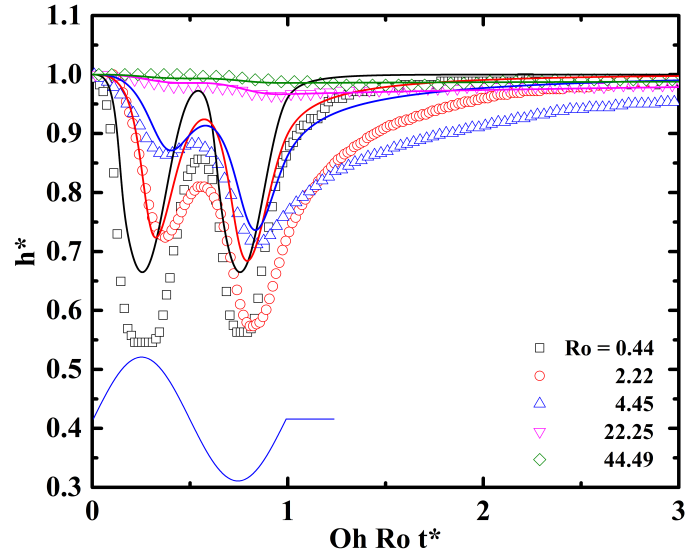


Figure 2.4: Transient variation of the droplet height for different Roshko numbers. The additional terms are fixed to $Oh = 0.009$, $\mu_r = 110.55$, and $\eta = 0.89$. The experimental results are represented by symbols and the results obtained from the proposed model are represented by the solid lines.

from the actuation cycle is imminent, which can be observed for case of $Ro = 2.22$ and above. As a result, the drop's response shifts from the sine form to an out of phase asymmetrical spreading. As noticed for all η , the drop attempts to regain its original height as the voltage is reversed during the first half cycle, but the time scale is too short for the drop to regain the original height. In this middle height regaining process, the second increment in the voltage magnitude triggers, i.e., the initiation of the second half of the cycle, and interrupts the recoiling and generates that the drop further spread. This caused the out-phase response, which intensifies along with the difference between the two valleys as Ro increases. As mentioned earlier, for higher Ro the drop spreading is minimal and is reversible in nature. The time to regain the original drop shape is strongly dependent on the viscosities of the drop and the medium. It would be interesting to see whether one can get similar reversibility in the air medium with the practical limitation of the contact angle

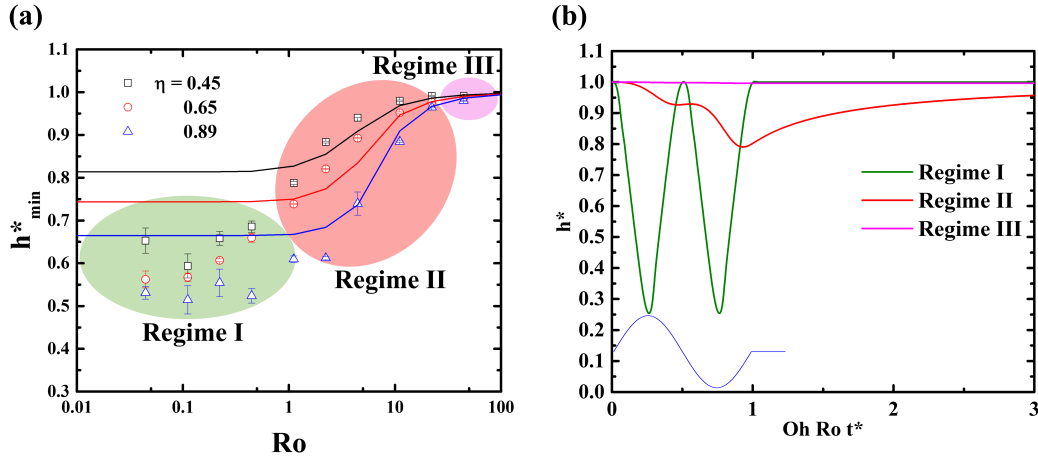


Figure 2.5: Effect of Roshko number on drop's spreading dynamics. (a) Minimum height achieved by a drop ($Oh = 0.009$ and $\mu_r = 110.55$) by a single electrowetting wave as a function of Roshko number, for different electrowetting numbers. The experimental results are represented by open symbols, and the lines represent the theoretical results. (b) Three different regimes proposed to study the transient reponse of drop spreading, which can be categorized into in-phase, out-phase, and non-responsive behaviour.

hysteresis. One very critical aspect of Young-Lippmann's equation is scrutinized here, this classical equation (Eq.2.1) never commented on the role of frequency. Here, we clearly demonstrated that for $Ro = 22.25$ and above, the drop's response completely deviates from the expected prediction proposed by Young-Lippmann's equation. One can argue that only one cycle of actuation is applied, which motivated us to study the role of number of cycles and the outcome was similar. The details of the role of number of cycles are presented in the upcoming sections, and prior to that, we have presented a quantified way to identify different regimes where the role of frequencies can be considered or ignored. In Fig.2.5 an attempt is made to present a phase plot that can clearly identify the range in which one has to study the electrospreading.

Interestingly, if the minimum height attained by the drop is studied as a function of the Roshko number, the response resembling to the "S"-shaped curve can be observed, as depicted in Fig.2.5(a). This phase plot can be categorized into three different regimes namely, Regime I ($1 \gtrsim Ro$), Regime II ($20 \gtrsim Ro \gtrsim 1$), and Regime III ($Ro \gtrsim 20$). For Regime I, where the applied frequency is smaller and can be approximated as DC electrowetting, the drop's response is approximately in phase with the applied actuation, hence, the minimum height is independent of the Ro . Regime I is the process where the maximum drop deformation can be witnessed, which is in phase with the actuation, whereas the Regime II is out of phase of the drop's response. As identified in Regime III, for very high actuation frequencies, the drop is irresponsive to the actuation, hence, it can be approximate as independent of the actuation. To further clarify the significance of the regimes, the theoretical response of the drop's height in three different regimes is presented in Fig.2.5(b). In the first regime (Regime I), when $Ro \ll 1$, the drop can closely follow the applied electrical field [98], but the minimum height deviates from the height calculated following the Young-Lippmann's equation using the root-mean-square value of the voltage. However, it is desirable to reiterate that, for low frequencies, the drop response resembles closer to DC voltage rather than to AC, where the drop can spread to a greater extent. This justifies the deviation in the theoretical model from the experiments, in Regime I, which underestimates the height reduction. On the contrary, by increasing the actuation frequency at which electrowetting is triggered (higher Ro), the model perfectly predicts the response of the drop. For the transitional regime (Regime II), when $20 \gtrsim Ro \gtrsim 1$, the drop can partially follow the actuation, which leads to the out of phase behaviour

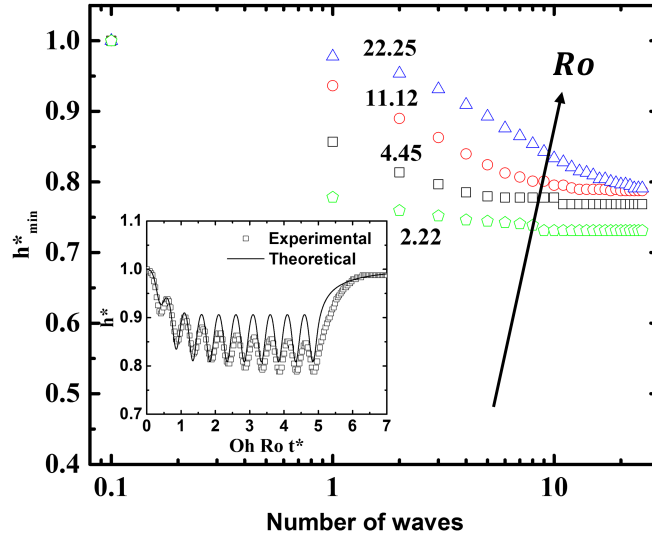


Figure 2.6: Minimum height achieved by a drop ($Oh = 0.009$ and $\mu_r = 110.55$) by a sequence of sine waves ($\eta = 0.65$) for different Roshko numbers. The initial height, when the number of waves is zero, is represented at 0.1 instead, because of the logarithmic nature of the plot. The maximum error obtained was $Error_{h_{min}^*} = \pm 0.013$.

as explained in the case of variation of η scenario. In this regime, the drop fails to attain the equilibrium maxima or minima in phase with the actuation. This has further consequences in terms of maximum spreading, which is a strong function of the number of actuation cycle that is studied in the upcoming section. For the last regime (Regime III), when $Ro > 20$, the drop is completely irresponsive to the actuation cycle. In this particular case, the spreading becomes independent of η and Ro .

The fact that a transitional regime exists can arise two questions: what would happen if more than a single sine wave is applied to the drop? and how many waves would be necessary to achieve the maximum reduction in height? Aiming to resolve the previous questions, the drop was subjected to a series of waves, and the minimum height achieved with respect to each cycle is studied as presented in Fig.2.6.

We believe the transition zone, i.e, Regime II, is in between $Ro = 2$ and $Ro = 22$. Due to additional continuous actuation for certain period, by means of higher number of actuation cycles, the drop further spreads and attains the maximum possible spreading. This maximum spreading, after certain number of actuation cycles, does not alter the maximum spreading or resulting change in the contact angle. It is worthwhile to notice that the number of actuation cycles is strongly dependent of Ro , as the Ro increases, one has to apply a larger number of cycles. Another interesting aspect was noticed regarding the drop's response after this equilibration. As the inset shows, once this critical number of actuation cycles are performed, the drop deforms in phase with the actuation cycle. During the in-phase oscillatory behaviour, the maximum and minimum drop height neither corresponds to the initial drop's height nor to the equivalent height predicted by Young-Lippmann's equation, respectively. In fact, as the Ro is increased, more cycles are required to approach towards the in-phase cyclic response, as shown in Fig.2.6. As a consequence of these higher number of cycles, the ultimate drop equilibrium height decreases with the increase in Ro . The higher Ro implies a faster spreading and a limited time for the drop to pursue the imposed actuation, which inevitably leads to a higher viscous dissipation and thus a longer time to achieve the equilibration. With the best of the authors' knowledge, based on all previous studies related with AC electrowetting, the researchers always comment that '*sufficient time*' was granted to the drop for this equilibration, but quantification of this '*sufficient time*' was missing which we have presented here. For the completeness of the analysis, it is important to study the role of medium viscosity as we have presented in the next section.

2.4.3 Effect of viscosity ratio

The viscosity ratio significantly affects the overall oscillatory response of the drops. For this study, only the liquid medium viscosity was varied. Thus, the viscosity ratio μ_r was always greater than one, which implies that the effect of the work due to the medium dissipation was significantly higher than the drop viscous dissipation. However, both the drop and medium viscosity directly influence the relaxation time of the drop, by causing additional energy losses associated with energy dissipation. The study of viscosity ratios below the unity can be easily performed in an air medium, but the existence of additional factors, such as evaporation and contact line friction, was restricting us to perform that spectrum. Figure 2.7 exhibits the experimental and theoretical response of a drop to a single wave for different viscosity ratios. A similar effect occurs for increasing the viscosity ratio, as in the case of increasing η and Ro , i.e., the drop cannot pursue the external actuation cycle. It requires more time to respond as the viscosity of the medium increases. The aforementioned delay is greatly reflected on the drop at the end of the first half of the cycle, where the drop cannot retract to its original height, and during the second half, the drop spreads in a completely different magnitude than the previous half. Thus, an irregular spreading is observed and more than one wave is required to attain the global minimum height. The irregular response can be avoided by reducing the medium dissipation, accomplished by reducing the viscosity ratio, which guarantees insignificant losses due to the medium. For the least viscous medium in Fig.2.7 ($\mu_r = 11.34$), the drop can retract to its original height by the end of the first half of the cycle, and the first and second valley are equal in magnitude. As μ_r increases, the drop's reaction diverges from the in-phase response and begins to

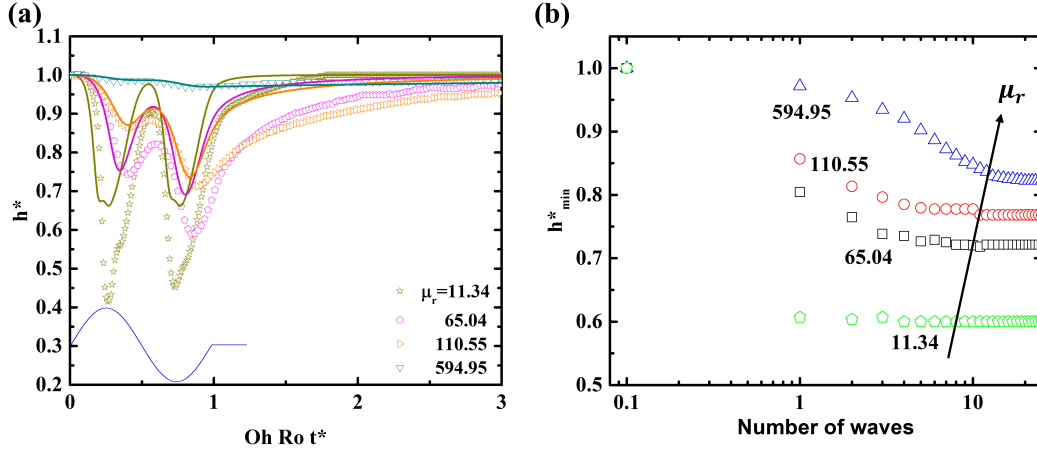


Figure 2.7: Effect of viscosity ratio on drop's spreading dynamics. (a) Transient variation of the droplet height with additional terms fixed to $Oh = 0.009$, $Ro = 4.45$, and $\eta = 0.89$. The experimental results are represented by symbols and the results obtained from the proposed model are represented by solid lines. (b) Minimum height achieved by a drop ($Oh = 0.009$ and $Ro = 4.45$) by a sequence of sine waves ($\eta = 0.65$) for different viscosity ratios. The initial height, when the number of waves is zero, is represented at 0.1 instead, because of the logarithmic nature of the plot. The maximum error obtained was $Error_{h_{min}^*} = \pm 0.037$.

lag. It can be observed in Fig.2.7 that the lagging phenomenon and the intensified out-phase response can be seen with the increase in the viscosity ratio. For more viscous medium, the difference between the first and second valley is more palpable and the reduction in the maximum height depression can be also witnessed. A clear similitude between Fig.2.4 and Fig.2.7 corroborates the statement that the transition of the drop's response from in-phase to out-phase is linked to the relationship between the drop's response and the actuation time scale.

As we studied the role of number of cycles with the variations in Ro , the similar analysis is presented with respect to medium viscosity in Fig. 2.7(b). Also, it is observed that a plateau is reached after the actuation of certain number of cycles beyond, in which the drop's response was in phase with the actuation independent

of the number of waves. For higher viscosity ratios, the drop reduces the maximum spreading and requires more waves to reach the oscillatory steady state response. Thus, the resemblance between the Ro and the viscosity ratio is evident. Here again, the same observation was made that suggests a minimum number cycles must be considered before commenting on the equilibration or even for the comparisons with the Young-Lippmann's equation.

2.5 Conclusion

This study has developed a theoretical model to predict the dynamic response of a drop to the actuation of an external electric perturbation. An overall energy balance (OEB) approach was selected to study the combined effects of the inertial, the surface tension, and the dissipation forces on the drop's oscillations. The model balances the energy delivered by the electrical actuation, which was simplified by defining an instantaneous contact angle as a function of a modified Young-Lippmann's equation. The energy balance resulted in a second order ordinary equation, which was solved by means of a Runge-Kutta technique. The results obtained from the theoretical model were compared with the results from the experiments. The theoretical and the experimental results presented a similar response in the drop's oscillations for electrowetting in a liquid medium. The model qualitatively predicts the dynamic drop's response in terms of height's variations. This model also commented on the retracting stage where the drop attempts to reacquire its original shape. The model predicted the change between the in-phase to out-phase spreading of the drop according to the applied frequency and the thermophysical properties of the liquids. Also, the comparison of the different energies revealed

the relevance of the work due to the medium dissipation in the electrowetting's response of a drop in liquid medium. Finally, the dynamic response of a drop for a single or a sequence of electrowetting waves was studied in detail. For a single wave perturbation, it was observed how the drop completely changed its reaction according to the relationship between the dissipation forces and the speed of the electric wave. Nondimensionalization of the governing equation resulted in three key parameters or nondimensional groups, i.e. η , Ro , and μ_r representing the importance of the magnitude of the actuation force, the dynamics involved in this force, and the viscosity of the system, respectively. The obtained results were presented in a nondimensional form and the analysis was corroborated with experiments. Three different regimes for the dynamic response of a sessile drop to electrowetting were identified. Special attention was dedicated to the transitional regime, where the number of waves applied to the drop dramatically changed the maximum spreading of the drop. Therefore, this mathematical model can provide with a better understanding of the electrowetting's dynamic response, and can be used for finding the optimal operating conditions of electrowetting-based devices.

Chapter 3

Sessile drop response to a single wave electrokinetic excitation¹

3.1 Introduction

Drop spreading and response of equilibrated drop to an external actuation has always been a topic of interest due to its relevance in numerous applications such as inkjet printing [113], droplet manipulation [114–116], pesticide deposition [117], raindrop impact [118] and so on [119–122]. The drop motion on a surface is governed by the inherent surface energies of the drop and the underlying interface along with the physical properties of the liquid, which is generally represented in terms of group of nondimensional numbers [123, 124]. For solid-air interface the surface roughness [125], inherent surface energy [126, 127] and stiffness [128, 129] influence the drop motion. Based on the surface energy interactions, the drop forms a sessile drop configuration attaining an equilibrium with a contact angle either termed as equilibrium or Young’s angle ascertaining the importance of only interfacial energies [101, 106]. After the actuation of external field by means of drag [130], magnetic field [100], acoustic field [131, 132], electrical field [133, 134],

¹A version of this chapter has been submitted for publication in Langmuir as: Juan S. Marin Quintero and Prashant R. Waghmare, “Sessile drop response to a single wave electrokinetic excitation”, 2019.

the sessile drop response is studied for a relevant applications. The continuous deformation of the drop with respect to the continuous deformative external actuation is widely investigated [100, 130–134]. Interestingly the responsive behaviour of drop to a single or series of waves has not been singled out, primarily permitting the drop to equilibrate after the actuation of external deformative force. In this study we attempt to investigate the response of a sessile drop to a wave perturbation by means of electric field and through the examination of the drop response, until it equilibrates, we commented on the generalized responsive behaviour of the drop.

The sessile drop configuration can be maneuvered in a precise way by applying an electric field which is commonly known as ‘electrowetting’ [7, 41]. In the case of electrowetting, an electrolyte drop attached to the electrode – generally a thin copper wire – spreads on the dielectric layer (PDMS or Teflon). The dielectric layer enhances the ability to spread the drop and avoid the unwarranted electrolysis. Prior to the application of an electric field, during the attainment of sessile drop configuration, ions instantaneously reconfigure to form an electric double layers at electrolyte-dielectric surface and dielectric-metal surface [135] as depicted in Fig. 3.1 (a). Commonly, the larger variation in the reversible wettability is attained with dielectric layer between the electrolyte and the metal substrate. By inducing an electrical voltage difference between the droplet and the substrate (electrode), coated with a dielectric layer, the ions inside the drop particularly at the three-phase contact line reorganize themselves, and slip at the three-phase contact line (TPCL) is witnessed. This slip ultimately reflects in the drop shape which can be quantified in terms of contact angle (CA) or the height of the drop [21, 103]. The presence of

charges at the solid-liquid interface, after the actuation of electric field, generates a repulsion between like charges causing the drop to spread. The resultant drop height variation after the single wave actuation is presented in Fig. 3.1(b) and the corresponding images depict the drop shapes at that particular instance. The voltage actuation cycle is shown in the continuous line in Fig. 3.1 (b).

In such cases, where the dielectric layer, for enhancement of maximum reversible displacement of the TPCL, is used in the electrowetting is referred as electrowetting on dielectric (EWOD) [15, 41]. The apparent contact angle θ_{app} attained due to electrowetting, is related to the applied voltage as explained by following Young-Lippmanns equation [41]:

$$\cos\theta_{app} = \cos\theta_Y + \frac{\varepsilon_o\varepsilon_d}{2d\sigma_{lv}}U^2 = \cos\theta_Y + \eta. \quad (3.1)$$

where θ_Y is the initial equilibrium contact angle or Young's contact angle, ε_o is the permittivity of free space, ε_d is the dielectric constant of an insulating layer of thickness d , σ_{lv} is the interfacial tension of the liquid and the surrounding medium, and U is the applied voltage. The change in contact angle due to the application of electric field is computed with the second term in Eq. 3.1 and this nondimensional group is known as electrowetting number (η). This superposition of contact angles suggests that the wide range of contact angle variation, in reversible way [47], can be achieved. It was discovered that by using alternating current (AC) voltage, the electrowetting saturation can be further prolonged even with higher voltage compared to direct current (DC) voltage [135]. Furthermore, the energy supplied using

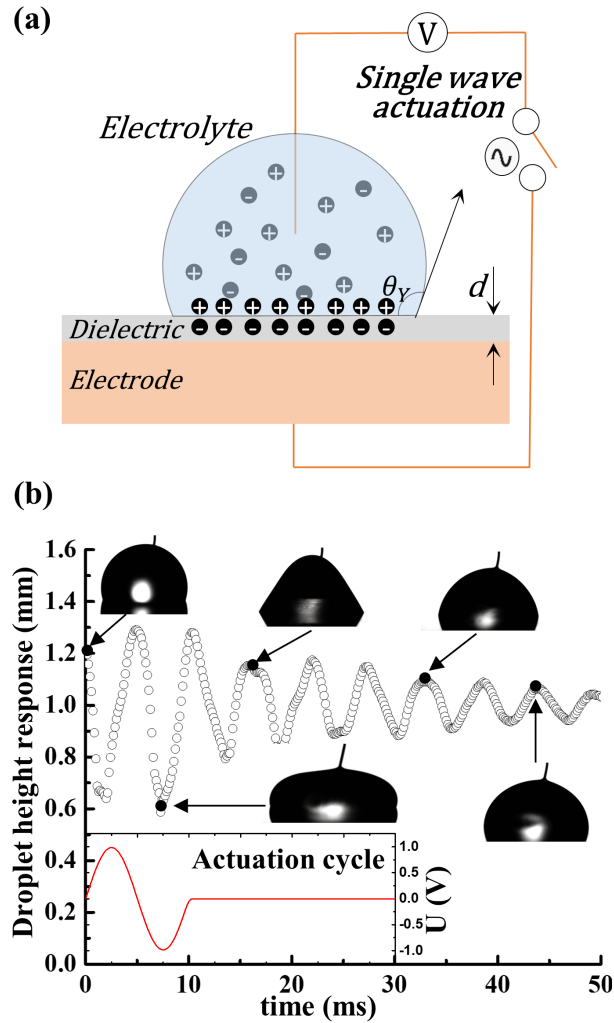


Figure 3.1: Schemes of the response of a sessile droplet to an external deformative force. (a) Electrowetting of a sessile droplet on a dielectric with a thickness d and an initial contact angle θ_Y . (b) Oscillatory response of the drop to a wave perturbation by means of electrowetting, snapshots of the drop evolution in time are presented. The inset figure symbolizes the wave perturbation, where the two main parameters in the wave are exemplified. The wave represents the actual wave which the drop received.

AC is used to reduce the possibility of permanent charge adsorption on the substrate [41, 97, 136]. By introducing an AC voltage, the frequency of the applied voltage will change hydrodynamic flows inside a droplet [94]. It was also found that the magnitude of driving frequency can suggest whether the system behaves as a perfect conductor at low frequencies or as a dielectric at high frequencies [137].

A single wave of an electrowetting force will create motion in the drop with oscillations by abruptly changing the shape of the drop. This force can be considered as an external force that will not considerably modify the properties of the system if the force is only applied at the beginning of the process. After the voltage has been applied, the drop will spread by reducing the CA and height and thus increasing the base radius. Yet, the base radius of the drop will experience additional forces such as the three-phase contact line friction and pinning effect with the substrate. These additional forces will provoke higher energy dissipation and therefore an erratic spreading. The drop height will present more noticeable oscillations, making the height to be a reliable parameter that can be studied. The primary objective of this paper is to observe and explain the effects of the applied voltage and frequency of the single wave. Additionally, the role of drop and medium viscosity is also investigated in the transient dynamic of drop spreading.

3.2 Material and Methods

During the experiments, an aqueous solution consisting of different concentrations of glycerol and 0.1M sodium chloride was used. The viscosity of the drop phase was

adjusted by varying the glycerol concentration. The role of viscosity was studied by changing the drop as well as the medium viscosity. Viscosity was measured using a bulk rheology rheometer (Rheolab QC, Anton Paar), and the surface tension and density were measured using a force tensiometer (K100, KRÜSS Scientific Instruments Inc.). Drops of approximately $3\mu L$ were created using a single software controlled syringe dispenser, installed on a goniometer (Drop Shape Analyzer (DSA100, KRÜSS Scientific Instruments Inc.) using disposable syringes (NORM-JECT 1mL, Henke-Sass Wolf GmbH). As a surrounding media, air and silicone oils with a wide range viscosity were used. Drops were deposited on a copper substrate covered by a PDMS layer with a dielectric constant of $\epsilon_d = 2.8$. The thickness of the film ($21\mu m$) was controlled by changing the time and rotational speed of the spinning coating process. The AC electrical signal, as shown in the inset of Fig. 3.1 was produced by a waveform generator (294 100MS/s, FLUKE), where the frequency was varied between $1Hz \leq f \leq 100Hz$. The voltage ranged between $200 \leq U_{AC} \leq 350V$ was achieved with the help of an amplifier (BOP 500, KEPCO). The range for these experimental operating parameters was decided based on the contact angle saturation [18, 42] for a considered combination. The negative electrode was connected to the copper substrate, and the positive electrode was connected to the copper wire ($60\mu m$ in diameter) which was positioned inside the droplet with a vertical separation distance from the copper substrate equal to the initial base radius of the drop. A high-speed camera (Phantom V711, Vision Research Inc.) with a frame rate of 3,000 and 7,000 frames per second was used to record the spreading and retracting stages of the drops. An extended macro lens assembly was used to obtain a spatial resolution of $\sim 5\mu m/\text{pixel}$ with an appro-

Table 3.1: Properties of liquids. Viscosity μ , density ρ , and interfacial tension σ of different liquids at room temperature

Liquid	$\mu(mPas)$	$\rho(kg/m^3)$	$\sigma(mN/m)$
Water	0.91	997.1	71.7
43% Glycerol/water	4.86	1120.8	65.6
60% Glycerol/water	13.34	1166.6	60.8
76% Glycerol/water	47.93	1205.4	64.0
85% Glycerol/water	121.71	1226.3	65.6
D10	10.32	846.2	40.6
N35	59.19	853.6	40.6
S60	100.60	857.0	40.4
D500	541.40	869.9	40.5
D1000	1138.00	870.7	40.5

appropriate magnification. The length scale of the image was calibrated by considering the needle image with known diameter as calibration target. Videos were analyzed by an image processing software (ImagePro Premier 9.2, Media Cybernetics, Inc.), where an edge detector function in the software was applied to identify the liquid/gas interface; thus, the transient variations in the height and the base diameter of the drops can be quantified. Parameters that influence the drop response noticeably such as applied voltage, amplitude, frequency, and viscosity were studied in a systematic way. Table 3.1 provides the details of viscosity μ , the density ρ , and the surface tension σ of liquids considered here. It is to be noted that the interfacial tension reported in Table 3.1 for viscosity standard oil is with respect to water since the water drop was placed inside the oil.

For a desired process, the optimization of the operating parameters is one of the main objectives and the applied voltage is the energy-consuming parameters that one has to optimize for the envisioned outcome. Hence, in this study a single wave

actuation is studied that can certainly help to comment on the role of time scale involved in the electrowetting process, for which Young-Lippmann equation fails to comment on. Dey et al. [138] already used the intermittent AC electrowetting to reduce the trapping of condensate droplets which has ultimately enhanced the condensate shedding efficiency. The Young-Lippmanns equation, despite describing the change in the CA accurately, is only valid for the equilibrium contact angle after some time has passed, which varies depending on the system's parameters. Although some researchers have studied the variation of the shape of the drop by applying an AC voltage [30, 94, 139], the electrical signal in these experiments was applied continuously. Also, some other studies regarding the transient dynamics of the drop spreading due to electrowetting have been performed [25, 102]. However they used a DC electric pulse as a step function, and the voltage was always kept at a non-zero value. Hence, the study of the spreading of the drop caused only by a single AC wave without any offset voltage has not been achieved yet.

3.3 Results and Discussions

The dynamic response of a sessile drop to the perturbation resembles to an inertial system, where the electric force will generate the perturbation in the system and induce the oscillations across the liquid-fluid and solid-fluid interface. The oscillation at the contact line are prone to get hampered or dampened due to the contact angle hysteresis but the oscillatory behaviour along the fluid-liquid is hampered only due to the surrounding and drop phase properties. Thus one can argue that the oscillatory behaviour at the interface decays over time either by the contact line friction or by the dissipation caused by the viscosity of drop and/or

medium. The behaviour studied in Fig. 3.1(b) reminded us the inertial capillarity studies [82, 140, 141] where the role of inertial and dampening viscous forces in relation with driving force were scrutinized. A simpler approach with mass-spring-dampener model analogy is commonly used to determine the characteristics of such systems [142, 143]. Here, mass represents the object in motion, which is subjected to the external actuation for short period of time, and resistance offered by the fluid due to viscosity acting as a dampener. In the case of liquid drops, one can infer that the mass of the system is related to the density and volume of the drop under consideration; the inherent energy source, i.e., surface tension at the drop-medium interface is spring, and as mentioned earlier the viscosity is dampener. For an ideal damped harmonic oscillator, the height of the drop, h , can be expressed as [142, 143]:

$$\frac{d^2h}{dt^2} + \zeta\omega_n \frac{dh}{dt} + \omega_n^2 h = 0 \quad (3.2)$$

The transition from oscillatory to non-oscillatory behaviour can be easily identified based on the magnitude of ζ which is ratio of the damping coefficient (C), and product of mass (m) and spring constant (K). By defining the natural frequency as $\omega_n = \sqrt{K/m}$, the underdamped ($\zeta < 1$) and overdamped ($\zeta > 1$) regimes can be established with the knowledge of C and K . For the underdamped system, the decayed oscillations can be witnessed, conversely, the exponential decay without any oscillatory behaviour is common outcome for overdamped system. In the case of a drop submitted to electrospreading, one can obtain both the regimes by appropriately changing the properties of the system, such as the viscosity of the drop, as depicted in Fig.3.2(a). The height of the sessile drop with two distinctly different

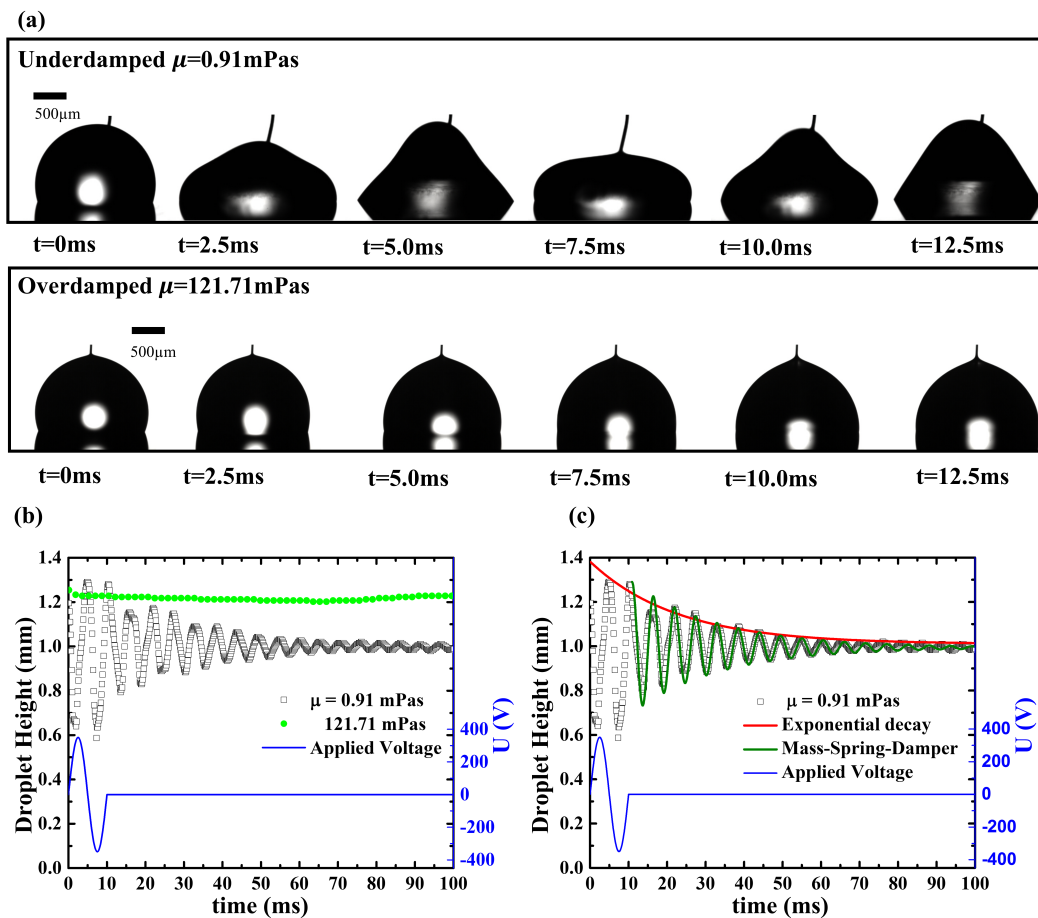


Figure 3.2: Drop's response to a wave perturbation by means of electric field (a) Snapshots presenting the drop evolution for the under damped and over damped regimes by applying a 350V sine wave at 100Hz to drops with viscosities of 0.91mPas and 121.71mPas . (b) Droplet height vs time, for both cases of under damped and overdamped regimes. The wave perturbation is represented in a second vertical axis. (c) Comparison between the drop's response of underdamped with a damping ratio $\zeta = 0.1$, along with the exponential decay and the mass-spring-dampener response associated to this experiment. The wave perturbation is again represented in a second vertical axis.

viscosities, 0.91mPas and 121.71mPas , is presented in Fig. 3.2(b). For a drop of 0.91mPas the decaying oscillations are evident in height of the drop for more than 100ms , even though the application of single wave perturbation was for 10ms . However, for the case of 121.71mPas , with the same actuation, the drop rapidly attains the new equilibrium position without any oscillations. With appropriate regression analysis, the decay along the peak of highest height from each oscillation, as shown in Fig.3.2(c), ζ , can be quantified [143]. Further, spring and damping coefficient can also be determined empirically. The continuous line, overlapping with the experimental results, in Fig.3.2(c), is theoretically predicted height response. It is evident that at the beginning of the process, the theoretical prediction is in phase with the experimental observation but with marginal over prediction. In the dying period, this model is not in phase and under predicts the behaviour. The deviation from the experimental results can be attributed to the contact line hysteresis. Another possibility for this discrepancy is the inability to dynamically change the spring and damping constant [143]. The pinning of the contact line or stick-slip [144] at the contact line results in disruptive representation in height. This was the prime motive for us to represent the entire analysis in terms of height of the drop rather than the base diameter or the contact angle. To circumvent the role of solid substrate roughness and in turn slip-stick or pinning effect at the contact line, one can perform similar analysis in liquid medium instead of air. After a single sinusoidal wave actuation, the drop continues to move due to the inertia and eventually stops when the dissipation forces overcome the inertia. The combination of the applied forces or parameters responsible for the actuation such as voltage and frequency along with the thermophysical properties of the drop and medium will

dictate the drop dynamics. Therefore, a parametric study with different operating parameters mainly the actuation parameters is worth to study. In the following sections, a more detailed analysis for each of these parameters and corresponding drop responses are presented.

3.3.1 Applied voltage effect

The driving actuation force is mainly controlled by the applied voltage, hence by increasing the applied voltage with constant wave frequency, the variations in the height is expected. Figure 3.3 represents the response of drop height to the varied range of applied voltage. The role of applied voltage (200 – 350V) is studied in the Fig. 3.3(a) where it can be observed that after the one cycle of actuation the drop continues to deform in the similar way as the applied signal. The selection of maximum voltage (350V) was based on the dielectric breakdown of PDMS, $E_{breakdown}$ ($19V\mu m^{-1}$, which in the case of the present study is 400V) and on the saturation criteria. The lower voltage (200V) was decided to observe the noticeable change in the drop shape. The continuous line in sine wave form at the left bottom corner represents the actuation signal and the numbers in the parenthesis for legends are corresponding electrowetting numbers for each voltage. In the first quarter of the actuation cycle, as the voltage is increased the drop apex is pulled further towards the solid interface. In the next quarter, drop attempts to regain its shape by attaining its original height. In the figures the drop height is normalized with the drop initial height whereas the time is normalized with frequency to get the same bounding limits for comparison of the observed phenomenon. In the regaining process, during

the second quarter of the cycle, the drop attains the height which is less or equal to the initial drop height.

In the case of $350V$, marginal overshoot is noticed which can be attributed to the inertial effects [141] or the non-symmetrical nature of the drop shape (refer to the Fig. 3.2(a) and drop shape at the nondimensional time 0.25 and 0.75). The inset presented, at the right bottom corner, depicts the magnified view of the quarter cycle response and the solid symbol representing the maximum deformation of drop in terms of height. Higher the applied voltage, smaller the out of phase behaviour for the drop deformation. For example, in the case of $350V$, the solid symbol, maximum deformation of the drop is observed closer to the peak of the applied voltage (point A presented in both the inset figures). It is to be noted that even though the magnitude of applied voltage is in the opposite direction, the electrospreading is governed by the square of the applied voltage as discussed in Eq. 3.1. Therefore, in the second half cycle, the similar observation is noticed. After one cycle actuation, in the absence of any external force, the drop continues to deform in a similar way and attains the equilibrium with dampening in the oscillatory changes in the height. In air medium (Fig. 3.3(a)), the non-continuous or abrupt change in the height is observed which is due to the contact angle hysteresis at the contact line at the solid-liquid interface at the substrate as well as at the electrode [80]. The abrupt change is due to the pinning or sudden slip at the three-phase contact line which can be clearly noticed for $300V$. In the case of liquid medium, as presented in Fig. 3.3(b), the liquid surrounding medium nullified the role of hysteresis and thus the continuous change in the drop height was observed. The moment actuation finishes, the

outer liquid medium instantly suppresses the oscillatory deformation of drop and returns to its original height monotonically. In the case of air, the oscillatory behaviour continues for longer period of time which is at least ten to twenty folds of the time required to complete the first cycle. The focus was to observe the first few cycles of the oscillations with high frame rate, hence the attainment of equilibrium or original shape of drop was not presented here. After attaining the equilibrium, the normalized final drop height response in air (empty squares) and liquid medium (empty circle) are shown in the inset of Fig. 3.3(b). The main difference between the liquid medium with the air medium is the origin of the dissipation of energy.

In liquid medium, the thin lubricated film at the drop base enhances the slip at the contact line but at the expense of dampening the movement of the interface due to the surrounding viscous medium. Due to the lower three-phase contact line friction in liquid medium, the droplet attains the initial position without any additional permanent spreading of drop, regardless of the applied voltage. In case of air medium, the permanent irreversible drop spreading was noticed which decreased the drop height accordingly. This change is in linear response with the applied voltage suggesting that the higher voltage indeed forced the drop to spread more but the drop could not regain its original shape due to the resistance at the contact line arises by contact angle hysteresis. It is well accepted fact that liquid medium or thin liquid film significantly reduces the contact angle hysteresis [145]. The careful observation of air medium case (Fig.3.3(a)), the continuous pinning, in a successive manner in each cycle, can be noticed by identifying the valleys of each cycle. The maximum diminution in the height for a given cycle decreases as the number of cy-

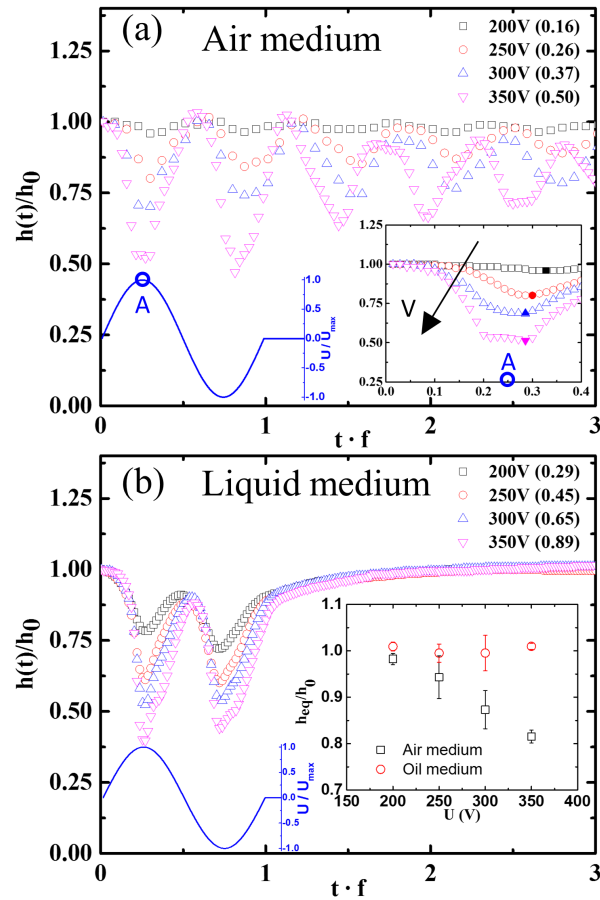


Figure 3.3: Effect of applied voltage on the drop spreading dynamics: (a) Drop in air medium with an electrical wave of 100Hz and different voltages for drops with viscosity of 0.91mPas ; and (b) 10Hz and different voltages for a liquid medium with 10.32mPas viscosity. The actuation time is located and increases with the applied voltage for both air and liquid medium.

cle increases. This reflects the permanent irreversible spreading of the drop. At the same time, for liquid medium, the two maximum decrements are more congruent with each other suggesting a marginal loss in the height due to the hysteresis.

3.3.2 Applied frequency effect

The second controlling parameter, in a sinusoidal wave, is the applied frequency which can be considered as the number of waves completed in one second. By increasing the frequency, the number of waves per second is increased which is opposite to the period – time to complete an individual cycle. In this study, the role of single wave actuation is studied and the consequence of changing the frequency is witnessed accordingly as shown in Fig. 3.4. The range of frequency (1 – 100Hz) was selected based on the limit for breakdown of the conductor [94] and minimum frequency to observe the change in the oscillation of the drop height. The separation between high- and low-frequencies is defined by a critical frequency f_c [96]. For $f \ll f_c$ the droplet behaves as a perfect conductor and the voltage drop is entirely concentrated in the dielectric layer. The critical frequency for a water drop is $f_c \approx 2kHz$, but the practical limitation of the system was selected to be 100Hz to avoid the inconsistency from a perfect conductor. In addition, the resonance frequencies of the drop can be expressed as $f_n = \sqrt{n(n-1)(n+2)\sigma/(R^3\rho)}/(4\pi)$, where n is the corresponding resonance mode, and R is the volume-averaged radius [30, 98]. For the case of a $3\mu L$ water drop, the resonance frequencies for nodes $n = 2$ and $n = 4$ are $f_2 = 50$ and $f_4 = 150Hz$, respectively. Therefore, frequencies above 100Hz were avoided aiming to remain below the second resonance

frequency and to prevent the formation of additional lobes and higher complexity in the drop geometry. For frequencies far below the first resonance frequency ($f \ll f_2$), i.e., $f < 5Hz$, the drop response does not present significant changes and the height remains constant. However, for frequencies in the vicinity of the first resonance frequency, the drop behaviour changes according to the applied frequency.

Interestingly, the drop response dramatically changes as a function of the applied frequency; the amplitude of the oscillations in drop motion and the equilibration time increase as the applied frequency increases. The advantage of normalizing the time with the frequency is necessary, since the comparison becomes cumbersome with respect to the dimensional time (as in the inset figure at the right bottom corner of Fig. 3.4(a)). The drop spreading is similar until the minimum height is reached in the first quarter of the actuation cycle, approximately at the time when the voltage is maximum ($t \cdot f = 0.25$). After the voltage starts returning to zero for the first time, the drop attempts to recover its original height, with the exception of $10Hz$. Hong et al. [98] observed that for certain frequencies, the drop oscillations are extremely weakened. The maximum drop height is always less than or equal to the original drop in all the cases except for $100Hz$. We speculate that this is due to the inertia in the system and the higher frequency actuation can verify this claim. For other frequencies, the drop height decay is noticed which eventually attains an equilibrium with a smaller height than the initial drop height due to the slip at the three phase contact line. For the frequencies far below the first resonance frequency (1 and $5Hz$), the drop simply follows the applied voltage [98], and the inertial ef-

fect is not significant enough to trigger any oscillations in the drop after the seizing of the actuation. For lower frequency, the actuation is smaller in magnitude hence the spreading or slip at the contact line is also lower. Moreover, the longer time between the actuation peaks allows the drop to reconfigure itself, therefore, nearly follows the actuation wave. The resultant spreading in the drop was marginal which is reflected in the final drop height which is almost 90 – 95% of the original height. On the contrary, by increasing the frequency, the period of the wave is shortened, and the drop struggles to be in phase with the actuation due to its response time. One can argue on the definition of the drop response time which can be the inertial or viscous time scale and in the later part of the manuscript we will comment on it briefly. During the actuation, the higher frequency increases the height drop that subsequently requires longer time to equilibrate the height even after the completion of the actuation cycle. Theoretically, the drop must regain its original height but, as mentioned earlier, the stick-slip at the contact line facilitates the irreversible spreading. The liquid medium avoids such a scenario as can be seen in Fig. 3.4(b).

For a liquid medium, an analogous behaviour, as witnessed in air medium, is observed by varying the frequency. There are two distinct behaviours noticed, i.e., in phase and out of phase with the actuation. The first resonance frequency associated with the liquid medium is similar compared to the air medium experiments ($f_2 \approx 35Hz$) [112]. It can be anticipated that for high frequencies the momentum transferred is highly restrained by the medium viscosity and at these high frequencies the drop will not oscillate by applying only a single wave due to the medium viscosity. Therefore, the selection of the frequencies in the case of viscous medium

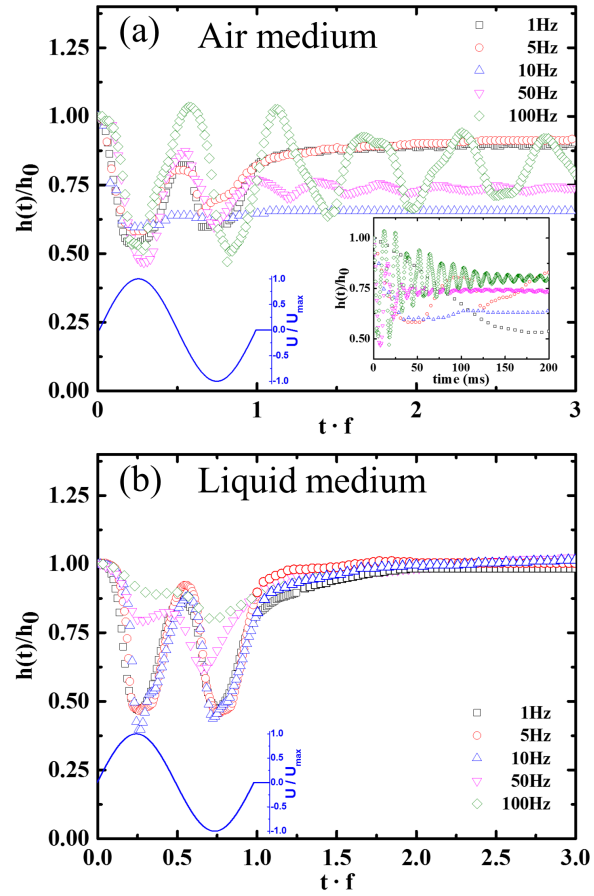


Figure 3.4: Effect of applied frequency on the drop spreading dynamics: (a) Drop in air medium with an electrical wave of $350V$ and $0.91mPas$ viscosity for different applied frequencies; and (b) $350V$ and $10.32mPas$ liquid medium viscosity for different applied frequencies.

was based on the limitations of the medium dissipation. For all the cases in the liquid medium, the drop always regains its original height reflecting a negligible penalty due to the contact angle hysteresis. In the case of $1 - 10Hz$, the drop height response is in phase with the actuation cycle and it is independent of the magnitude of the frequency as presented in Fig. 3.4(b). For these three cases, the maximum depression in the height, with maximum (at quarter of the cycle) and minimum (at the middle of the cycle) voltage, is approximately the same. A marginal increment in the drop depression with respect to the actuation frequency is witnessed from $1 - 10Hz$ due to inertia. Whereas, for $50Hz$ and $100Hz$ the response in height is completely different. It is evident that for these two frequencies the drop response is much slower than the actuation. By the end of the first quarter, as observed for both cases, a local maximum deformation is attained. The occurrence of the minimum height is delayed, perceptible on how the drop does not immediately stop spreading at the end of the first quarter. In the next quarter, the drop tries to regain its original shape with its own response/relaxation time scale which is significantly slower than the actuation frequency. Therefore, in the second quarter of the actuation, the process of regaining the original shape is interrupted and a non-symmetric change in the height is observed [95]. The interrupted spreading in the case of $50Hz$ and $100Hz$ can be interpreted in terms of height change which suggests that the drop has not settled into defined limits, as commonly reported in studies of AC electrowetting [21]. Hence, a single cycle is not sufficient to stabilize the dynamic response of the drop due to electrowetting. This justifies the difference in the minimum drop height during both halves of the cycle. This effect is also reflected on the delay in the occurrence of the minimum heights. Such a behaviour was absent

in the case of air medium, hence we attribute this to a role of surrounding medium. This is supported by the observations reported in next section where a similar outcome was witnessed as we increased the medium viscosity.

3.3.3 Viscosity effect

Drop response which is in phase with the actuation cycle is observed in most of the cases. The out of phase response and the non-intuitive obstruction in the regaining of the shape without attaining original height during the subsequent second half of the actuation cycle – which is observed only for liquid medium beyond a certain frequency – motivated us to investigate the role of surrounding medium viscosity. For the completeness of the study, the response of drops with different viscosities is also studied as shown in Fig. 3.5(a) whereas the drop response with different medium viscosities is demonstrated in Fig. 3.5(b). The viscosity represents the loss due to energy dissipation, so if the magnitude of the viscosity is increased, a higher energy loss is expected. For a constant deformation rate, the loss due to viscous dissipation can be approximated to the velocity gradient, higher the gradient larger will be the losses. The same observation is noticed, as stipulated in the case of change in frequency. For higher applied frequency the difference in the first and second valley of the drop height was higher compared to the lower ones. In air medium, to study the role of viscosity, other parameters were chosen in such a way that the contact angle hysteresis was as minimum as possible. As expected, in air medium, the increase in drop viscosity decreased the amplitude of the oscillatory change in drop height without hampering the frequency. The maximum reduction

in height is lower for more viscous drops, having repercussions in the amplitude although the applied voltage was identical. The argument of the inertial effect for overshoot in the height can be witnessed by observing the 0.91mPas case. Based on a similar hypothesis, it has been demonstrated that, with the sudden release in the voltage, the drop recoils and jumps from the substrate [146]. Nevertheless, for drops that remain on the substrate, as in all the cases observed here, the first and second valley witnessed marginal difference, regardless the drop viscosity. Thereafter, after the actuation cycle is completed, the drops continue to oscillate with a similar frequency until the energy is dissipated and the new equilibrium shape is attained. Complete dampening of these oscillations can be observed in the case of 121.71mPas , as seen in the inset figure. A similar phenomenon of the delay in the minimum height is observed as in the case of varying the frequency. By increasing the viscosity, the response time of the drop is increased and the drop demands more time to restructure. Therefore, the drop still spreads after the first quarter of the cycle, which is intensified as the viscosity of the drop is increased. Yet, the retraction stage for all the different viscosities follows the same fashion, and finishes exactly at the end of the second quarter of the cycle. With the understanding of drop response based on its viscosity, the role of medium viscosity is studied.

For the case of varying the medium properties, the drop also changes the spreading behaviour according to the surrounding medium viscosity. For low viscous medium (10.32 mPas), the drop does not experience a resistance from the medium and it spreads following the applied sine wave of the voltage as seen in Fig.3.5(b). But as the viscosity is increased, the responsive behaviour changes as a consequence

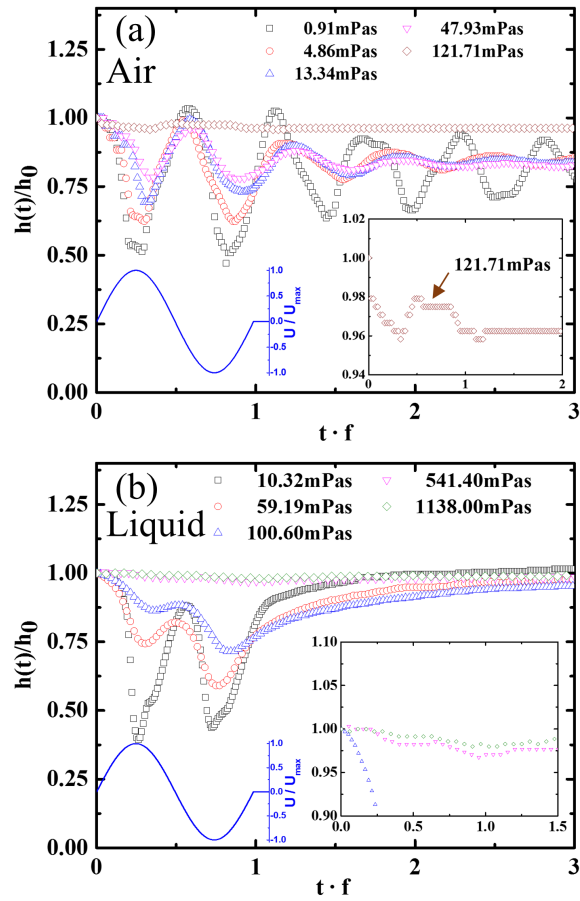


Figure 3.5: Effect of viscosity on the drop spreading dynamics: (a) Drop in air medium with an electrical wave of 350V and 100Hz with drops of different viscosities; and (b) 350V and 10Hz for different liquid medium viscosities.

of a dissimilar retraction response which is evident in the height variations. In other words, an alike effect with the frequency is noticed, where the drop initially spreads to an intermediate position in the first half, and then further spreads in the second half. Hence, it can be recognized that as the viscosity increases, the dynamic response of the drop differs more from the sine wave shape. Furthermore, for higher viscous mediums, as in the case of 541.40 and 1138.00 *mPas*, the drop seems not to oscillate and barely spread. However, in the inset figure, at the right bottom corner in Fig. 3.5(b), it can be seen that the amplitude is highly dampened. Consequently, the occurrence of the minimum height is delayed which depends on the medium viscosity. This irregular spreading is not attributed to the polarity of the voltage, but to the relationship between the relaxation time and the applied frequency. By comparing the height response for both frequency and medium viscosity, it can be affirmed that the actuation time of the drop is directly proportional to the viscosity and inversely proportional to the frequency. As the viscosity is increased, the relaxation time of the drop is also being raised and it needs more time to reorganize itself. To understand the role of the time scale a detailed study on the response time scale is presented in the next section.

3.3.4 Response time of the drop

The response time of the drop (τ_{drop}) is defined as the longest time required for the drop to attain maximum deformation with the first attempt of maximum perturbation, i.e., the time required for the drop to reach the minimum height in the first half of the actuation cycle. If there was no influence of any thermophysical

property, this time should exactly match the imposed actuation time of the applied frequency (τ_f). In other words, the drop should reach the maximum deformation exactly at the end of the first quarter of the cycle when the voltage is maximum (at $t = 0.25f$). However, as previously discussed, the drop has a different response time based on its thermophysical properties, either inertial viscous or capillary time scale [147]. Hence, the first choice was viscous time scale to observe its influence on the response time of the drop. We can contemplate that the maximum force per unit length exerted to the drop on the three-phase contact line is $F_{max}^* = \sigma(Cos\theta_{app} - Cos\theta_Y) = \eta\sigma$, and an opposite force due to the friction is $F = A(\mu\mu_o)^{1/2}u$, where μ and μ_o are the viscosity of the drop and the surrounding fluids, respectively, u is the contact line velocity, and A is an empirical constant that is a function of the surface properties [102]. In our case, we are analyzing the results without any correction factor A . Thereafter, the balance of these two forces will lead to a characteristic velocity at the three-phase contact line of $U = \eta\sigma/(\mu\mu_o)^{1/2}$. The viscous time scale for electro-spreading of the drop can be found as ($\tau_v = (\mu\mu_o)^{1/2}(R_{max} - R_0)/\eta\sigma$), where R_{max} and R_0 are the maximum and initial base radius of the drop. The response time of the drop will never be smaller than the imposed actuation time, yet it can be delayed by the different factors considered in this study. Thus, if this viscous time scale is considered as an additional time for the drop to respond, the total response of the drop is the sum of τ_f and τ_v , and the universality of the response time of the drop due to AC electrowetting can be studied, as seen in Fig.3.6.

Based on the present study, the drop response time is noticed to be dominated

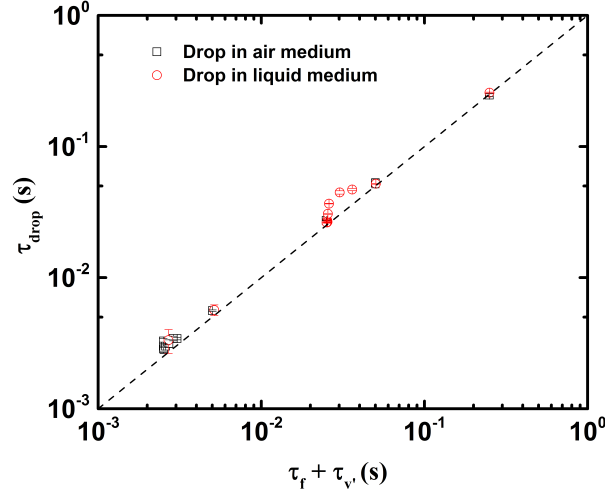


Figure 3.6: Response time of the drops for different conditions of electrowetting. Linear relationship between the response time of the drop τ_{drop} and the combined effect of the actuation time of the applied wave and the viscous time scale ($\tau_f + \tau_v$). For τ_v calculations, all liquids in Table 3.1 are considered.

by the actuation time of the external force, with marginal influence from the applied voltage and the viscosity of both drop and liquid medium. Results for different operational conditions present an agreement with the proposed corrected drop response time, where these modifications are based on the viscous effect and electrowetting numbers η . The drop response is highly influenced by the frequency and the viscosity due to the application of a single electrowetting perturbation. Therefore, it is crucial to consider the relationship between the time scales and the actuation time of the applied wave.

3.4 Conclusions

The present study details a thorough experimental investigation on the dynamic response of a sessile droplet to a single wave perturbation which is similar to the electrowetting scenario. This investigation includes the careful analysis of the drop

deformation before and after the perturbation. The similarity with a mass-spring-dampener system is explained and a simple approach is presented to correlate the fluid properties with the damping ratio. Furthermore, the comprehensive analysis includes the different implications of variation in the perturbation of the applied electrowetting actuation, and the thermophysical properties of the system. It was demonstrated that the periodic self-similar oscillatory behaviour was a strong function of the applied frequency of the electric wave and the systems properties primarily, viscosities of drop as well as medium. Out of phase response in the oscillations in the drop shape, compared to the applied frequency, was an outcome of viscous nature of the system and electrowetting properties. In the case of air medium drop dynamics, increase in the frequency witnessed the irreversible and marginal over-spreading along with the out of phase response. The irreversible spreading can be attributed to the contact line friction or contact angle hysteresis which has been avoided by performing the similar in liquid medium. The presence of viscous surrounding medium not only demonstrated the reversible spreading but the reduction in out of phase response was also noticed. Evidence was presented regarding the relationship between the drop response time to maximum spread in comparison with the actuation time. Interestingly the linear relationship was established between these two responses provided the time scale contributing the electrowetting in addition to the viscous time scale of the system is considered. The additive time response is a representation of electrowetting number which is required to be studied for a better understanding of attainment of equilibrium configuration in electrowetting where the equilibrium contact angle is presented as the outcome of the initial actuation.

Chapter 4

Induced coalescence of sessile droplets by a single wave of electrowetting¹

4.1 Introduction

As we discussed in the Introduction chapter (Chapter 1), coalescence and electrocoalescence are important for numerous applications [148–151]. Electrocoalescence is the merging of two liquid drops under the influence of an electrical field [149]. The drop can be either a sessile drop or a pendant drop, but interestingly the majority of the literature focuses on electrocoalescence of pendant or suspended drops [149, 152–155]. The importance of studying the coalescence of drops is related to cloud formation [156], viscous sintering [157], two-phase separation [158], emulsion stability [159], and spray cooling [160]. Drop coalescence is linked with the minimization of surface energy [87]; upon coalescing, the surface area of the final drop is less than the combined surface area of the two separate drops. In the case of sessile drop coalescence, apart from the charged liquid-fluid interface, the

¹A modified version of Chapter 4 of this thesis will be prepared for submission to a suitable journal as: Juan S. Marin Quintero, Hafijur Rahman, Markus Cäsar, and Prashant R. Waghmare, “Induced coalescence of sessile droplets by a single wave of electrowetting”

charged solid-liquid interface is also an additional factor that must be considered. A key aspect for studying the sessile drop or the spreading drop coalescence is the merging of two drops at the three phase contact line (TPCL) rather than at the liquid-fluid interface. Coalescence without any electric field is also a classical subject that has been studied in detail and a universality for the coalescence or mass transfer between drop has been established [150]. Different techniques have been developed to deposit two drops on a flat substrate in such a way that the desired coalescence occurs. Some techniques include: a) allowing both the drops to attain an equilibrium differently and the operation distance between two drops managed so that coalescence at TPCL can be observed [85]; b) generating the second drop from the hole drilled to the substrate and pumping the liquid from the bottom of the substrate until the coalescence can be noticed at the TPCL [161, 162]; and c) producing drops with jetting systems and observing the coalescence of two spreading drops [87]. For the benefit of maintaining consistency, the coalescence terminology used in this chapter is associated with sessile drop coalescence.

In the process of coalescence, a small bridge is formed at the TPCL connecting the two drops for the purpose of mass transfer. The growth of the bridge is the representation of the mass transfer rate. Hence, for such scenario, the bridge growth with respect to time is the key quantifying parameter [85]. The coalescence can be characterized by the behaviour of the bridge growth dynamics, which has two dimensions namely, the vertical height (with respect to the substrate) and the radius of the bridge (which is measured parallel to the substrate). It is found that the radius growth of the bridge, which grows in lateral direction, has a dependency on

the viscosity of the liquid that can be seen as $r \sim t$ for high viscosities [88, 89] or as $r \sim t^{(1/2)}$ for low viscosities [89, 90]. Yet, for both viscosities, the bridge height grows as $h \sim t^{1/3}$ in the initial stage, and later in time slows down [86]. The surface tension drives a motion of the TPCL that merges the two drops to form a larger drop with a smaller surface area [88]. Once the bridge is formed, the thermophysical properties of the liquid start playing a role; as the initial bridge growth starts, the viscosity and the density of the liquid, in combination with the surface tension, decide the growth dynamics [89]. This role can be represented by the Reynolds number $Re \sim \rho \sigma_{DF} R / \mu_d^2$, where ρ is the fluid density, σ_{DF} is the interfacial tension of the drop and the surrounding medium, and μ_d is the viscosity of the drop. Here, the capillarity velocity ($U_c = \sigma_{DF} / \mu_d$) is the characteristic speed and the radius of the bridge (R) is the characteristic size [89]. For Reynolds numbers smaller than the unit, it is a viscous coalescence, where the early stage is characterized by a significantly larger capillarity in the droplets that relaxes very quickly by linking the two drops [163]. However, for Reynolds numbers greater than one, the dynamics are dominated by the inertial forces. For water, it is considered to be always in the inertial regime.

In the case of electrocoalescence, the interface is charged and for pendant drop electrocoalescence, drops are charged by the needle and the coalescence dynamics at drop-medium interface are studied [152, 153]. If the suspended or interacting traveling drop coalescence is investigated, the drops are surrounded by an immiscible fluid through which the interface is charged before the coalescence [149, 154, 155]. For sessile drop coalescence, the drop is charged during the flight

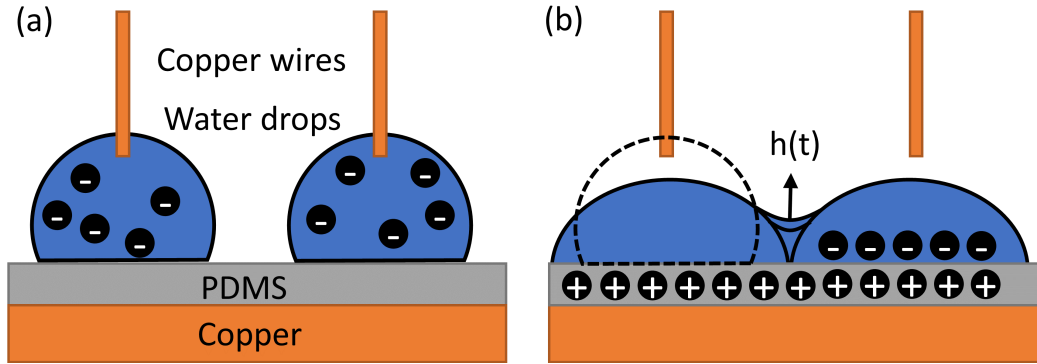


Figure 4.1: Schematic of two water drops on a PDMS layer on top of a copper substrate, with a wire of copper on top of each. (a) No voltage is being applied, the charges and dipoles are freely distributed inside the drops. (b) Voltage is applied, the charges reorganize, and the drops spread and eventually detach from the top electrode. The base diameters increase to generate the drop coalescence where the minimum height $h(t)$ characterizes the bridge height and growth. Dashed lines represent the original drop before the voltage is applied.

before impinging on the substrate [164, 165], or the drop spreading is influenced by electric field and eventually this electrospreading results in electrocoalescence [84, 166–168]. The later one is commonly used for studying the electrocoalescence and the externally actuation of the electric field, which is similar to the electrowetting case of a drop. Thus, the coalescence of two spreading drops influenced by electrowetting is researched. Here, we have adopted the same approach for which we have devised a specialized drop deposition mechanism and the details of it will be discussed in the experimental section.

A simple sketch is presented to illustrate the different stages of the proposed experiments; in Fig.4.1(a)(before applying an electric field) two drops are placed over a copper substrate with a PDMS (Polydimethylsiloxane) coating on top of it. This additional coating acts as a dielectric that enhances the breakdown limit [15]. The drop has ions which are dispersed at will inside the drop, and a copper wire is

inserted inside the drop at the centre to transmit the electricity. In Fig.4.1(b), when the electric field is applied, and the ions get reoriented and reorganized, both the drops spread instantaneously. Based on the separation distance between the wires, i.e., drops, the attainment of the equilibrium sessile drop formation or coalescence of two sessile drops can be witnessed. The initial insertion depth of electrodes inside the drop and the applied voltages will decide whether the electrode will remain in contact with the drop for the entire duration. One can also study the electrocoalescence by triggering the electrospreading of only one drop, in which case the coalescence can also take place with the electrode being immersed in the drop or detached from the drop. The consequences of the electrode being in contact with the drop can result in numerous unwarranted cases. The results of different arrangements of electrodes is discussed in detail in Fig. 4.2.

The first observations are pertinent to the single electrode electrocoalescence, panel presented in Fig. 4.2(a). It is noteworthy to mention that there is a significant difference in the response of the electrocoalescence according to the way in which the electric field is applied to a single drop or both drops. For instance, if the electric field is applied to only one drop, at the initial stage the drop connected to the wire will spread and, as the moving TPCL approaches to a stagnant drop's TPCL, the stagnant drop marginally gets attracted towards the spreading drop and eventually coalescence initiates. Albeit this method can effectively induce coalescence, it will be always an asymmetric coalescence, and during the bridge formation and growth process, the shape of the drops are not symmetric as depicted at all times (except $t = -1.86ms$) in Fig.4.2(a). Please note that the initial time $t = 0ms$ is always con-

sidered at the onset of the bridge formation. The asymmetric coalescence inevitably generates a horizontal displacement of the bridge towards the drop with the lower contact angle [85], which in this case is the drop spreading due to electrowetting. The initial coalescence is governed by the bridge geometry, which can be described with the contact angles of the drops just before coalescence. Therefore, the bridge growth dynamics will be significantly different in every case with respect to the applied voltages [86, 87]. However, this additional lateral displacement restricts us to characterize the bridge growth since the bridge and liquid-medium interface are of irregular shape. This motivated us to use two electrodes instead of a single electrode.

Figure 4.2(b) demonstrates the arrangements with two electrodes for electrocoalescence of two electrospreeding drops. In this particular case, both droplets spread until both moving TPCL are in contact. Surprisingly, a repulsion between the two drops, instead of coalescence, was witnessed, as shown in Fig.4.2(b). The effect of the charges accumulated at the interface of the droplets in the spreading, in this case similar in nature, creates a electrostatic repulsion [34, 167, 169]. Quillet et al. [34] observed the presence of charges at the interface of the drop that create repulsion forces and prevent coalescence. This electric field near the contact line has a high magnitude, but it rapidly decreases above the contact line [84] that causes a varied repulsion magnitude along the drop-drop interface. However, the coalescence sporadically occurs along the interface at a location where the electrostatic repulsion is low, which leads to induce coalescence at a random location at the liquid-liquid interface, i.e., above the TPCL rather than at the TPCL. Therefore, this

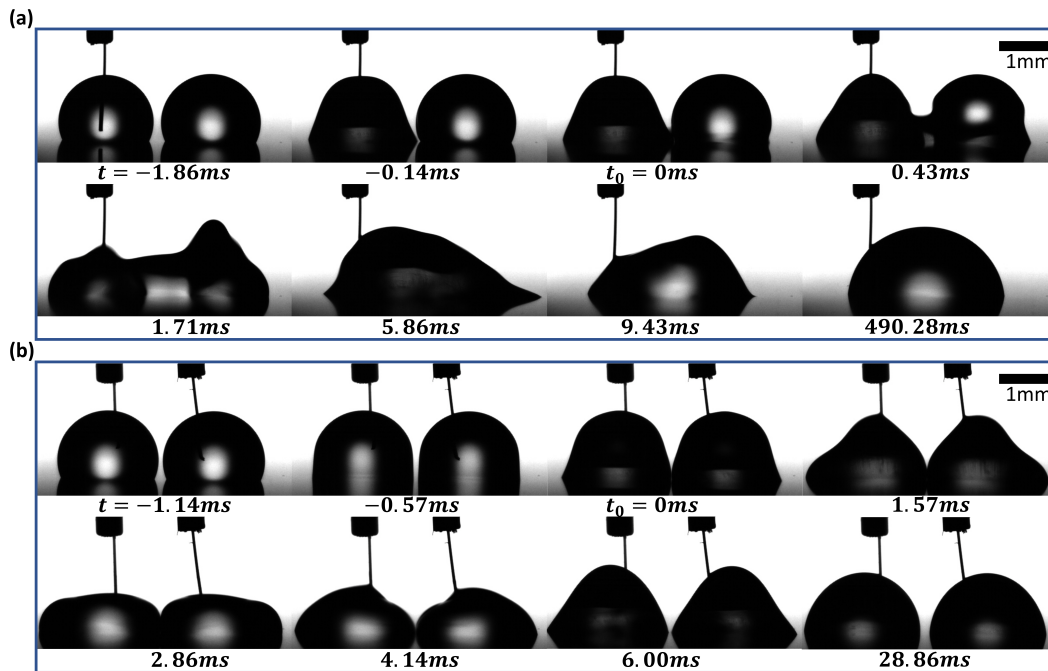


Figure 4.2: Drops response to a single wave perturbation by electrowetting. The drops, with a viscosity of $0.91mPas$ and separated approximately by $2.2mm$ centre to centre distance, were submitted to a wave of $350V$ at $100Hz$. (a) Snapshots presenting the induced electrocoalescence by applying the electric field to a single drop. The right drop is slightly attracted to the left drop which is spreading. Once the drops coalesce, the bridge grows vertically and moves horizontally simultaneously. (b) Snapshots presenting the repulsion experienced by both drops submitted to electrowetting. Once the drops spread and touch each other, the repulsion forces prevented the coalescence and generated that the drops spread outwards and do not coalesce.

method also guarantees an inconsistent and highly likely asymmetric coalescence. Another alternative is to use one electrode in a horizontal orientation instead of a vertical one. In this case, the two drops will spread and eventually coalesce [170], but the drop shape gets altered due to the horizontal wire arrangement. Moreover, the location of the wire inside the drop from the surface or from the tip of the drop influence the outcome significantly, and a critical distance for coalescence is required for successful coalescence [170]. Therefore, we diverted our attention to an arrangement where we can spread the drop by means of an electric field, but at the same time the role of the electrode can be avoided. This can be achieved by allowing the drop to detach from the electrode after it starts electrospreading. The single drop detachment from the electrode due to electrowetting on dielectric (EWOD) has already been studied [139, 171], and it was observed that after the detachment, at low frequencies, the contact angle remained close to the apparent contact angle predictions made by Young-Lipmann's equation. The ultimate motive for drop's detachment from the electrode is to eliminate the repulsion between charges at the drop-drop interface, particularly at TPCL. Therefore, if the drop detaches from the electrodes, the inertia will facilitate the drop spreading with a spreading equivalent to the electrospreading and, as the two TPCL merge, a bridge growth similar to the symmetric coalescence can be observed.

For a symmetric coalescence, the bridge growth and its shape have a universal behaviour. For the coalescence of two sessile drops, in the absence of an electric field, the $1/3$ power law of the bridge growth is assumed respect to time [86], and it is desired to verify if it is applicable for this electrocoalescence scenario

achieved by a novel method. The experiments for sessile drop coalescence, in the absence of any electric field, have always been developed with a fixed separation distance between the two drops. The considered drop-liquid combination enables to achieve a coalescence without a finite velocity of the TPCL. Yet, it has not been understood the role of the moving TPCL on the coalescence dynamics and bridge growth. Though a few studies relate electrowetting and coalescence, a relationship between the voltage, the frequency, the number of electrical/actuation waves, and the size and viscosity of the drop has not been presented in detail. Following this order of ideas, the present chapter was thought as a chance to correlate two different phenomena, which are the sessile drop coalescence and electrowetting, where nowadays there are not many studies with respect to this. It was expected to develop an innovative technique that can initiate an additional application for EW, and a simplified experimental setup for drop coalescence. Also, in this current study, the transient bridge growth in electrocoalescence, and the coalescence response as a function of the EW parameters were considered and analyzed. In like manner, the critical distance for the drop coalescence was observed and discussed, looking for a dependency on the EW or drop liquid properties. The main purpose of using EW for the drop coalescence was to observe the growth of the bridge by the union of two symmetrical drops, separated by a controlled initial distance, which is practically impossible to study for the case of sessile drop coalescence due to engineering as well to physical limitations. First, two drops of equal volume and same properties were deposited on the PDMS coated substrate. Then, by applying a voltage, the CA decreased and the base diameter increased, causing the two drops to reduce the separation distance between each other, until they started unifying. By

using this procedure, it could be studied how the coalescence can change according to the separation distance, the initial volume of the drops, the initial CA, and the spreading rate, i.e., TPCL velocity, which can be controlled by the applied electric field and the duration of it.

4.2 Experimental setup

The electrocoalescence experiments were conducted using an aqueous solution consisting of glycerol and $0.1M$ sodium chloride. Please refer to Table 3.1 for details of the thermophysical properties of the liquids. Drops with $3\mu L$ volume were generated using a goniometer (Drop shape Analyzer (DSA100), KRÜSS Scientific Instruments Inc.) equipped with disposable syringes (NORM-JECT 1mL, Henke-Sass Wolf GmbH). The droplets were positioned with a centre-to-centre distance in the range of $2mm < D < 3mm$, based on the volume of the drops and the maximum spreading of an individual drop. The drops were deposited on a copper substrate coated with a PDMS layer with a dielectric constant of $\epsilon_d = 2.8$. The copper substrates were cleaned with acetone to remove any oil particles on the surface and then with isopropyl alcohol to remove the acetone residue. The dielectric layer was deposited on the substrate by spin coating, so the thickness of the film was controlled by changing the time and rotational speed of the spinning process. Uniform thickness of $21\mu m$ was maintained in all cases. The AC voltage was applied using a waveform generator (294 100MS/s, FLUKE). The wave's frequency was set to be $f = 15Hz$ and $100Hz$ considering the first resonance frequency (at the second resonance node $n = 2$), which for a drop of $3\mu L$ in air medium is ap-

proximately $f_2 \approx 40 - 60Hz$ [30, 98]. The voltage produced by the waveform generator was strengthened by an amplifier (BOP 500, KEPCO), where the voltage applied to the drops was set to $200V \leq U \leq 350V$. The negative and positive electrodes of the circuit were connected to the copper substrate and the copper wires, respectively. The copper wires had a $60\mu m$ diameter and were positioned at the centre of the droplet with a vertical separation distance equal to the initial radius of the drop, and the location of the tip of the wire was maintained in such a way, that after the actuation of electrowetting, the drops detached from the wires. The drop spreading and the bridge growth due to coalescence were recorded at a frame rate of 15,000 frames per second by a high-speed camera (Fastcam Nova S9, Photron). The recorded videos were analyzed by an image processing software (ImagePro Premier 9.2, Media Cybernetics Inc.), where an edge detector function in the software was used to identify the liquid/gas interface; thus, the height of the bridge and the diameter of the drops could be measured with respect to time. Also, in an initial stage, the dynamic contact angle was measured by a shape analyzer software (ADVANCE, KRÜSS Scientific Instruments Inc.) until it reached equilibrium.

An ingenious mechanism was devised to precisely control the position of the two top electrodes as seen in Fig.4.3, where the separation distance between the wires could be adjusted, as well as the vertical position of the tip of the electrode with respect to the drop. The main objective of this instrument is to enable the placement of the wires at the centre of the drops to induced a symmetric spreading for both droplets. Also, as the insertion depth of the electrode inside the drop can be controlled, the detachment of the drops was facilitated for the drop coalescence.

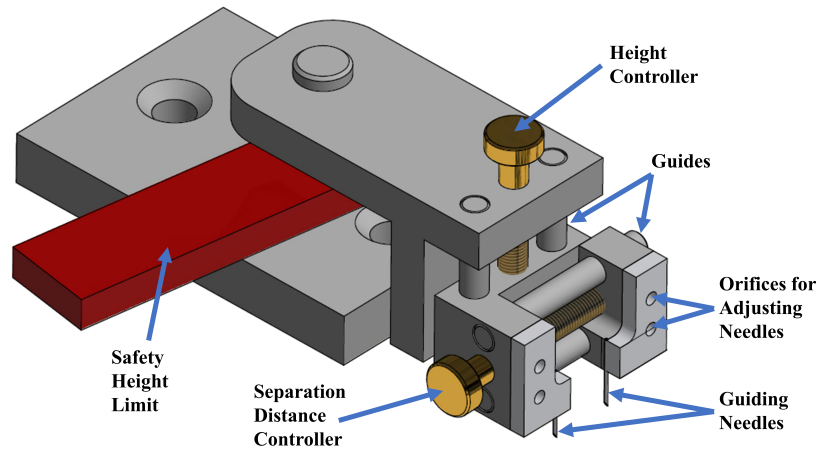


Figure 4.3: Experimental setup used to locate the two top electrodes at the centre of the droplets, with a desired separation distance. Both vertical and horizontal position could be controlled precisely to induce drop detachment after the voltage is applied.

And finally, the quick time span to make the arrangements (maximum 10 seconds) and to get the electrodes placed inside the drop at a desired and specific location allowed us to eliminate the role of evaporation before the coalescence. Thereafter, an extensive parametric study was performed to study the effect of the influencing parameters on the response of the electrocoalescence. The main parameters studied were the frequency and amplitude of the applied electrical signal, the separation distance between the drops, and the viscosity of the drops.

4.3 Prediction of the bridge growth

The governing equation for the growth of the liquid bridge can be obtained using the knowledge of the creeping flow approximation of Navier-Stokes equation. Since the velocity of the liquid bridge growth is very small, the creeping flow approximation

is introduced here to neglect the non-linear terms of the Navier-stokes equations. For steady flow conditions, the Navier-Stokes equations for a 2-D system under gravitational and electrostatic forces can be written as follows [172]:

$$\frac{\partial P}{\partial x} = \mu_d \left(\frac{\partial^2 u}{\partial x^2} + \frac{\partial^2 u}{\partial z^2} \right) + f_e \quad (4.1)$$

where, the drop spreading direction is in x direction, whereas the bridge growth is in z direction. In addition, u represents the horizontal component of the fluid velocity along the x axis, P is the pressure of the fluid, μ_d is the drop's viscosity, and f_e is the electrostatic force per unit volume. The properties of the liquid drop are assumed to be homogeneous. Since the drop is already detached from the electrodes during coalescence, in this case, electrostatic force can be considered as zero ($f_e \approx 0$). This is a preliminary attempt to get the theoretical modeling and we are working on developing the extensive model with f_e being non zero. Thus, Eq.4.1 can be reduced to:

$$\frac{\partial P}{\partial x} = \mu_d \frac{d^2 u}{dz^2} \quad (4.2)$$

In order to solve Eq.4.2, two boundary conditions are required. Since this is a bridge growth process, we are assuming there is no-slip at the TPCL during the bridge growth. And for the second boundary condition, we decided to consider the medium viscosity by considering the interface boundary condition $\mu_d \frac{\partial u}{\partial z} = \mu_m \frac{\partial u_m}{\partial z}$: $z = h(x, t)$, which implies the tangential stress balance at the drop-fluid interface. Then the solution of Eq.4.2 can be found as:

$$\mu_d u = \frac{\partial p}{\partial x} \frac{z^2}{2} + \left[\left(\mu_d \frac{\partial u}{\partial z} \right)_{=h} - \frac{\partial p}{\partial x} h \right] z \quad (4.3)$$

If air medium is considered, the viscosity of the drop is several orders of magnitude above the viscosity of the medium ($\mu_d \gg \mu_m$), thus the first term inside the square bracket can be neglected. In addition, another boundary condition at the liquid-drop interface can be derived from the Young-Laplace equation, in which the normal stress balance can be written as [20, 173]:

$$\frac{\partial p}{\partial x} = -\rho_m g \frac{\partial h}{\partial x} - \sigma \frac{\partial^3 h}{\partial x^3} \quad (4.4)$$

where σ is the surface tension of the drop-medium interface. The first term is the static pressure head due to medium and the second one is the pressure along the curvature. Using Eqs. 4.3 and 4.4, the flow rate can be simplified to:

$$Q = \int_0^h u(x, z, t) dz = \frac{h^3}{3\mu_d} \left(\rho_m g \frac{\partial h}{\partial x} + \sigma \frac{\partial^3 h}{\partial x^3} \right) \quad (4.5)$$

Utilizing the conservation of mass for a thin strip of fluid film of thickness dx , the relationship between the change in the height of the strip and the flow rate per unit depth can be obtained as:

$$\frac{dh}{dt} + \frac{dQ}{dx} = 0 \quad (4.6)$$

Now, for an air medium scenario, after combining Eqs.4.5 and 4.6, the lubrication equation in one dimension, for symmetric drop coalescence, can be expressed as:

$$\frac{dh}{dt} = -\frac{1}{3\mu_d} \frac{d}{dx} \left[h^3 \left(\sigma \frac{\partial^3 h}{\partial x^3} \right) \right] \quad (4.7)$$

The resulting equation is a non-linear partial differential equation that describes the growth rate of a liquid bridge between two spreading drops. Aiming to reduce the governing parameters, a nondimensional study of the governing equation (Eq.4.7) can be performed. The initial base radius of the drop (R_0) was selected as the length scale, while the time scale found in Chapter 3 ($\tau_{sum} = \tau_f + \tau_{v'}$) was used as the characteristic time scale. Involvement of this timescale allows us to consider the electrowetting effects even though we have not considered the equivalent body force in the momentum equation (Eq.4.1). In this time scale $\tau_f = \frac{1}{4f}$ is the imposed actuation time of the applied frequency, and $\tau_{v'} = \mu_d(R_{max} - R_0)/\eta\sigma$ is the viscous time scale for a electrospreading drop. Subsequently, the nondimensional form of Eq.4.7 can be found as:

$$\frac{\partial h^*}{\partial t^*} = -\frac{1}{3} \times \frac{d}{dx^*} \left[h^{*3} \frac{\tau_{sum}}{\tau_v} \frac{\partial^3 h^*}{\partial x^{*3}} \right] \quad (4.8)$$

Owing to the high complexity involved in obtaining the numerical solution of Eq.4.8, a scaling analysis was incorporated into the investigation to obtain approximate results. The final expression for the dimensionless height (h^*) can be obtained as a function of the dimensionless time (t^*) as [86]:

$$h^* \sim \phi \left\{ \frac{t^*}{\left(\frac{\tau_{sum}}{\tau_v} \right)} \right\}^{\frac{1}{3}} \quad (4.9)$$

where an empirical constant $\phi = f(\mu_d, \eta, f)$ was used. Therefore, the results were focused on the effect of η , $D/(2R_0)$, and Oh which correspond to the governing factors of electrowetting number, separation distance, and Ohnesorge number, respectively. In addition, the effect of the frequency was also considered, but only for one frequency below and one frequency above the first resonance frequency. It is noteworthy to mention that this is a preliminary attempt to get the theoretical model, and a detailed modeling approach is warranted to get the desired accurate solution.

4.4 Results and Discussions

In the case of the electrode being in contact with the drops, a repulsion at the TPCL was observed. In order to reduce or eliminate the repulsion effects of the electrostatic forces, a detachment mechanism was developed that allowed to observe similar coalescence for both drops with equal spreading rate. For a predetermined separation distance that is larger than the base diameter of the equilibrium sessile drop configuration, the coalescence can be studied while maintaining the separation distance smaller than the base diameter of the drop representing the Young-Lippmann's contact angle. Once the drops detach and continue to spread, the coalescence takes place at the moment both TPCL meet with each other, provided the electrode is not in contact with the drop. With different separation distances or

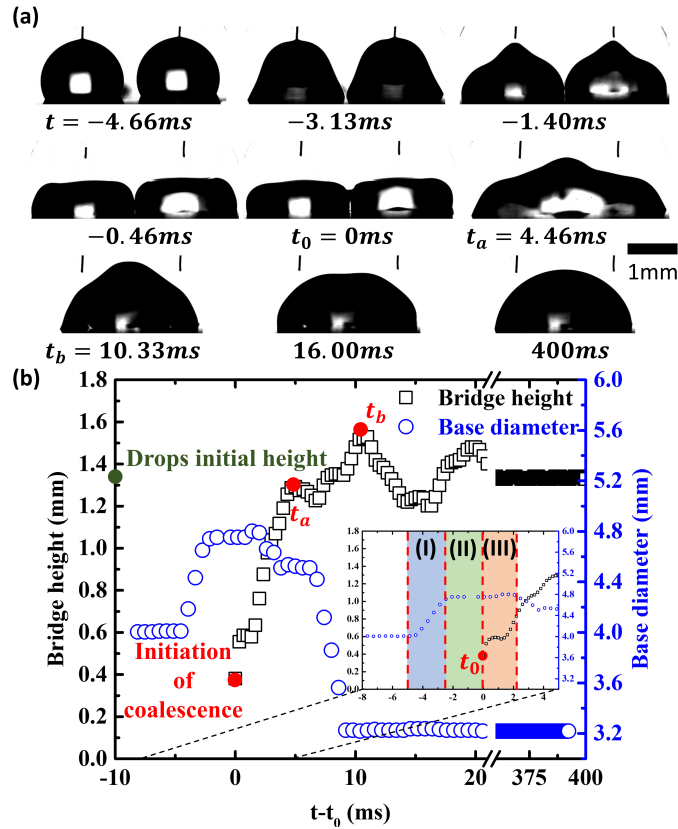


Figure 4.4: Drops response to a single wave perturbation by electrowetting. The drops, with a viscosity of 0.91mPas and separated approximately by 2.4mm centre to centre distance, were submitted to a wave of 350V at 100Hz . (a) Snapshots presenting the induced electrocoalescence by applying the electric field to both drops and inducing the detachment from the top electrode. (b) Bridge height vs time, for the previous case. After the drops started to coalesce, the relevant events are highlighted in the plot. The moment when the drops started to coalesce was set to be $t_0 = 0\text{ms}$, therefore, times before coalescence have negative values.

drop volumes, along with an applied voltage and frequency, a varied range of coalescence mechanisms can be studied. Figure 4.4(a) shows the case where the drops coalesced with an actuation wave of $350V$ at $100Hz$. As mentioned earlier, the arrangements are made in such a way that the bridge growth starts at the moment the drops are detached from the electrodes. In all the cases, the drop liquid properties, along with the applied voltages and frequencies, dictate the contact line velocity. Based on the contact line velocity we have observed different coalescence mechanisms. This contact line velocity can be altered by changing the electrowetting parameters, which can be studied by varying the electrowetting number (η) and the drop liquid properties, that can be represented in terms of the Ohnesorge number (Oh). Before we scrutinize the role of these two primary nondimensional numbers, we would like to explain the coalescence process as depicted in Fig. 4.4(b).

The inset figure of Fig. 4.4(b) demonstrates the drop spreading before the coalescence (Zone I), therefore the bridge height is not measurable before t_0 , i.e., the initiation of coalescence. Before the electrowetting is triggered (approximately at $t = -5ms$), the base diameter is constant. Please note that the distance between the two extreme positions of TPCL of both drops is termed as base diameter, which is not a base diameter of the single drop. After the drops get actuated due to electrowetting, the rapid spreading can be witnessed and eventually both TPCL merge for the coalescence. Before the coalescence starts, the base diameter momentarily attains a constant magnitude (Zone II). Thereafter, the bridge rapidly grows with no change in the base diameter (Zone III). Then, as the bridge becomes larger than the initial single drop base radius, the drop starts to demonstrate dewetting or re-

ceding at TPCL. At this point the bridge height is smaller than the initial height of the drops. The instant at which the bridge attains the height equal to the initial drop height is denoted as t_a , as presented in Fig.4.4(b). At the noncoalescing side of TPCL for both drops, where the influence of the other drop is absent, drop recoiling or receding dominates, which can be attributed to the minimization of the surface area or energy. Therefore, despite the oscillatory growth in the middle (coalescing side of the TPCL), the drop's base continues to recoil from the noncoalescing side. The maximum recoiling continues until the maximum bridge height is observed (t_b) and after that, even if the drop-medium interface oscillates, the base diameter remains constant. The sudden decrement in the base diameter is facilitated when the bridge oscillated and assisted the further spreading.

4.4.1 Effect of electrowetting number

The applied electric field is the actuation force that provokes the drops to spread and come into contact. The magnitude of this actuation force can be estimated based on the electrowetting number η . The range of η was decided based on the applied voltage U , and was fixed for the dielectric constant ε_d , the dielectric thickness d , and the surface tension σ parameters. The lowest limit for the applied electrowetting number ($\eta = 0.16$) was selected based on the experimental observation of sufficient applied force to create drop motion and drop-fluid interface oscillations. However, for this low η , the drops did not detach from the electrode and could not spread to observe the coalescence. Hence, the lowest electrowetting number for successful coalescence was observed to be $\eta = 0.26$, as seen in Fig.4.5. For the upper limit, the maximum applied electrowetting number ($\eta = 0.50$) was based on the contact

angle saturation to prevent the deviation from Young-Lippmann's equation [18, 42], so we restricted the upper bound below this actuation. After applying the actuation force, both drops equally spread and detach from the top electrode. It was observed that the drops did not immediately start coalescing after coming together due to the remaining repulsion forces at the interface. When the ions inside the drops reorganized and the repulsion force weakened, coalescence began. However, it is beyond the scope of this study to comment on the delayed coalescence or the timescale pertinent to this delay. It is reported that the oscillations of the interface of the sessile drop depend on the applied frequency and its proximity to the resonance frequency [30, 98]. The first associated resonance frequency (f_2) for a water drop of $3\mu L$ is approximately $f_2 \approx 40Hz$. Therefore, in order to avoid the influence due to the closeness to the resonance frequency, the bridge growth was studied for two applied frequencies ($15Hz$ and $100Hz$), which are under and above the resonance frequency, respectively.

For the frequency below the resonance frequency ($f \leq f_2$), we observed a significant influence of η on the coalescence that can be seen in Fig.4.5(a). The initial bridge growth – growth until the bridge height is approximately equivalent to the drop radius – is presented in the inset figure, where it can be noticed that the initial growth rate is independent of η . It can be clearly seen that the initial bridge growth follows an exponential growth with an exponent of $1/3$. This prediction matches with the proposed bridge growth from Eq.4.9. Yet, after the bridge had a height close to the initial base radius of the drops, the influence of η can be noticed. For lower electrowetting numbers, the drops coalesced with larger initial contact angles

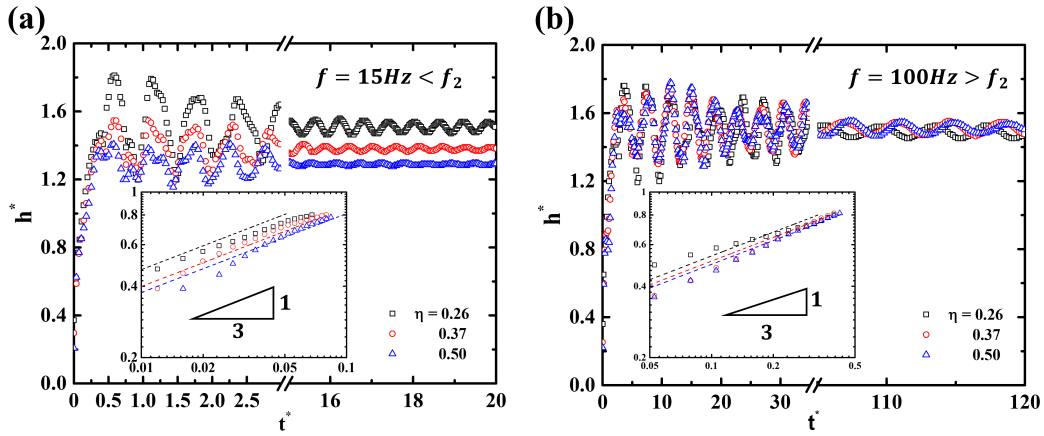


Figure 4.5: Effect of electrowetting number on the bridge growth for drops in air with $Oh = 0.0035$ and separated by a distance $D/(2R_0) = 1.15$. (a) Bridge growth for applied frequency under the resonance frequency, and (b) Bridge growth for applied frequency above the resonance frequency. The initial bridge growth is presented in the inset figures.

compared to the drops with higher electrowetting numbers or stronger actuation forces, i.e. higher voltages. It has been demonstrated that the bridge growing velocity is affected by the initial contact angle of the drops immediately before the coalescence [87]. In the case of sessile drops with contact angles lower than 90° , a larger initial contact angle speeds up the bridge growth. For the considered scenario where the drop's contact angle is always greater than 90° , the first point of contact for the coalescence is in function of the separation distance and the actuation magnitude, and it can be either at TPCL or at the drop-medium interface. As the actuation force is increased (increment in η), the larger spreading can be witnessed for a given time, due to which the first point of contact to initiate the coalescence, comes closer to the TPCL. Unfortunately, due to experimental limitations as well as the repulsion at the TPCL, the ideal scenario could not be achieved where the drops can always coalesce at TPCL. This reveals the importance of the location of the first contact point where the coalescence triggers. If this point is

farther from the TPCL, the bridge growth was faster and if it came closer to the TPCL with the increment in η , a slower bridge growth was noticed. Once the coalescence begins, based on the initial rate of the bridge growth, the dynamics in the bridge growth can be witnessed. Interestingly, with this growth rate, the oscillatory behaviour in the bridge growth, resembling the inertial oscillatory motion, is also observed. Here, as the first point of contact comes closer to the TPCL, the growth rate decreases, and thus the maximum height in this oscillatory motion decreases. After attaining the maximum bridge growth, the newly formed drop attempts to regain a new equilibrium through the decayed oscillatory motion in bridge height. It is evident that larger the bridge growth rate is, the longer the waiting period for the drop to attain the equilibrium. These oscillations can be studied by following a similar analysis from Chapter 3, i.e., an ideal damped harmonic oscillator described by Eq.3.2. The sudden growth and oscillatory motion at the drop-medium interface has consequences on the drop's base as well. The finite pinning force at the TPCL of both drops is primarily function of the contact angle hysteresis, but also of the surface energy of the substrate and the interfacial tension of the fluids. At certain growth rate, the induced force at the TPCL during the coalescence is sufficient to overcome the adhesion due to the contact angle hysteresis and to slip the TPCL. This slip is the indication of a change in the base diameter, as detailed in Fig.4.4(b). One can completely eliminate this slip-stick motion by performing experiments of a substrate without contact angle hysteresis, but it is challenging in air medium. Nevertheless, one can argue that if the actuation frequency is kept high enough, that will always ascertain the higher force at TPCL to depin the TPCL. Therefore, we performed a similar study with a frequency with at least one order of magnitude

higher ($f = 100$), and we also made sure that this frequency avoided the natural frequency. As anticipated, at the higher frequency the role of η was diminished.

4.4.2 Effect of separation distance

As mentioned earlier, the first point of contact for the coalescence can be maneuvered by the separation distance, therefore we attempted to study this hypothesis. In spite of the fact that the separation distance is only a geometrical parameter, it greatly affected the dynamics of the coalescence bridge. The range of the separation distance was based on the minimum and maximum distance where the coalescence can be witnessed. The minimum distance is equal to the base diameter of the sessile drop when the drop's contact angle is less than 90° , and to the spherical diameter of the drop for drops with a contact angle of $\geq 90^\circ$. The details of the geometrical parameters of a drop under the spherical cap assumption can be found in Chapter 2, as presented in Fig.2.1. From the closer observation of Eq.4.10, it can be seen how the initial bridge height is mainly a function of the separation distance D and θ , in which the later can be approximated to be θ_{app} as a function of the electrowetting number η from the Young-Lippmann's equation as:

$$h_0 = -r\cos\theta \pm \sqrt{r^2 - \frac{D^2}{4}} \quad (4.10)$$

where r is the radius of the sphere by assuming a spherical cap geometry. Hence, the initial bridge height can be presented as a function of $D/(2R_0)$ and η , as seen in Fig.4.6(a). If the theoretical initial height occurred below the substrate, i.e.,

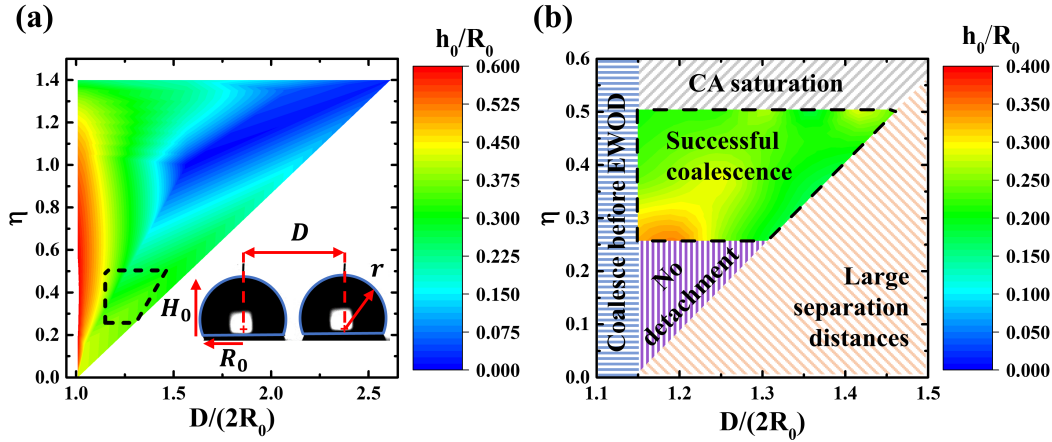


Figure 4.6: Initial bridge height of water drops in air with $Oh = 0.0035$ as a function of the nondimensional separation distance $D/(2R_0)$ and electrowetting number η . (a) Theoretical results of initial bridge height obtained from Eq.4.10 from all possible ranges. Inset figure presents all the geometrical parameters of the drops, including the initial height of the drops H_0 , the initial base radius of the drops R_0 , the equivalent radius of the sphere r , and the separation distance between the drops D . (b) Experimental results of initial bridge height for successful conditions, along with the four different experimental limitations.

$h_0 < 0$, the drops in reality will not coalesce. The range of η was selected based on the Young-Lippmann's equation in which the maximum η is approximately 1.4 with a corresponding apparent contact angle of zero. The expected height, calculated from Eq.4.10, is compared with the experimental results obtained from the water drops, shown in Fig.4.6(b). For the practical case, as mentioned in the previous sections, the range of η ($[0.26, 0.50]$) was based on sufficient driven forces to induce the spreading, detachment, and coalescence of the drops, but always below the contact angle saturation. While the separation distance range $D/(2R_0)$ ($[1.15, 1.30]$) was established for successful coalescence conditions, it was also observed that coalescence could also be obtained for separation distances of $D/(2R_0) = 1.44$, but above this value the drops never merged. It is interesting to observe how the initial bridge height is reduced by increasing the separation distance and the electrowetting

number simultaneously, which occurs due to the possibility of the drops to further spread and collide in a position closer to the TPCL. Yet, in reality, the electric field, and therefore the repulsion forces, are higher close to the three phase contact line [84, 174]. This additional effect, which is not considered in the purely geometrical observations from Eq.4.10, will prevent the coalescence at the TPCL as observed at $t = -1.40ms$ from Fig.4.4(a). Thus, the coalescence will be delayed until the drops touch in a higher height, where the repulsion forces are lower, and start to fuse, as observed at $t = 0ms$ in Fig.4.4(a).

After finding out the appropriate domain of the separation distance, a detailed parametric study was performed to observe the variations in the coalescence. Figure 4.7 shows the role of the separation distance on the bridge growth and, as anticipated, this observation is similar to the previous one where the first point of contact for coalescence dictated the outcome of the coalescence behaviour. As we have noticed for lower η , similarly for the case of the low frequency, the drop's response was affected by the increment in the separation distance, as observed in Fig.4.7(a). The drops separated by smaller distances could meet with a greater contact angle prior to coalesce and with a reduced separation distance between the two extremes of the TPCL. All these factors generated a faster bridge growth with a greater maximum height, that will eventually influence the reduction of the base diameter and increment the magnitude of the equilibrium height. The additional distance created elongated final drops with a bigger base diameter that reduced the height of the final drop. As in the case of the electrowetting effect, for the high frequency, a lessen effect of the separation distance was observed, as seen in Fig.4.7(b). The

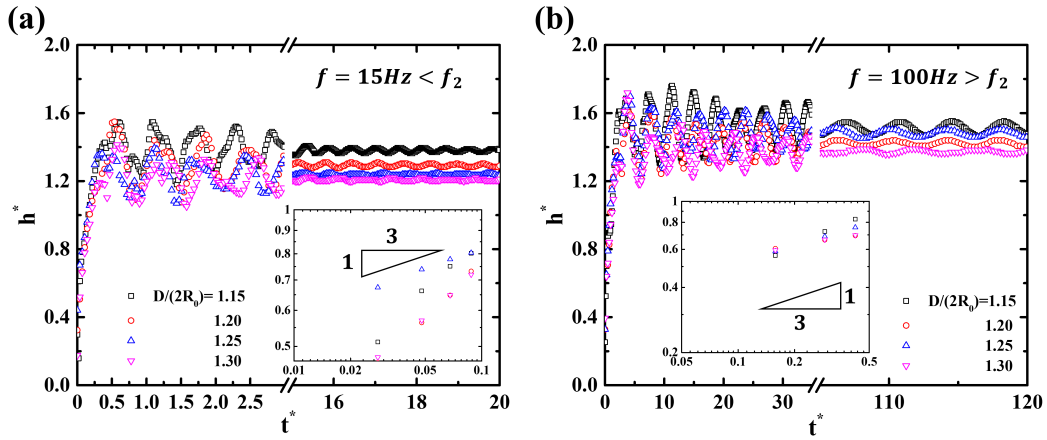


Figure 4.7: Effect of separation distance on the bridge growth for drops in air with $Oh = 0.0035$ submitted to an applied wave of $\eta = 0.37$. (a) Bridge growth for applied frequency under the resonance frequency, and (b) Bridge growth for applied frequency above the resonance frequency. The initial bridge growth is presented in the inset figures.

initial bridge growth remained unchanged for all the separation distances. The inset figures for Figs. 4.5, 4.7, and 4.8 demonstrate the linear bridge growth, and if we compare that with the proposed theory, it is evident that it follows the $1/3$ scaling law. However, all these considerations still ignore the influence of the viscosity of the drops, which is known to be a governing parameter in coalescence. A change in the viscosity will generate a different dissipation rate in the drops, and will affect the velocity at which the drops encounter before coalescence, as well as the attainment of the equilibrium. Hence, the following section is dedicated to study the influence of the Ohnesorge number in the bridge growth.

4.4.3 Effect of Ohnesorge number

The Ohnesorge number, $Oh = \mu/\sqrt{\rho\sigma R_0}$, was mainly modified by changing the viscosity of the drops. The selected range considered for Oh was from 0.0035 to

0.4386. The appropriate ratio between glycerol and water allowed us to attain this range. As studied in previous chapters (Chapter 2 and 3), the gain in the viscosity of the drop increased the response time of the drop, which implies a lower spreading velocity. Also, the higher Oh implies a stronger effect of the viscous forces compared to the surface and inertial forces, which will generate a higher energy dissipation and will decelerate the bridge growth [85, 175]. The Ohnesorge number has a bigger effect on the bridge growth response in the case of the frequency below the resonance frequency, as shown in Fig.4.8. The increment of Oh implies a longer time required for the drop to respond to the external actuation force and to restructure, as studied in Chapter 3. Hence, this delay will prompt smaller perturbations in the drop during the coalescence. The eventuality of the oscillatory motion and the magnitude of the maximum bridge height becomes less pronounced as Oh is increased. The change in the magnitude of the bridge height and the frequency of oscillatory motion is associated to the underdamped regime, in which the drop oscillates and the magnitude of these oscillations decay exponentially over time [143]. The deformation of the drops in the overdamped regime did not show capillary waves, and the time to reach the maximum bridge height was delayed [176]. An additional effect is witnessed for high Ohnesorge numbers, where the base diameter of both drops were completely pinned during the coalescence time. Thus, the base diameter of the new drop is larger to justify the spherical cap assumption, therefore, the drop flattens and lowers the equilibrium height.

The frequency above the resonance frequency induced more oscillation in the bridge growth after attaining the maximum height, as seen in Fig.4.8(b). The higher

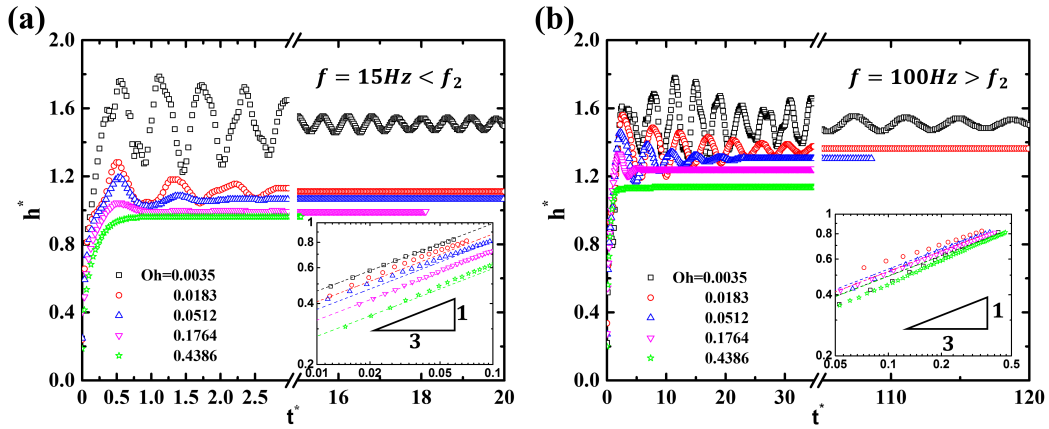


Figure 4.8: Effect of Ohnesorge number on the bridge growth for drops in air submitted to an applied wave of $\eta = 0.50$ and separated by a distance $D/(2R_0) = 1.15$. (a) Bridge growth for applied frequency under the resonance frequency, and (b) Bridge growth for applied frequency above the resonance frequency. The initial bridge growth is presented in the inset figures.

frequency implied a faster abrupt change in the shape of the drop, which increases the drop-fluid interface oscillations. In addition, it causes a higher velocity of the drops prior to coalesce, which also increases the velocity at which the bridge grows. All this additional considerations resulted in more kinetic energy and presented more oscillations than the experiments from the frequency below the resonance frequency. At the same time, these oscillations aided the depinning of the three phase contact line and reduced the base diameter of the new drop. The initial bridge growth was almost identical for all the Ohnesorge numbers following an exponential growth with an exponent approximately of $h^* \approx t^{*1/3}$. However, it is important to mention that the scaling analysis performed for the governing equation, resulting in Eq.4.9, can accurately predict the liquid bridge growth at the initial coalescence interval, within which the liquid bridge is smaller of the initial base radius of a single drop.

4.5 Conclusions

The electrocoalescence of sessile drops in air medium has been investigated where coalescence was triggered by a single actuation cycle of electrowetting. The electrocoalescence of sessile drops was achieved by generating the detachment of the drops from the electrode and by reducing the repulsion forces existing at the interacting interfaces of the drops. The sudden change in the contact angle of the drops will also generate some interface oscillations that will promote the drop coalescence. A modified theoretical approach, developed primarily based on the lubrication approximation, contemplates the electrowetting effect in the drop's coalescence and predicts the bridge growth between two coalescing drops. The time scale used in the nondimensional process was the sum of the actuation time of the applied frequency and the viscous time scale modified with the electrowetting number. This time scale considers the time required to reach the maximum spreading of the drops and, by using it as a time scale for electrocoalescence, the initial bridge growth presented a universal response. The effects of the electrowetting number, the separation distance, and the Ohnesorge number were investigated separately for two different frequencies, i.e., above and below the resonance frequency. For the case below the resonance frequency, all the parameters influenced the bridge formation by affecting the maximum bridge growth magnitude and corresponding oscillatory motion at the drop-medium interface. It was demonstrated that for a frequency above the resonance frequency, the operating parameters had less impact in the growth dynamics. In the case of a frequency higher than the resonance frequency, the dynamics at the three phase contact line were much quicker and in-

fluenced in the coalescence accordingly. Yet, for both frequencies, it was observed that the separation distance and the Ohnesorge number influenced the bridge growth and the equilibrium height. The higher separation distances reduced the contact angle at which the drops approached prior to the mass transfer, so it slowed down the bridge growth and reduced the magnitude of the maximum height attained by the bridge. Also, the combined effect of the electrowetting number and the separation distance was studied on the influence of the initial bridge height. The lower Ohnesorge numbers allowed the new drop to acquire a higher maximum height that was reflected in terms of motions at the three phase contact line. For the same scenario of low Ohnesorge numbers, the oscillations in the bridge height were granted in resemblance with the case of an underdamped mass-spring-dampener system. For higher viscous cases, i.e., higher Ohnesorge numbers, the equilibrium height was lower but with minimum oscillations, therefore, the attainment of equilibrium was in shorter period of time.

Chapter 5

Conclusion and Future Work

5.1 Overview and summary

The primary objective of this thesis was to investigate the dynamic response of sessile drops to perturbation cycles triggered by means of electrowetting. Therefore, this thesis addressed the transient dynamic response of sessile drops to an external actuation force. Our efforts were dedicated to understand the implications of applying an individual actuation wave to the drops aiming to reduce the operational time and power consumption involved in electrowetting.

First, in Chapter 2, a mathematical model was proposed based in an overall energy balance that contemplates the combined effects of the inertial, the surface tension, and the dissipation forces on the drop's oscillations. The capillary time scale was used as the characteristic time scale for the nondimensionalization of the governing equation, in which the key nondimensional numbers were the electrowetting number, the Roshko number, and the viscosity ratio. The theoretical results were compared with the experimental results to describe the transient response of drops due to electrowetting in a liquid medium. The proposed model

illustrates a notorious shift of the transient response depending on the applied frequency and the medium viscosity. It was noticed that, for low frequencies and/or viscous mediums, the drop closely follows the applied actuation wave. Yet, as the frequency or the medium viscosity increase, the drop lags from the response and cannot longer spread equally for both halves of the applied wave. This special case of out-phase response was studied thoroughly for additional waves. It was observed that the drops further spread after each applied cycle until attaining a steady oscillatory response. However, it was discerned that the time scale used did not consider the viscous effect nor the properties of the applied wave, as the voltage or the frequency. Hence, the natural extension of this investigation involved scrutinizing the first half of the applied wave and finding a time scale that quantifies all the thermodynamic properties of the liquids, as well as the parameters of the applied wave.

In Chapter 3, the transient dynamics of EWOD were studied for a single wave perturbation. The change in the drop's response was investigated considering the effects of the applied electrowetting perturbation and the thermophysical properties of the liquids. Special attention was dedicated for the maximum deformation of the drop in the first half of the cycle and the time required to reach this point. For the completeness of the study, drops in liquid and air medium were considered, which provided a better understanding of the transient response of the drop. In the case of air medium, interface oscillations that resemble the mass-spring-dampener system were perceived, and these oscillations remained after the application of the electrical wave. However, these oscillations were not observed in the liquid medium due to the different nature of the energy dissipation, which was provoked by the

liquid medium viscosity rather than the contact line hysteresis, as in the case of air medium. The time required to reach the maximum spreading, called as the response time of the drop, was compared with a new time scale that considers the thermo-physical properties of the liquids, as well as the applied frequency and voltage of the perturbation. It was observed a universal linear relationship between the response time of the drop and the proposed time scale.

Finally, the associated drop oscillations inspired us to use them to induce electrocoalescence of sessile drops by electrowetting. Based on the results obtained in the previous chapters, in Chapter 4 a method to guarantee electrocoalescence by applying a single actuation cycle of EWOD was experimentally investigated. The repulsion forces between the drops were reduced by inducing the detachment of the drops from the electrode. It was observed that the coalescence at the three phase contact line was entangled by the repulsion forces, but coalescence could be achieved by applying a single actuation cycle. The initial bridge growth was studied in detail, and compared with a theoretical model for drop coalescence that considers the effect of electrowetting. Hence, the bridge growth was studied as a function of the electrowetting number, the separation distance, and the Ohnesorge number. The combined effect of the electrowetting number and the separation distance on the initial bridge height were observed mostly as a geometrical consideration. Greater values of these two parameters allowed the drops to spread further and to initiate the coalescence at a point closer to the three phase contact line. The lower initiation height point slowed down the bridge growth and the magnitude of the maximum height attained by the bridge. In addition, it was observed how the Ohnesorge num-

ber affected the occurrence of droplet-medium interface oscillations, which affected the motion of the three phase contact line. As the Ohnesorge number increased, the oscillations were minimum and the new equilibrium height was attained faster.

In summary, this thesis contributes to the literature as follows:

- Describing the initial transient response of the drop to electrowetting experimentally and theoretically, which was commonly ignored.
- Developing a theoretical model, based on an overall energy balance, able to predict the dynamic response of a drop in liquid medium.
- Identifying and categorizing the transient response of a drop to electrowetting into in-phase, transitional, and non-responsive, as a function of the system parameters.
- Establishing a corrected timescale for AC electrowetting that incorporates the delayed time due to the thermophysical properties of the drop, but that also considers the electrical wave properties as the voltage and the frequency.
- Proposing a novel method to induce drop coalescence of a pair of sessile drops by means of electrowetting, where the repulsion forces were minimized by generating a drop detachment from the electrode.
- Delineating the bridge growth in drop coalescence and studying the influence of system parameters as the separation distance between the drops, the applied voltage and frequency, and the viscosity of the droplets.

5.2 Future works

The better understanding of the dynamic response of sessile drops due to AC electrowetting in air and liquid medium provides the opportunity for further studies as an extension of the current research. The conclusions presented facilitate the full description of the drop spreading due to electrowetting and explained how the shape of the drop evolves in time. Therefore, the time required to achieve the maximum spreading, or to attain a steady state oscillation, it can improve the usage of electrowetting for different applications. Also, the observations raised due to electrocoalescence can be used as a basis to study further drop's coalescence due to the application of external forces. These future works can be mainly divided into the study of liquid medium electrocoalescence and the design and characterization of a liquid lens.

5.2.1 Liquid medium electrocoalescence

Coalescence in a liquid medium presents a completely different nature from air medium scenario. The additional resistance generated by the surroundings prevents the fast process of coalescence, in which all the liquid trapped between the two drops needs to be removed before the drops can merge [177]. The time required to completely drain the liquid between the drop, referred as drainage time (t_{drain}), is in function of the Capillary number ($Ca = \mu V/\sigma$), where V is the characteristic velocity of the drops [178]. The increment of the medium viscosity leads to longer time required to move the trapped liquid due to the additional energy dissipation [179]. Thus, the film drainage decelerates which can delay or prevent coalescence

to occur [180]. However, the inherent nature of a drop in a liquid medium generates greater contact angles of the drops which speed up the coalescence of partially wetting drops [87, 163]. The induced detachment of the drops from the top electrodes is required to reduce the repulsion forces between the drops that prevents the electrocoalescence [34, 84]. Yet, due to the additional restriction from the medium viscosity, the drop detachment is reduced for liquid mediums, and is completely abolished for high viscous mediums.

Therefore, electrocoalescence prompted by a single actuation wave of electrowetting has an entirely different dynamic and considerations from the case of air medium. The reduced time granted for the drops to touch each other by the application of an external force is quickly removed to the oscillatory nature of the actuation force. Time for which drops are allowed to come into contact with each other is not sufficient to completely drain the confined liquid and start the coalescence. However, we observed that, under certain conditions, the electrocoalescence in a liquid medium can be generated by a single actuation cycle of electrowetting as shown in Fig.5.1.

The electrocoalescence process in liquid medium provokes that the initial bridge formed by the coalescence is considerably far from the merging three phase contact line or the substrate. Although two drops merge by removing the liquid between them, some liquid still remains underneath the bridge that needs to be drained as well. The time required to drain this liquid cramped under the bridge is also a function of the liquid medium properties. Hence, further investigation is required

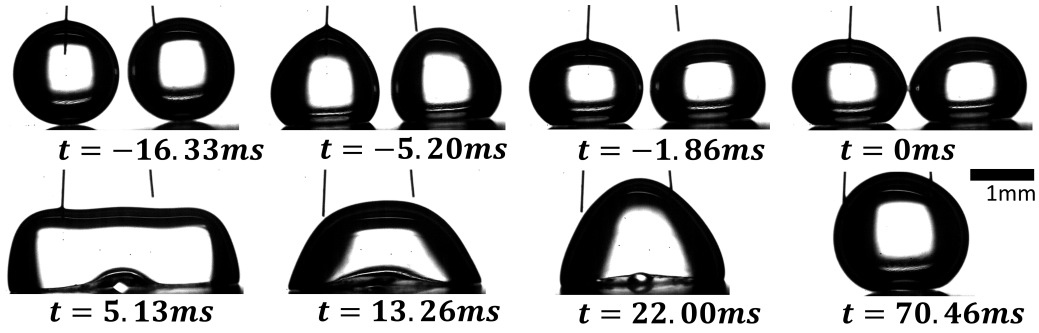


Figure 5.1: Liquid medium electrocoalesce for a single wave perturbation of electrowetting. The drops, with a viscosity of 0.91mPas and separated approximately by 2.2mm center to center distance, were surrounded by a liquid medium with a viscosity of 0.91mPas . The applied wave 350V and 35Hz was submitted for both drops. The snapshots present the initial spreading and detachment of the drops, and at $t = 0\text{ms}$ the drops started to coalesce. Once the bridge started growing for a height above the three phase contact line, some liquid remained under the bridge which was drained after some oscillations of the drop. After multiple oscillations in the shape of the final drop, all the oil is drained and the final drop acquired a spherical geometry.

to generate and describe the electrocoalescence of two sessile drops by means of a single actuation cycle of electrowetting.

5.2.2 Design and characterization of a liquid lens

Minimizing the size of the optical devices and the reduction in the number of mechanical components necessary for its operation allows a compact design and a faster focusing process. Existing mechanisms provide the feasibility to build tunable micro-lenses, but they have limited control on the change in the focal length of the optic device [73–76, 181]. Manufacturing a lens from a liquid interface has the potential to completely fulfill the operation requirements for a photonic device and can be driven by the surface tension forces [182, 183]. This concept can be achieved by depositing a liquid droplet on a transparent substrate and surrounding

it by an oil medium. Therefore, the focal length of the lens can be varied by modifying the curvature of the droplet-medium interface [77, 184]. The shape of the interface is usually characterized by the contact angle measured at the three-phase contact line [185]. Hence, electrowetting provides a reversible alternative to alter the shape of the drop by several tens of degrees, with low power consumption [18, 51, 105, 186]. Bearing in mind that the drop acts as a lens, the drop can be considered to be a plano-convex lens. The liquid-liquid interface acts as the convex side with a radii of curvature equal to the radius of the drop (r), while the liquid-solid interface is the planar side with an infinite radius of curvature. Following this idea, the Lensmaker's equation for a plano-convex lens can be simplified to [187]:

$$\frac{1}{f} = \frac{n_L - n_M}{r} \quad (5.1)$$

where f is the focal length of the lens, n_L and n_M are the refractive indexes of the liquid drop and the oil medium, respectively. If the drop's shape is assumed to always maintain the spherical cap geometry, Eq.5.1 can be rewritten as [22, 59]:

$$f = \frac{3V}{\pi(2 + \cos\theta)(1 - \cos\theta)^2(n_L - n_M)^3} \quad (5.2)$$

V represents the volume of the drop, and θ is the aforementioned contact angle of the sessile drop. Thus, the focal length of the lens can be mainly modified as a function of the applied voltage, described by the Young-Lippmann's equation as presented in Fig.5.2. Therefore, it can be seen how the focal length increases as the applied voltage increases. This result is intuitive by thinking that as the voltage is

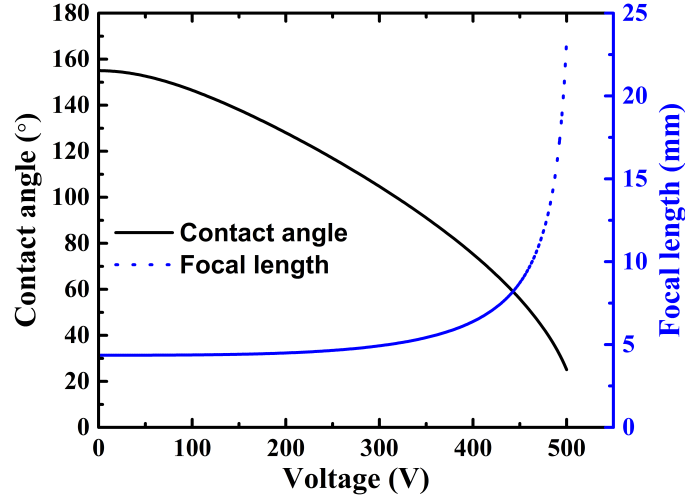


Figure 5.2: Theoretical results of contact angle and focal length of a liquid lens as a function of the applied voltage. Results are based on a drop of $3\mu L$ volume, submitted to AC EWOD with PDMS as an insulator layer with a thickness $d = 21\mu m$ and dielectric constant $\varepsilon_d = 2.8$.

applied, the drop spreads and increases the curvature of the drop which ultimately increases the focal length. However, due to the contact angle saturation, the drop no longer spreads following Young-Lippmann's equation beyond a critical voltage. Thus, the increment in the focal length after this point decelerates and reaches its maximum value.

These results are based on the assumption of steady conditions for AC EWOD, when the drop has completely reached the new equilibrium contact angle after numerous cycles. However, it is desired to reduce the operational times and costs involved in controlling a liquid lens, so the results obtained in this thesis can be extended into this context to obtain the minimum time required to achieve the desired focal length. It would be interesting to observe the effect of the transient dynamics of electrowetting on optimizing the operation of a liquid lens, which can be continued as future work.

Bibliography

- [1] J. Drelich, E. Chibowski, D. D. Meng, and K. Terpilowski, “Hydrophilic and superhydrophilic surfaces and materials,” *Soft Matter*, vol. 7, no. 21, pp. 9804–9828, 2011.
- [2] H. M. Ali, M. A. Qasim, S. Malik, and G. Murtaza, “Techniques for the fabrication of super-hydrophobic surfaces and their heat transfer applications,” *Heat Transfer: Models, Methods and Applications*, p. 283, 2018.
- [3] R. K. Upadhyay and P. R. Waghmare, “Green preparation of copper surfaces with wettability contrast for guided fluid transport and fog harvesting application,” *Materials Letters*, vol. 246, pp. 223–226, 2019.
- [4] A. Baldan, “Adhesively-bonded joints and repairs in metallic alloys, polymers and composite materials: adhesives, adhesion theories and surface pre-treatment,” *Journal of materials science*, vol. 39, no. 1, pp. 1–49, 2004.
- [5] D. Myers, *Surfactant science and technology*. Wiley Online Library, 2006.
- [6] J. Rafiee, X. Mi, H. Gullapalli, A. V. Thomas, F. Yavari, Y. Shi, P. M. Ajayan, and N. A. Koratkar, “Wetting transparency of graphene,” *Nature materials*, vol. 11, no. 3, p. 217, 2012.

- [7] G. Lippmann, *Relations entre les phénomènes électriques et capillaires*. PhD thesis, Gauthier-Villars Paris, France:, 1875.
- [8] G. Quincke, “Electrische untersuchungen,” *Annalen der Physik*, vol. 255, no. 8, pp. 545–588, 1883.
- [9] J. Sondag-Huethorst and L. Fokkink, “Potential-dependent wetting of electroactive ferrocene-terminated alkanethiolate monolayers on gold,” *Langmuir*, vol. 10, no. 11, pp. 4380–4387, 1994.
- [10] V. Peykov, A. Quinn, and J. Ralston, “Electrowetting: a model for contact-angle saturation,” *Colloid and Polymer Science*, vol. 278, no. 8, pp. 789–793, 2000.
- [11] E. Bormashenko and O. Gendelman, “A generalized electrowetting equation: Its derivation and consequences,” *Chemical Physics Letters*, vol. 599, pp. 139–141, 2014.
- [12] J. Lee, H. Moon, J. Fowler, T. Schoellhammer, and C.-J. Kim, “Electrowetting and electrowetting-on-dielectric for microscale liquid handling,” *Sensors and Actuators A: Physical*, vol. 95, no. 2-3, pp. 259–268, 2002.
- [13] H. Matsumoto and J. Colgate, “Preliminary investigation of micropumping based on electrical control of interfacial tension,” in *IEEE Proceedings on Micro Electro Mechanical Systems, An Investigation of Micro Structures, Sensors, Actuators, Machines and Robots.*, pp. 105–110, IEEE, 1990.
- [14] N. E. Cousens and A. R. Kucernak, “Reversible ultralow-voltage liquid–

- liquid electrowetting without a dielectric layer,” *Faraday discussions*, vol. 199, pp. 63–73, 2017.
- [15] B. Bruno, “Electrocapillarité et mouillage de films isolants par l’eau,” *Comptes Rendus de L’Academie des Sciences Paris, Serie, II*, vol. 317, pp. 157–163, 1993.
- [16] J. Lee and C.-J. Kim, “Surface-tension-driven microactuation based on continuous electrowetting,” *Journal of Microelectromechanical Systems*, vol. 9, no. 2, pp. 171–180, 2000.
- [17] W. C. Nelson and C.-J. C. Kim, “Droplet actuation by electrowetting-on-dielectric (ewod): A review,” *Journal of Adhesion Science and Technology*, vol. 26, no. 12-17, pp. 1747–1771, 2012.
- [18] H. Verheijen and M. Prins, “Reversible electrowetting and trapping of charge: model and experiments,” *Langmuir*, vol. 15, no. 20, pp. 6616–6620, 1999.
- [19] J.-Y. Yoon and R. L. Garrell, “Preventing biomolecular adsorption in electrowetting-based biofluidic chips,” *Analytical Chemistry*, vol. 75, no. 19, pp. 5097–5102, 2003.
- [20] T. Young, “iii. an essay on the cohesion of fluids,” *Philosophical transactions of the royal society of London*, no. 95, pp. 65–87, 1805.
- [21] W. J. Welters and L. G. Fokkink, “Fast electrically switchable capillary effects,” *Langmuir*, vol. 14, no. 7, pp. 1535–1538, 1998.

- [22] C. B. Gorman, H. A. Biebuyck, and G. M. Whitesides, “Control of the shape of liquid lenses on a modified gold surface using an applied electrical potential across a self-assembled monolayer,” *Langmuir*, vol. 11, no. 6, pp. 2242–2246, 1995.
- [23] S. Kuiper and B. Hendriks, “Variable-focus liquid lens for miniature cameras,” *Applied physics letters*, vol. 85, no. 7, pp. 1128–1130, 2004.
- [24] J. Hong, Y. K. Kim, K. H. Kang, J. Kim, and S. J. Lee, “Spreading dynamics and oil film entrapment of sessile drops submerged in oil driven by dc electrowetting,” *Sensors and Actuators B: Chemical*, vol. 196, pp. 292–297, 2014.
- [25] Q. Vo, H. Su, and T. Tran, “Universal transient dynamics of electrowetting droplets,” *Scientific reports*, vol. 8, no. 1, p. 836, 2018.
- [26] T. B. Jones, K.-L. Wang, and D.-J. Yao, “Frequency-dependent electromechanics of aqueous liquids: electrowetting and dielectrophoresis,” *Langmuir*, vol. 20, no. 7, pp. 2813–2818, 2004.
- [27] C. Decamps and J. De Coninck, “Dynamics of spontaneous spreading under electrowetting conditions,” *Langmuir*, vol. 16, no. 26, pp. 10150–10153, 2000.
- [28] F. Li and F. Mugele, “How to make sticky surfaces slippery: Contact angle hysteresis in electrowetting with alternating voltage,” *Applied Physics Letters*, vol. 92, no. 24, p. 244108, 2008.

- [29] B. Berge and J. Peseux, “Variable focal lens controlled by an external voltage: An application of electrowetting,” *The European Physical Journal E*, vol. 3, no. 2, pp. 159–163, 2000.
- [30] J. M. Oh, S. H. Ko, and K. H. Kang, “Shape oscillation of a drop in ac electrowetting,” *Langmuir*, vol. 24, no. 15, pp. 8379–8386, 2008.
- [31] M. G. Pollack, R. B. Fair, and A. D. Shenderov, “Electrowetting-based actuation of liquid droplets for microfluidic applications,” *Applied Physics Letters*, vol. 77, no. 11, pp. 1725–1726, 2000.
- [32] F. Mugele, J.-C. Baret, and D. Steinhauser, “Microfluidic mixing through electrowetting-induced droplet oscillations,” *Applied Physics Letters*, vol. 88, no. 20, p. 204106, 2006.
- [33] D. ‘t Mannetje, C. Murade, D. Van Den Ende, and F. Mugele, “Electrically assisted drop sliding on inclined planes,” *Applied physics letters*, vol. 98, no. 1, p. 014102, 2011.
- [34] C. Quilliet and B. Berge, “Electrowetting: a recent outbreak,” *Current opinion in colloid & Interface science*, vol. 6, no. 1, pp. 34–39, 2001.
- [35] A. Kumar, M. Pluntke, B. Cross, J.-C. Baret, and F. Mugele, “Finite conductivity effects and apparent contact angle saturation in ac electrowetting,” *MRS Online Proceedings Library Archive*, vol. 899, 2005.
- [36] T. D. Blake, A. Clarke, and E. Stattersfield, “An investigation of electrostatic assist in dynamic wetting,” *Langmuir*, vol. 16, no. 6, pp. 2928–2935, 2000.

- [37] S. Chevalliot, S. Kuiper, and J. Heikenfeld, "Experimental validation of the invariance of electrowetting contact angle saturation," *Journal of Adhesion Science and Technology*, vol. 26, no. 12-17, pp. 1909–1930, 2012.
- [38] S. Zhang, X. Hu, C. Qu, Q. Zhang, X. Ma, L. Lu, X. Li, X. Zhang, and Y. Deng, "Enhanced and reversible contact angle modulation of ionic liquids in oil and under ac electric field," *ChemPhysChem*, vol. 11, no. 11, pp. 2327–2331, 2010.
- [39] Y. S. Nanayakkara, S. Perera, S. Bindiganavale, E. Wanigasekara, H. Moon, and D. W. Armstrong, "The effect of ac frequency on the electrowetting behavior of ionic liquids," *Analytical chemistry*, vol. 82, no. 8, pp. 3146–3154, 2010.
- [40] J. Chen, X. Xiong, Q. Zhang, L. Shui, S. Shen, H. Yang, Z. Zhu, and F. Zhang, "P (vdf-trfe)/pmma blended films with enhanced electrowetting responses and superior energy storage performance," *Polymers*, vol. 11, no. 3, p. 526, 2019.
- [41] F. Mugele, A. Klingner, J. Buehrle, D. Steinhauser, and S. Herminghaus, "Electrowetting: a convenient way to switchable wettability patterns," *Journal of physics: condensed matter*, vol. 17, no. 9, p. S559, 2005.
- [42] M. Vallet, M. Vallade, and B. Berge, "Limiting phenomena for the spreading of water on polymer films by electrowetting," *The European Physical Journal B-Condensed Matter and Complex Systems*, vol. 11, no. 4, pp. 583–591, 1999.

- [43] B. Shapiro, H. Moon, R. L. Garrell, and C.-J. C. Kim, “Equilibrium behavior of sessile drops under surface tension, applied external fields, and material variations,” *Journal of Applied Physics*, vol. 93, no. 9, pp. 5794–5811, 2003.
- [44] E. Seyrat and R. A. Hayes, “Amorphous fluoropolymers as insulators for reversible low-voltage electrowetting,” *Journal of Applied Physics*, vol. 90, no. 3, pp. 1383–1386, 2001.
- [45] A. Quinn, R. Sedev, and J. Ralston, “Contact angle saturation in electrowetting,” *The journal of physical chemistry B*, vol. 109, no. 13, pp. 6268–6275, 2005.
- [46] J.-L. Lin, G.-B. Lee, Y.-H. Chang, and K.-Y. Lien, “Model description of contact angles in electrowetting on dielectric layers,” *Langmuir*, vol. 22, no. 1, pp. 484–489, 2006.
- [47] Z. Rui, L. Qi-Chao, W. Ping, and L. Zhong-Cheng, “Contact angle hysteresis in electrowetting on dielectric,” *Chinese Physics B*, vol. 24, no. 8, p. 086801, 2015.
- [48] P. Mach, T. Krupenkin, S. Yang, and J. Rogers, “Dynamic tuning of optical waveguides with electrowetting pumps and recirculating fluid channels,” *Applied physics letters*, vol. 81, no. 2, pp. 202–204, 2002.
- [49] J. M. Oh, S. H. Ko, and K. H. Kang, “Analysis of electrowetting-driven spreading of a drop in air,” *Physics of Fluids*, vol. 22, no. 3, p. 032002, 2010.

- [50] M. Prins, W. Welters, and J. Weekamp, "Fluid control in multichannel structures by electrocapillary pressure," *Science*, vol. 291, no. 5502, pp. 277–280, 2001.
- [51] X. Tan, Z. Zhou, and M. M.-C. Cheng, "Electrowetting on dielectric experiments using graphene," *Nanotechnology*, vol. 23, no. 37, p. 375501, 2012.
- [52] R. S. Hale and V. Bahadur, "Electrowetting-based microfluidic operations on rapid-manufactured devices for heat pipe applications," *Journal of Micromechanics and Microengineering*, vol. 27, no. 7, p. 075004, 2017.
- [53] R. B. Fair, "Digital microfluidics: is a true lab-on-a-chip possible?," *Microfluidics and Nanofluidics*, vol. 3, no. 3, pp. 245–281, 2007.
- [54] E. M. Miller and A. R. Wheeler, "Digital bioanalysis," *Analytical and bioanalytical chemistry*, vol. 393, no. 2, pp. 419–426, 2009.
- [55] S. K. Cho, H. Moon, and C.-J. Kim, "Creating, transporting, cutting, and merging liquid droplets by electrowetting-based actuation for digital microfluidic circuits," *Journal of Microelectromechanical systems*, vol. 12, no. 1, pp. 70–80, 2003.
- [56] V. Srinivasan, V. K. Pamula, and R. B. Fair, "An integrated digital microfluidic lab-on-a-chip for clinical diagnostics on human physiological fluids," *Lab on a Chip*, vol. 4, no. 4, pp. 310–315, 2004.
- [57] P. Paik, V. K. Pamula, and R. B. Fair, "Rapid droplet mixers for digital microfluidic systems," *Lab on a Chip*, vol. 3, no. 4, pp. 253–259, 2003.

- [58] B. Hendriks, S. Kuiper, M. V. As, C. Renders, and T. Tukker, “Electrowetting-based variable-focus lens for miniature systems,” *Optical review*, vol. 12, no. 3, pp. 255–259, 2005.
- [59] T. Krupenkin, S. Yang, and P. Mach, “Tunable liquid microlens,” *Applied Physics Letters*, vol. 82, no. 3, pp. 316–318, 2003.
- [60] R. A. Hayes and B. J. Feenstra, “Video-speed electronic paper based on electrowetting,” *Nature*, vol. 425, no. 6956, p. 383, 2003.
- [61] J. Heikenfeld and A. Steckl, “High-transmission electrowetting light valves,” *Applied Physics Letters*, vol. 86, no. 15, p. 151121, 2005.
- [62] V. A. Lifton, S. Simon, and R. E. Frahm, “Reserve battery architecture based on superhydrophobic nanostructured surfaces,” *Bell Labs Technical Journal*, vol. 10, no. 3, pp. 81–85, 2005.
- [63] V. Lifton, J. Taylor, B. Vyas, P. Kolodner, R. Cirelli, N. Basavanahally, A. Papazian, R. Frahm, S. Simon, and T. Krupenkin, “Superhydrophobic membranes with electrically controllable permeability and their application to “smart” microbatteries,” *Applied Physics Letters*, vol. 93, no. 4, p. 043112, 2008.
- [64] B. R. Acharya, T. Krupenkin, S. Ramachandran, Z. Wang, C. Huang, and J. A. Rogers, “Tunable optical fiber devices based on broadband long-period gratings and pumped microfluidics,” *Applied physics letters*, vol. 83, no. 24, pp. 4912–4914, 2003.

- [65] S. K. Thio, D. Jiang, and S.-Y. Park, “Electrowetting-driven solar indoor lighting (e-sil): an optofluidic approach towards sustainable buildings,” *Lab on a Chip*, vol. 18, no. 12, pp. 1725–1735, 2018.
- [66] Y. Chen, N. Doshi, B. Goldberg, H. Wang, and R. J. Wood, “Controllable water surface to underwater transition through electrowetting in a hybrid terrestrial-aquatic microrobot,” *Nature communications*, vol. 9, no. 1, p. 2495, 2018.
- [67] H.-H. Jeong, B. Lee, S. H. Jin, S.-G. Jeong, and C.-S. Lee, “A highly addressable static droplet array enabling digital control of a single droplet at pico-volume resolution,” *Lab on a Chip*, vol. 16, no. 9, pp. 1698–1707, 2016.
- [68] H. A. Stone, A. D. Stroock, and A. Ajdari, “Engineering flows in small devices: microfluidics toward a lab-on-a-chip,” *Annu. Rev. Fluid Mech.*, vol. 36, pp. 381–411, 2004.
- [69] P. R. Gascoyne and J. V. Vykoukal, “Dielectrophoresis-based sample handling in general-purpose programmable diagnostic instruments,” *Proceedings of the IEEE*, vol. 92, no. 1, pp. 22–42, 2004.
- [70] A. Renaudin, P. Tabourier, V. Zhang, and C. Druon, “Plateforme saw dédiée à la microfluidique discrète pour applications biologiques,” in *Actes du 2ème Congrès Français de Microfluidique*, 2004.
- [71] A. A. Darhuber, J. P. Valentino, S. M. Troian, and S. Wagner, “Thermocapillary actuation of droplets on chemically patterned surfaces by programmable

- microheater arrays,” *Journal of Microelectromechanical Systems*, vol. 12, no. 6, pp. 873–879, 2003.
- [72] R. B. Fair, A. Khlystov, T. D. Taylor, V. Ivanov, R. D. Evans, V. Srinivasan, V. K. Pamula, M. G. Pollack, P. B. Griffin, and J. Zhou, “Chemical and biological applications of digital-microfluidic devices,” *IEEE Design & Test of Computers*, vol. 24, no. 1, pp. 10–24, 2007.
- [73] L. Commander, S. Day, and D. Selviah, “Variable focal length microlenses,” *Optics communications*, vol. 177, no. 1-6, pp. 157–170, 2000.
- [74] N. Sugiura and S. Morita, “Variable-focus liquid-filled optical lens,” *Applied Optics*, vol. 32, no. 22, pp. 4181–4186, 1993.
- [75] C. Monat, P. Domachuk, and B. Eggleton, “Integrated optofluidics: A new river of light,” *Nature photonics*, vol. 1, no. 2, p. 106, 2007.
- [76] J. Chen, W. Wang, J. Fang, and K. Varahramyan, “Variable-focusing microlens with microfluidic chip,” *Journal of Micromechanics and Microengineering*, vol. 14, no. 5, p. 675, 2004.
- [77] J. Lee, Y. Park, and S. K. Chung, “Multifunctional liquid lens for variable focus and aperture,” *Sensors and Actuators A: Physical*, vol. 287, pp. 177–184, 2019.
- [78] P. Sen and C.-J. C. Kim, “Capillary spreading dynamics of electrowetted sessile droplets in air,” *Langmuir*, vol. 25, no. 8, pp. 4302–4305, 2009.
- [79] J. Hong, Y. K. Kim, K. H. Kang, J. Kim, and S. J. Lee, “Effects of drop

- viscosity on oscillation dynamics induced by ac electrowetting,” *Sensors and Actuators B: Chemical*, vol. 190, pp. 48–54, 2014.
- [80] A. Tröls, T. Voglhuber-Brunnmaier, S. Clara, B. Mayrhofer, and B. Jakoby, “The oscillation dynamics of droplets subject to electrowetting actuation,” *IEEE Sensors Journal*, vol. 19, no. 4, pp. 1379–1387, 2018.
- [81] X. Noblin, A. Buguin, and F. Brochard-Wyart, “Vibrated sessile drops: Transition between pinned and mobile contact line oscillations,” *The European Physical Journal E*, vol. 14, no. 4, pp. 395–404, 2004.
- [82] D. Quéré, “Inertial capillarity,” *EPL (Europhysics Letters)*, vol. 39, no. 5, p. 533, 1997.
- [83] D. Erickson, B. Blackmore, and D. Li, “An energy balance approach to modeling the hydrodynamically driven spreading of a liquid drop,” *Colloids and Surfaces A: Physicochemical and Engineering Aspects*, vol. 182, no. 1-3, pp. 109–122, 2001.
- [84] S. Bansal and P. Sen, “Effect of electrowetting induced capillary oscillations on coalescence of compound droplets,” *Journal of colloid and interface science*, vol. 530, pp. 223–232, 2018.
- [85] J. Hernández-Sánchez, L. Lubbers, A. Eddi, and J. Snoeijer, “Symmetric and asymmetric coalescence of drops on a substrate,” *Physical review letters*, vol. 109, no. 18, p. 184502, 2012.
- [86] W. Ristenpart, P. McCalla, R. Roy, and H. Stone, “Coalescence of spread-

- ing droplets on a wettable substrate,” *Physical review letters*, vol. 97, no. 6, p. 064501, 2006.
- [87] M. W. Lee, D. K. Kang, S. S. Yoon, and A. L. Yarin, “Coalescence of two drops on partially wettable substrates,” *Langmuir*, vol. 28, no. 8, pp. 3791–3798, 2012.
- [88] J. Eggers, J. R. Lister, and H. A. Stone, “Coalescence of liquid drops,” *Journal of Fluid Mechanics*, vol. 401, pp. 293–310, 1999.
- [89] D. G. Aarts, H. N. Lekkerkerker, H. Guo, G. H. Wegdam, and D. Bonn, “Hydrodynamics of droplet coalescence,” *Physical review letters*, vol. 95, no. 16, p. 164503, 2005.
- [90] M. Wu, T. Cubaud, and C.-M. Ho, “Scaling law in liquid drop coalescence driven by surface tension,” *Physics of Fluids*, vol. 16, no. 7, pp. L51–L54, 2004.
- [91] G. Beni and S. Hackwood, “Electro-wetting displays,” *Applied Physics Letters*, vol. 38, no. 4, pp. 207–209, 1981.
- [92] J. Sondag-Huethorst and L. Fokkink, “Potential-dependent wetting of octadecanethiol-modified polycrystalline gold electrodes,” *Langmuir*, vol. 8, no. 10, pp. 2560–2566, 1992.
- [93] M. Vallet, B. Berge, and L. Vovelle, “Electrowetting of water and aqueous solutions on poly (ethylene terephthalate) insulating films,” *Polymer*, vol. 37, no. 12, pp. 2465–2470, 1996.

- [94] S. H. Ko, H. Lee, and K. H. Kang, "Hydrodynamic flows in electrowetting," *Langmuir*, vol. 24, no. 3, pp. 1094–1101, 2008.
- [95] F. Mugele, A. Staicu, R. Bakker, and D. van den Ende, "Capillary stokes drift: a new driving mechanism for mixing in ac-electrowetting," *Lab on a Chip*, vol. 11, no. 12, 2011.
- [96] T. B. Jones, J. D. Fowler, Y. S. Chang, and C.-J. Kim, "Frequency-based relationship of electrowetting and dielectrophoretic liquid microactuation," *Langmuir*, vol. 19, no. 18, pp. 7646–7651, 2003.
- [97] J. S. Hong, S. H. Ko, K. H. Kang, and I. S. Kang, "A numerical investigation on ac electrowetting of a droplet," *Microfluidics and Nanofluidics*, vol. 5, no. 2, pp. 263–271, 2008.
- [98] F. Hong, D. Jiang, and P. Cheng, "Frequency-dependent resonance and asymmetric droplet oscillation under ac electrowetting on coplanar electrodes," *Journal of Micromechanics and Microengineering*, vol. 22, no. 8, p. 085024, 2012.
- [99] Y. Gu and D. Li, "A model for a liquid drop spreading on a solid surface," *Colloids and Surfaces A: Physicochemical and Engineering Aspects*, vol. 142, no. 2-3, pp. 243–256, 1998.
- [100] A. Ahmed, A. J. Qureshi, B. A. Fleck, and P. R. Waghmare, "Effects of magnetic field on the spreading dynamics of an impinging ferrofluid droplet," *Journal of colloid and interface science*, vol. 532, pp. 309–320, 2018.

- [101] J. C. Bird, S. Mandre, and H. A. Stone, “Short-time dynamics of partial wetting,” *Phys. Rev. Lett.*, vol. 100, p. 234501, Jun 2008.
- [102] Q. Vo and T. Tran, “Contact line friction of electrowetting actuated viscous droplets,” *Physical Review E*, vol. 97, no. 6, p. 063101, 2018.
- [103] C. Hao, Y. Liu, X. Chen, Y. He, Q. Li, K. Li, and Z. Wang, “Electrowetting on liquid-infused film (ewolf): complete reversibility and controlled droplet oscillation suppression for fast optical imaging,” *Scientific reports*, vol. 4, p. 6846, 2014.
- [104] D. R. Lide, *CRC handbook of chemistry and physics*, vol. 85. CRC press, 2004.
- [105] R. Sedev, “Electrowetting: Electrocapillarity, saturation, and dynamics,” *The European Physical Journal Special Topics*, vol. 197, no. 1, p. 307, 2011.
- [106] Y. Gu and D. Li, “Liquid drop spreading on solid surfaces at low impact speeds,” *Colloids and Surfaces A: Physicochemical and Engineering Aspects*, vol. 163, no. 2-3, pp. 239–245, 2000.
- [107] M. Pasandideh-Fard, Y. Qiao, S. Chandra, and J. Mostaghimi, “Capillary effects during droplet impact on a solid surface,” *Physics of fluids*, vol. 8, no. 3, pp. 650–659, 1996.
- [108] F. Brochard-Wyart and P. De Gennes, “Dynamics of partial wetting,” *Advances in colloid and interface science*, vol. 39, pp. 1–11, 1992.

- [109] D. 't Mannetje, F. Mugele, and D. van den Ende, "Stick-slip to sliding transition of dynamic contact lines under ac electrowetting," *Langmuir*, vol. 29, no. 48, pp. 15116–15121, 2013.
- [110] F. M. White and I. Corfield, *Viscous fluid flow*, vol. 3. McGraw-Hill New York, 2006.
- [111] A. Roshko, "On the development of turbulent wakes from vortex streets," 1954.
- [112] C. Miller and L. Scriven, "The oscillations of a fluid droplet immersed in another fluid," *Journal of fluid mechanics*, vol. 32, no. 3, pp. 417–435, 1968.
- [113] B. Derby, "Inkjet printing of functional and structural materials: fluid property requirements, feature stability, and resolution," *Annual Review of Materials Research*, vol. 40, pp. 395–414, 2010.
- [114] Y.-C. Tan, J. S. Fisher, A. I. Lee, V. Cristini, and A. P. Lee, "Design of microfluidic channel geometries for the control of droplet volume, chemical concentration, and sorting," *Lab on a Chip*, vol. 4, no. 4, pp. 292–298, 2004.
- [115] F. Mugele, M. Duits, and D. Van den Ende, "Electrowetting: a versatile tool for drop manipulation, generation, and characterization," *Advances in colloid and interface science*, vol. 161, no. 1-2, pp. 115–123, 2010.
- [116] M. Washizu, "Electrostatic actuation of liquid droplets for micro-reactor applications," *IEEE transactions on industry applications*, vol. 34, no. 4, pp. 732–737, 1998.

- [117] V. Bergeron, D. Bonn, J. Y. Martin, and L. Vovelle, “Controlling droplet deposition with polymer additives,” *Nature*, vol. 405, no. 6788, p. 772, 2000.
- [118] R. Zhao, Q. Zhang, H. Tjugito, and X. Cheng, “Granular impact cratering by liquid drops: Understanding raindrop imprints through an analogy to asteroid strikes,” *Proceedings of the National Academy of Sciences*, vol. 112, no. 2, pp. 342–347, 2015.
- [119] D. Bonn, J. Eggers, J. Indekeu, J. Meunier, and E. Rolley, “Wetting and spreading,” *Reviews of modern physics*, vol. 81, no. 2, p. 739, 2009.
- [120] E. Bertrand, D. Bonn, D. Broseta, H. Dobbs, J. Indekeu, J. Meunier, K. Ragil, and N. Shahidzadeh, “Wetting of alkanes on water,” *Journal of Petroleum Science and Engineering*, vol. 33, no. 1-3, pp. 217–222, 2002.
- [121] N. Shahidzadeh, E. Bertrand, J. P. Dauplat, J. C. Borgotti, P. Vié, and D. Bonn, “Effect of wetting on gravity drainage in porous media,” *Transport in Porous Media*, vol. 52, no. 2, pp. 213–227, 2003.
- [122] A. Ahmed, B. A. Fleck, and P. R. Waghmare, “Maximum spreading of a ferrofluid droplet under the effect of magnetic field,” *Physics of Fluids*, vol. 30, no. 7, p. 077102, 2018.
- [123] M. J. De Ruijter, J. De Coninck, and G. Oshanin, “Droplet spreading: partial wetting regime revisited,” *Langmuir*, vol. 15, no. 6, pp. 2209–2216, 1999.
- [124] A.-L. Biance, C. Clanet, and D. Quéré, “First steps in the spreading of a liquid droplet,” *Physical Review E*, vol. 69, no. 1, p. 016301, 2004.

- [125] D. Quéré, “Wetting and roughness,” *Annu. Rev. Mater. Res.*, vol. 38, pp. 71–99, 2008.
- [126] H. Fox and W. Zisman, “The spreading of liquids on low energy surfaces. i. polytetrafluoroethylene,” *Journal of Colloid Science*, vol. 5, no. 6, pp. 514–531, 1950.
- [127] A.-M. Cazabat, “How does a droplet spread?,” *Contemporary Physics*, vol. 28, no. 4, pp. 347–364, 1987.
- [128] M. van Gorcum, B. Andreotti, J. H. Snoeijer, and S. Karpitschka, “Dynamic solid surface tension causes droplet pinning and depinning,” *Physical review letters*, vol. 121, no. 20, p. 208003, 2018.
- [129] M. R. Rahman, H. N. Mullagura, B. Kattamalalawadi, and P. R. Waghmare, “Droplet spreading on liquid–fluid interface,” *Colloids and Surfaces A: Physicochemical and Engineering Aspects*, vol. 553, pp. 143–148, 2018.
- [130] A. Milne and A. Amirfazli, “Drop shedding by shear flow for hydrophilic to superhydrophobic surfaces,” *Langmuir*, vol. 25, no. 24, pp. 14155–14164, 2009.
- [131] Z. Wang and J. Zhe, “Recent advances in particle and droplet manipulation for lab-on-a-chip devices based on surface acoustic waves,” *Lab on a Chip*, vol. 11, no. 7, pp. 1280–1285, 2011.
- [132] T. Dung Luong and N. Trung Nguyen, “Surface acoustic wave driven microfluidics-a review,” *Micro and Nanosystems*, vol. 2, no. 3, pp. 217–225, 2010.

- [133] A. Bateni, S. Susnar, A. Amirfazli, and A. Neumann, “Development of a new methodology to study drop shape and surface tension in electric fields,” *Langmuir*, vol. 20, no. 18, pp. 7589–7597, 2004.
- [134] A. Bateni, A. Ababneh, J. Elliott, A. Neumann, and A. Amirfazli, “Effect of gravity and electric field on shape and surface tension of drops,” *Advances in Space Research*, vol. 36, no. 1, pp. 64–69, 2005.
- [135] H. Moon, S. K. Cho, R. L. Garrell, and C.-J. Kim, “Low voltage electrowetting-on-dielectric,” *Journal of applied physics*, vol. 92, no. 7, pp. 4080–4087, 2002.
- [136] Z. Wang and Y.-P. Zhao, “Wetting and electrowetting on corrugated substrates,” *Physics of Fluids*, vol. 29, no. 6, p. 067101, 2017.
- [137] T. B. Jones, “On the relationship of dielectrophoresis and electrowetting,” *Langmuir*, vol. 18, no. 11, pp. 4437–4443, 2002.
- [138] R. Dey, J. Gilbers, D. Baratian, H. Hoek, D. van den Ende, and F. Mugele, “Controlling shedding characteristics of condensate drops using electrowetting,” *Applied Physics Letters*, vol. 113, no. 24, p. 243703, 2018.
- [139] J.-C. Baret, M. M. Decré, and F. Mugele, “Self-excited drop oscillations in electrowetting,” *Langmuir*, vol. 23, no. 9, pp. 5173–5179, 2007.
- [140] D. Quéré, É. Raphaël, and J.-Y. Ollitrault, “Rebounds in a capillary tube,” *Langmuir*, vol. 15, no. 10, pp. 3679–3682, 1999.
- [141] O. Shardt, P. R. Waghmare, J. Derksen, and S. K. Mitra, “Inertial rise in short capillary tubes,” *Rsc Advances*, vol. 4, no. 28, pp. 14781–14785, 2014.

- [142] D. Banks, C. Ajawara, R. Sanchez, H. Surti, and G. Aguilar, “Effects of liquid and surface characteristics on oscillation behavior of droplets upon impact,” *Atomization and Sprays*, vol. 24, no. 10, 2014.
- [143] S. Lin, B. Zhao, S. Zou, J. Guo, Z. Wei, and L. Chen, “Impact of viscous droplets on different wettable surfaces: Impact phenomena, the maximum spreading factor, spreading time and post-impact oscillation,” *Journal of colloid and interface science*, vol. 516, pp. 86–97, 2018.
- [144] M. R. Rahman and P. R. Waghmare, “Double-emulsion drop evaporation and formation of a daughter droplet,” *Langmuir*, vol. 35, no. 12, pp. 4403–4411, 2019.
- [145] J. D. Smith, R. Dhiman, S. Anand, E. Reza-Garduno, R. E. Cohen, G. H. McKinley, and K. K. Varanasi, “Droplet mobility on lubricant-impregnated surfaces,” *Soft Matter*, vol. 9, no. 6, pp. 1772–1780, 2013.
- [146] A. Cavalli, D. J. Preston, E. Tio, D. W. Martin, N. Miljkovic, E. N. Wang, F. Blanchette, and J. W. Bush, “Electrically induced drop detachment and ejection,” *Physics of fluids*, vol. 28, no. 2, p. 022101, 2016.
- [147] S. Das, P. R. Waghmare, and S. K. Mitra, “Early regimes of capillary filling,” *Physical Review E*, vol. 86, no. 6, p. 067301, 2012.
- [148] S. Bradley and C. Stow, “Collisions between liquid drops,” *Philosophical Transactions of the Royal Society of London. Series A, Mathematical and Physical Sciences*, vol. 287, no. 1349, pp. 635–675, 1978.

- [149] P. Atten, “Electrocoalescence of water droplets in an insulating liquid,” *Journal of Electrostatics*, vol. 30, pp. 259–269, 1993.
- [150] J. Eggers, “Coalescence of spheres by surface diffusion,” *Physical review letters*, vol. 80, no. 12, p. 2634, 1998.
- [151] Y.-H. Lai, M.-H. Hsu, and J.-T. Yang, “Enhanced mixing of droplets during coalescence on a surface with a wettability gradient,” *Lab on a Chip*, vol. 10, no. 22, pp. 3149–3156, 2010.
- [152] G. I. Taylor, “The coalescence of closely spaced drops when they are at different electric potentials,” *Proceedings of the Royal Society of London. Series A. Mathematical and Physical Sciences*, vol. 306, no. 1487, pp. 423–434, 1968.
- [153] J. C. Bird, W. D. Ristenpart, A. Belmonte, and H. A. Stone, “Critical angle for electrically driven coalescence of two conical droplets,” *Physical review letters*, vol. 103, no. 16, p. 164502, 2009.
- [154] S. Mhatre, S. Deshmukh, and R. M. Thaokar, “Electrocoalescence of a drop pair,” *Physics of Fluids*, vol. 27, no. 9, p. 092106, 2015.
- [155] P. Atten, L. Lundgaard, and G. Berg, “A simplified model of electrocoalescence of two close water droplets in oil,” *Journal of Electrostatics*, vol. 64, no. 7-9, pp. 550–554, 2006.
- [156] A. Kovetz and B. Olund, “The effect of coalescence and condensation on rain formation in a cloud of finite vertical extent,” *Journal of the Atmospheric Sciences*, vol. 26, no. 5, pp. 1060–1065, 1969.

- [157] C. Bellehumeur, M. Bisaria, and J. Vlachopoulos, “An experimental study and model assessment of polymer sintering,” *Polymer Engineering & Science*, vol. 36, no. 17, pp. 2198–2207, 1996.
- [158] V. S. Nikolayev, D. Beysens, and P. Guenoun, “New hydrodynamic mechanism for drop coarsening,” *Physical review letters*, vol. 76, no. 17, p. 3144, 1996.
- [159] T. Dreher, J. Glass, A. O’Connor, and G. Stevens, “Effect of rheology on coalescence rates and emulsion stability,” *AIChE Journal*, vol. 45, no. 6, pp. 1182–1190, 1999.
- [160] W. M. Grissom and F. Wierum, “Liquid spray cooling of a heated surface,” *International Journal of Heat and Mass Transfer*, vol. 24, no. 2, pp. 261–271, 1981.
- [161] N. Kapur and P. H. Gaskell, “Morphology and dynamics of droplet coalescence on a surface,” *Physical Review E*, vol. 75, no. 5, p. 056315, 2007.
- [162] M. Sellier and E. Treluyer, “Modeling the coalescence of sessile droplets,” *BiOMICROFLUIDICS*, vol. 3, no. 2, p. 022412, 2009.
- [163] R. Narhe, D. Beysens, and Y. Pomeau, “Dynamic drying in the early-stage coalescence of droplets sitting on a plate,” *EPL (Europhysics Letters)*, vol. 81, no. 4, p. 46002, 2008.
- [164] H. T. Ochs III and R. R. Czys, “Charge effects on the coalescence of water drops in free fall,” *Nature*, vol. 327, no. 6123, p. 606, 1987.

- [165] C. W. Visser, P. E. Frommhold, S. Wildeman, R. Mettin, D. Lohse, and C. Sun, “Dynamics of high-speed micro-drop impact: numerical simulations and experiments at frame-to-frame times below 100 ns,” *Soft matter*, vol. 11, no. 9, pp. 1708–1722, 2015.
- [166] A. Klingner, J. Buehrle, and F. Mugele, “Capillary bridges in electric fields,” *Langmuir*, vol. 20, no. 16, pp. 6770–6777, 2004.
- [167] J. Barman, A. K. Nagarajan, and K. Khare, “Controlled electro-coalescence/non-coalescence on lubricating fluid infused slippery surfaces,” *RSC Advances*, vol. 5, no. 128, pp. 105524–105530, 2015.
- [168] Z. Liu, X. Fu, B. P. Binks, and H. C. Shum, “Coalescence of electrically charged liquid marbles,” *Soft Matter*, vol. 13, no. 1, pp. 119–124, 2017.
- [169] S. Mhatre, V. Vivacqua, M. Ghadiri, A. Abdullah, M. Al-Marri, A. Hassanpour, B. Hewakandamby, B. Azzopardi, and B. Kermani, “Electrostatic phase separation: A review,” *Chemical Engineering Research and Design*, vol. 96, pp. 177–195, 2015.
- [170] G. G. Chase and A. S. Aljuhani, “Electro-coalescence of water droplets in air medium by electrowetting,” in *SPE Eastern Regional Meeting*, Society of Petroleum Engineers, 2013.
- [171] J.-C. Baret and F. Mugele, “Electrical discharge in capillary breakup: controlling the charge of a droplet,” *Physical review letters*, vol. 96, no. 1, p. 016106, 2006.

- [172] R. Temam and A. Chorin, “Navier stokes equations: Theory and numerical analysis,” 1978.
- [173] P. S. Laplace, *Traité de mécanique céleste*, vol. 1. de l’Imprimerie de Crapelet, 1799.
- [174] J. Buehrle, S. Herminghaus, and F. Mugele, “Interface profiles near three-phase contact lines in electric fields,” *Physical review letters*, vol. 91, no. 8, p. 086101, 2003.
- [175] S. Mitra and S. K. Mitra, “Symmetric drop coalescence on an under-liquid substrate,” *Physical Review E*, vol. 92, no. 3, p. 033013, 2015.
- [176] S. Thoroddsen, K. Takehara, and T. Etoh, “The coalescence speed of a pendant and a sessile drop,” *Journal of Fluid Mechanics*, vol. 527, pp. 85–114, 2005.
- [177] G. MacKay and S. Mason, “The gravity approach and coalescence of fluid drops at liquid interfaces,” *The Canadian Journal of Chemical Engineering*, vol. 41, no. 5, pp. 203–212, 1963.
- [178] M. Borrell, Y. Yoon, and L. G. Leal, “Experimental analysis of the coalescence process via head-on collisions in a time-dependent flow,” *Physics of Fluids*, vol. 16, no. 11, pp. 3945–3954, 2004.
- [179] H. Wang, A. Z. Zinchenko, and R. H. Davis, “The collision rate of small drops in linear flow fields,” *Journal of fluid mechanics*, vol. 265, pp. 161–188, 1994.

- [180] G. Jeffreys and J. Hawksley, “Stepwise coalescence of a single droplet at an oil-water interface,” *Journal of Applied Chemistry*, vol. 12, no. 8, pp. 329–336, 1962.
- [181] R. Sun, H. Yang, D. M. Rock, R. Danaei, R. Panat, M. R. Kessler, and L. Li, “Manufacturing pdms micro lens array using spin coating under a multiphase system,” *Journal of Micromechanics and Microengineering*, vol. 27, no. 5, p. 055012, 2017.
- [182] R. Shamai, D. Andelman, B. Berge, and R. Hayes, “Water, electricity, and between. . . on electrowetting and its applications,” *Soft Matter*, vol. 4, no. 1, pp. 38–45, 2008.
- [183] C. Murade, J. Oh, D. Van den Ende, and F. Mugele, “Electrowetting driven optical switch and tunable aperture,” *Optics express*, vol. 19, no. 16, pp. 15525–15531, 2011.
- [184] I. S. Park, Y. Park, S. H. Oh, J. W. Yang, and S. K. Chung, “Multifunctional liquid lens for variable focus and zoom,” *Sensors and Actuators A: Physical*, vol. 273, pp. 317–323, 2018.
- [185] P.-G. De Gennes, F. Brochard-Wyart, and D. Quéré, *Capillarity and wetting phenomena: drops, bubbles, pearls, waves*. Springer Science & Business Media, 2013.
- [186] S. Rong, Y. Li, and L. Li, “Electrowetting optical switch with circular tunable aperture,” *Optical Engineering*, vol. 57, no. 8, p. 087102, 2018.

- [187] J. E. Greivenkamp, *Field guide to geometrical optics*, vol. 1. SPIE press Bellingham, WA, 2004.
- [188] J. H. Masliyah and S. Bhattacharjee, *Electrokinetic and colloid transport phenomena*. John Wiley & Sons, 2006.
- [189] N. L. Salvaggio, N. Salvaggio, L. D. Stroebel, and R. D. Zakia, *Basic photographic materials and processes*. Taylor & Francis, 2009.

Appendix

A-1 Derivation of Young-Lippmann equation

A droplet which partially wets an homogeneous, rigid, and chemically stable substrate attains an equilibrium geometry, usually characterized by a contact angle. This contact angle is a function of the interaction between the interfacial energies (σ) of the solid substrate (S), liquid droplet (D) and fluid medium (F). Hence, the total free energy of the drop can be written as:

$$F = \sum A_i \sigma_i - V \Delta P \quad (\text{A-3})$$

where A represents the area of A_{SD} solid-drop, solid fluid A_{SF} , and drop-fluid A_{DF} interfaces, V is the drop volume, and P is the pressure drop across the drop-fluid interface. Please note that an index notation (i) was used to denote all the different interfacial energies and areas. If an additional external electric field is applied to the drop, the total free energy will be modified. The free energy of a drop as stated in Eq. A-3, when submitted to electrowetting on dielectric, has an additional term from the electrostatic energy:

$$F = \sum A_i \sigma_i - V \Delta P - E_E \quad (\text{A-4})$$

where E_E is the total electric potential energy stored in a capacitor. For instance, if a dielectric layer is used for electrowetting, the total capacitance of the system can be approximated to the capacitance of the dielectric, and the capacitance of the electric double layer can be ignored. A dielectric material can prevent the flow of the electric charges through it, but allows the reposition of some charges that grants the polarization of the material. A dielectric in an external electric field will induce a charge separation within each atom [188]. By applying Gauss law, the electric field E between two plates through a dielectric medium is:

$$E = \frac{Q}{\varepsilon_0 \varepsilon_d A} \quad (\text{A-5})$$

where Q is the charge of each plate, ε_0 is the vacuum permittivity, ε_d is the dielectric constant of the medium, and A is the cross-section area of the plates. The electric field can also be represented as $E = U/d$, where U is the potential difference between plates and d is the separation distance of the plates (or dielectric thickness). Thus, by combining this with Eq. A-5, the potential difference can be obtained as:

$$U = \frac{Q}{\varepsilon_0 \varepsilon_d A/d} \quad (\text{A-6})$$

Now, the energy stored by the dielectric could be obtained following Verheijen and Prins derivation [18], which considered the differential electrostatic energy per unit area. However, we proposed to use the total electric potential energy stored in a capacitor $E_E = \frac{QU}{2}$, which incorporated with Eq. A-6 can give the expression of:

$$E_E = \frac{\varepsilon_0 \varepsilon_d A}{2d} U^2 \quad (\text{A-7})$$

This electric potential energy is only for the area in which the drop wets the dielectric, i.e. the area of the solid-drop interface (A_{SD}). With these assumptions, and bearing in mind that the area of the solid-drop and solid-fluid interface are the same, the total free energy of a drop with an electrical field can be written as:

$$F = (\sigma_{SD} - \sigma_{SF} - \frac{\varepsilon_0 \varepsilon_d}{2d} U^2) A_{SD} + \sigma_{SV} A_{SV} - V\lambda \quad (\text{A-8})$$

where λ is a Lagrangian multiplier. The previous equation can be treated as the minimum energy required to be in equilibrium, in which all the components are a function of the base radius of the drop R or the contact angle θ , as reported in Table A-1. Therefore, the partial derivation of Eq. A-8 with respect to R and θ should be considered. Hence the partial derivatives of the energy in the drop are:

$$\frac{\partial F}{\partial R} = (\sigma_{SD} - \sigma_{SF} - \frac{\varepsilon_0 \varepsilon_d}{2d} U^2) \frac{\partial A_{SD}}{\partial R} + \sigma_{SV} \frac{\partial A_{SV}}{\partial R} - \lambda \frac{\partial V}{\partial R} = 0 \quad (\text{A-9})$$

Hence, by substituting terms from Table A-1 into Eq. A-9 and reorganizing terms, it can be obtained that:

$$k \sin^2 \theta + 2(1 - \cos \theta) = \frac{R}{2\sigma_{DF}} (2 + \cos \theta)(1 - \cos \theta)^2 \quad (\text{A-10})$$

where for the simplicity of the calculations representation $k = \frac{\sigma_{SD} - \sigma_{SF}}{\sigma_{DF}} - \frac{\varepsilon_0 \varepsilon_d}{2d\sigma_{DF}} U^2$.

Following this order of ideas, a similar procedure was performed with the partial derivative with respect to θ , and it was found that:

$$k \cos\theta + 1 = \frac{R}{2\sigma_{DF}} (1 - \cos^2\theta) \quad (\text{A-11})$$

Thereafter, if Eq. A-10 is divided by Eq. A-11, it can be found that $k = -\cos\theta$. Now, by substituting back the values into k , the classical formulation of Young-Lippmann equation for electrowetting on a dielectric can be written as:

$$\cos\theta_{app} = \frac{\sigma_{SF} - \sigma_{SD}}{\sigma_{DF}} + \frac{\varepsilon_0 \varepsilon_d}{2d\sigma_{DF}} U^2 = \cos\theta_Y + \eta. \quad (\text{A-12})$$

in which $\theta_Y = \frac{\sigma_{SF} - \sigma_{SD}}{\sigma_{DF}}$ is the Young's contact angle that can be obtained with the same procedure as before but starting from Eq. A-3 which ignores the electrostatic contribution. And $\eta = \frac{\varepsilon_0 \varepsilon_d}{2d\sigma_{DF}} U^2$ is the dimensionless electrowetting number.

Table A-1: Areas and volume equations, with the corresponding partial derivatives with respect to R and θ .

Parameter	$\frac{\partial}{\partial R}$	$\frac{\partial}{\partial \theta}$
$A_{SD} = \pi R^2 \sin^2\theta$	$2\pi R \sin^2\theta$	$2\pi R^2 \sin\theta \cos\theta$
$A_{DF} = 2\pi R^2 (1 - \cos\theta)$	$4\pi R (1 - \cos\theta)$	$2\pi R^2 \sin\theta$
$V = \frac{\pi R^3}{3} (2 + \cos\theta)(1 - \cos\theta)^2$	$\pi R^2 (2 + \cos\theta)(1 - \cos\theta)^2$	$\pi R^3 \sin\theta (1 - \cos^2\theta)$

A-2 Optical setup considerations

For all the experiments performed in this thesis, the spreading, the oscillations, and the coalescence of the droplets caused by electrowetting were recorded with a high speed camera. The drop was visualized by a shadowgraph technique in which the drop generates a shadow that is captured by the optic system. Figure A-3 presents an schematic of the main components of the optical system used in this project. For the functionality of shadowgraph technique, the system requirements can be divided into image acquisition, illumination, and data acquisition/processing. Therefore, in the following sections these main components will be described in detail.

A-2.1 Image acquisition

Both the cameras used in this project have a CMOS sensor with a dimension of 25.6mm by 16.0mm , with a pixel size of $20\mu\text{m}$ by $20\mu\text{m}$. Then, if a spatial resolution of $5\mu\text{m}/\text{pixel}$ is desired, the magnification factor is equal to four. Also, if a spatial resolution of 800 by 600 pixels is used for the images, the field of view will be 3.2mm by 2.4mm in horizontal and vertical direction, respectively. The minimum working distance can be calculated by considering the thickness of the cuvette and the base radius of the deposited drop after the spreading and/or coalescence. The thickness of the cuvette wall is approximately 2.5mm and the radius of the drops after the maximum spreading will be assumed to be 3mm . In addition, the drop must be deposited away from the wall to avoid any effect that the cuvette might produce in the fluid flow. An additional distance is included to separate the lens and the cuvette. Following this order of ideas, an additional distance of 10mm is required for the separation distance from the drop and the lens, leading to a total

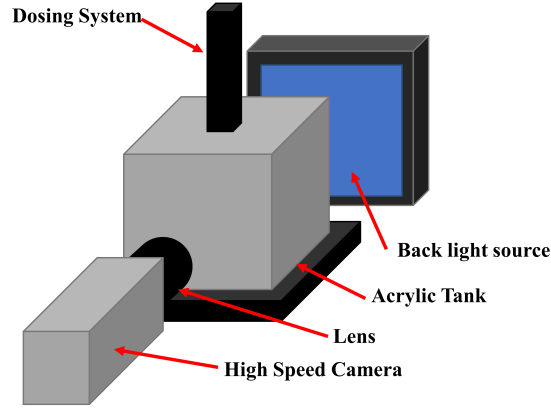


Figure A-3: Schematic of the optical setup used for the experiments. The main components of the optical setup include the high speed camera, the lens, and the back light source.

separation distance of $15.5mm$. Therefore, the viewing angle of the lens can be calculated as [189]:

$$\tan(\theta/2) = \frac{L/2}{f_2} \quad (\text{A-13})$$

where θ denotes the angle of view, L the length of field of view, and f_2 the separation distance between the droplet and the lens. As mentioned previously, if the separation distance is assumed to be $15.5mm$ and the lengths of field of view $3.2mm$ and $2.4mm$, the angle of view is 11.85° and 8.88° for horizontal and vertical direction, respectively. Now, in order to calculate the focal length, the following expression can be used [189]:

$$\frac{f_1}{f_2} = \frac{l}{L} \quad (\text{A-14})$$

where f_1 denotes the focal length and l the corresponding length of the sensor. Hence, it can be calculated that the focal length equals $77.5mm$. Therefore, a lens

with a focal of 80mm can be selected for the analysis. Therefore, the separation distance should be recalculated considering the fixed focal length of the lens, and for the same reason the angle of view must be recalculated. If the field of view remains constant, the new separation distance is equal to 16mm and the new angle of view is 11.48° and 8.60° for horizontal and vertical direction, respectively. As the height of the drop was the main parameter studied in this study, reducing the angle of view is essential for an accurate measurement of the droplet height. For high angles, the tangential rays of light might not be at the top of the drop, which will lead to an erroneous observation of the drop's shape. However, for low angles, the tangential rays are closer to be completely horizontal, so the height observed by the optic system corresponds with the height of the drop. This can also be verified by comparing the height obtained from the equation of the volume of a spherical cap (Eq. 2.2), with the measured height of the system. Therefore, the separation distance and focal length were set to produce a small angle of view, and so the measured height of the drop did not deviate more than 5% from the theoretical estimation of the droplet height.

The system f-number is used to control the size of the circular opening that allows light to reach the camera sensor. It is a nondimensional number that measures the lens speed and can be determined by the ratio of the system's focal length with respect to the diameter of the entrance pupil [189]:

$$N = \frac{f_1}{D} \quad (\text{A-15})$$

where N denotes the f-number and D is the diameter of aperture. The $f\#$ for most of the lenses can be tuned from defined limits, in which by increasing the $f\#$, the relative brightness is being reduced. If the f-number is increased, the exposure time should be increased to obtain an image with the same exposure. For this main reason, the f-number is selected to be equal to $f/4$ for capturing images with the maximum possible brightness.

The only two missing parameters related to the specification of the image are the depth of field and the depth of focus. The depth of field (DOF) is the missing spatial resolution parameter and the depth of focus measures the tolerance at which the image can be placed in comparison to the lens. The main difference between the depth of field and depth of focus is that the first is the area in front of the lens to obtain an acceptable focus, and the second denotes the zone behind the lens wherein the sensor is positioned to generate an in-focus image. The depth of field and the depth of focus can be calculated as [189]:

$$DOF \approx \frac{2Ncf_1^2f_2^2}{f_1^4 - N^2c^2f_2^2} \quad (\text{A-16})$$

$$t \approx \frac{2Ncf_2}{f_1} \quad (\text{A-17})$$

where c is the circle of confusion and t is the total depth of focus. The depth of field and depth of focus can be calculated by assuming the circle of confusion is $0.02mm$, the f-number is four. Also, by using the previous values of focal length,

and separation distance, the depth of field and depth of focus are approximately 6.4 and $32\mu m$, for the depth of field and depth of focus, respectively. With these values, the interface of the drop and the medium is well focused, with a high resolution of pixels to identify the change in the height of the droplet.

A-2.2 Illumination

The basic principle of shadowgraph is to detect the object by interrupting the rays of light of the back-light source. Therefore, a high illumination is required, specially when high speed imaging is used and the exposure time is reduced. Thus, the light source can be selected based on the camera saturation. The image saturation refers to the condition when the cell in a pixel becomes occupied. This limit, or amount of charge that can be accumulated in a single pixel, is a function of the area. As the pixel reaches the saturation, there is a smaller probability of trapping an electron, leading to the degrade of the linear relationship between the light intensity and the signal. The full well capacity describes the amount of charge that a single pixel can hold before saturating. This value depends mainly on the size of the sensor and the operating voltage for the sensor. The quantum efficiency is another key parameter that will determine the saturation of a system; it compares the number of photons hitting the devices and the number of charge carriers produce by the device at a specific wavelength. If any other kind of losses in the system is ignored, the number of incident photons can be calculated as:

$$N_{photon} = \frac{N_{electron}}{QE_{\lambda}} \quad (A-18)$$

where $N_{electron}$ is the number of electrons produced, N_{photon} is the number of photons absorbed, and QE_{λ} is the quantum efficiency at a specific wavelength λ . The high speed cameras used in this project have a Quantum efficiency (QE) of 31% approximately at a wavelength $\lambda = 530nm$ with a full well capacity of $23,000e$, which will be considered as the number of photons absorbed to saturate a pixel. Therefore, the number of electrons produced to saturate a pixel is 74,193. Knowing the number of photons to saturate a pixel, the amount of energy involved in this process can be calculated with the Planck-Einstein relation:

$$E_{sat} = N_{saturation} h \frac{c}{\lambda} \quad (\text{A-19})$$

Here, E_{sat} denotes the total energy of the light source, h is the Planck constant, and c is the speed of light. Hence, the total energy of the photons is equal to $173,538eV$. Now, in order to calculate the total energy to completely saturate the camera, this energy must be multiplied by the number of pixels that the sensor has. The total number of pixels in the sensor is 1,024,000 pixels, therefore the total energy is $1.78 * 10^{11}eV$. Thus, the light source should be selected accordingly to considered the energy required to saturate the sensor of the camera.

A-2.3 Data acquisition and processing

The first step of the data processing is the image calibration. An adequate spatial calibration is required to produce valid data and to reduce errors or distortion associated with the geometric measurements of digital cameras. The spatial calibration is performed to convert measurements from pixels (taken with the camera or sensor) to SI units or spatial units that can be compared with other images or data

obtained. Usually the calibration is achieved by measuring the number of pixels in the image which are associated to a known distance. Hence, the pixel domain can be converted to the physical domain. In this project, a needle with a known outside diameter of 0.51mm was used to create, to position, and to deposit the droplets for the experiments of electrowetting. Also, these needles were used to locate the top electrode to transmit the electric field to the droplets and generate the spreading. Therefore, the needle with known size can be used to calibrate the image from the pixel domain to the spatial domain. By locating the needle on the field of view of the camera and using the same conditions as in the experiments (light, zoom, and separation distance), the camera can capture the needle. Then, the number of pixels used to cover the outer diameter of the needle can be counted and used to calculate the aspect ratio of a pixel per unit length. Also, it is vital to clearly specify that the calibration is completed by maintaining the acrylic tank perpendicular to the front of the camera.

Finally, after the image calibration was completed, the height of the drop was measured by detecting the drop-medium interface. The interface was detected by the raise in the intensity of the pixels along the vertical center line of the droplet. Hence, the interface occurs when the pixels go from a low intensity (black) to a high intensity (white), as presented in Fig. A-4. All the optical parameters will influence how many pixels will be required to change from a low to a high intensity. For reducing the error associated with the height measurements, these number of pixels should be reduced as much as possible, which indicates a well defined interface in the image captured. If the condition of a well defined interface is maintained, the

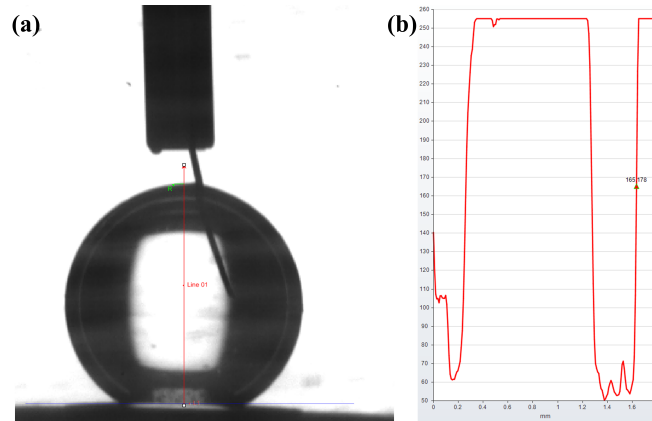


Figure A-4: Line profile for detecting drop's interface of a water drop in a liquid medium. (a) Experimental snapshot of a droplet with a submerged wire for inducing electrowetting. The line profile is located at the center of the droplet, in which R represents the rise of the pixel's intensity. (b) Intensity measurements, based on a grayscale, along the line profile in which the height of the drop is measured as 1.65mm .

height measurement process by this technique can be repeated for all the frames and the measurement of the height in time can be obtained.